AFWAL-TR-84-4041

B. N. Leis, D. P. Goetz, J. Ahmad,
A. T. Hopper and M. F. Kanninen

MECHANICS ASPECTS OF MICROCRACK GROWTH IN INCONEL 718-IMPLICATIONS FOR ENGINE RETIREMENT FOR CAUSE ANALYSIS

Battelle's Columbus Laboratories
505 King Avenue
Columbus, Ohio 43201

March 18, 1985

Report for period July, 1982 - January, 1984

MATERIALS LABORATORY
AIR FORCE WRIGHT AERONAUTICAL LABORATORIES
AIR FORCE SYSTEMS COMMAND
WRIGHT-PATTERSON AFB, OHIO 45433

NOTICE

When Government drawings, specifications, or other data are used for any purpose other than in connection with a definitely related Government procurement operation, the United States Government thereby incurs no responsibility nor any obligation whatsoever, and the fact that the government may have formulated, furnished, or in any way supplied the said drawings, specifications, or other data, is not to be regarded by implication or otherwise as in any manner licensing the holder or any other person or corporation, or conveying any rights or permission to manufacture, use, or sell any patented invention that may in any way be related thereto.

This technical report has been reviewed and is approved for publication.

James M. Larsen

JAMES M. LARSEN, Project Engineer
Metals Behavior Branch
Metals & Ceramics Division

John P. Henderson

JOHN P. HENDERSON, Chief
Metals Behavior Branch
Metals & Ceramics Division

FOR THE COMMANDER:

Lawrence N. Hjelm

LAWRENCE N. HJELM, Asst Chief
Metals and Ceramics Division
Materials Laboratory

"If your address has changed, if you wish to be removed from our mailing list, or if the addressee is no longer employed by your organization please notify AFWAL/MLLN, W-P AFB, OH 45433 to help us maintain a current mailing list".

Copies of this report should not be returned unless return is required by security considerations, contractual obligations, or notice on a specific document.

SECURITY CLASSIFICATION O S PAGE (When Data Entered)

REPORT DOCUMENTATION PAGE

READ INSTRUCTIONS BEFORE COMPLETING FORM

1. REPORT NUMBER: AFWAL-TR-84-4041	2. GOVT ACCESSION NO: AD-A162 886
3. RECIPIENT'S CATALOG NUMBER	
4. TITLE (and Subtitle): MECHANICS ASPECTS OF MICROCRACK GROWTH IN INCONEL 718-IMPLICATIONS FOR ENGINE RETIREMENT FOR CAUSE ANALYSIS	5. TYPE OF REPORT & PERIOD COVERED: Final Report July 1, 1982 - January, 1984
	6. PERFORMING ORG. REPORT NUMBER
7. AUTHOR(s): B. N. Leis, D. P. Goetz, J. Ahmad, A. T. Hopper, and M. F. Kanninen	8. CONTRACT OR GRANT NUMBER(s): F33615-81-C-5051
9. PERFORMING ORGANIZATION NAME AND ADDRESS: Battelle's Columbus Laboratories 505 King Avenue Columbus, Ohio 43201	10. PROGRAM ELEMENT, PROJECT, TASK AREA & WORK UNIT NUMBERS: P. E. 62102F Project 2420 03 09
11. CONTROLLING OFFICE NAME AND ADDRESS: Materials Laboratory (AFWAL/MLLN) Air Force Wright Aeronautical Laboratories Wright-Patterson AFB, Ohio 45433	12. REPORT DATE: March 18, 1985
	13. NUMBER OF PAGES: 162
14. MONITORING AGENCY NAME & ADDRESS (if different from Controlling Office)	15. SECURITY CLASS. (of this report): Unclassified
	15a. DECLASSIFICATION/DOWNGRADING SCHEDULE

16. DISTRIBUTION STATEMENT (of this Report)

Approved for public release; distribution unlimited.

17. DISTRIBUTION STATEMENT (of the abstract entered in Block 20, if different from Report)

18. SUPPLEMENTARY NOTES

19. KEY WORDS (Continue on reverse side if necessary and identify by block number) Inconel 718, short crack, small crack, fatigue, linear elastic fracture mechanics, inelastic fracture mechanics, threshold, notches, closure, models, engine materials, crack initiation, crack propagation, crack tip opening displacement, similitude, microstructure, oxidation, creep, engine retirement for cause, transients, 3D crack geometry, biaxial stress

20. ABSTRACT (Continue on reverse side if necessary and identify by block number)

Fatigue crack-growth rate predictions based on linear elastic fracture mechanics have been successfully applied in damage tolerance analyses for many years. These successes have prompted the Air Force Wright Aeronautical Laboratories to undertake the research needed to develop the technology to track the growth of defects in engine components. This application is not trivial because there is a growing body of experimental data that indicate that linear elastic fracture mechanics concepts do not always consolidate crack-growth-rate data. The lack of consolidation is particularly acute for

DD FORM 1 JAN 73 1473

SECURITY CLASSIFICATION OF THIS PAGE (When Data Entered)

CONT

physically short cracks and often the trend is toward much higher crack growth rates than expected.

A literature review led to the conclusion that this short-crack effect arose primarily because of crack tip plasticity, transients from initiation to microcracking, and incorrect or incomplete implementation of LEFM. However, the data did not discriminate between these possible causes to that it was not clear which were significant. An experimental program was undertaken to isolate or emphasize the factors thought to promote the short-crack effect. The material used in the study was Inconel 718 in a heat-treatment condition found in current advanced engines. This report presents the results of those experiments.

Two specimen geometries were used in the experiments--a center cracked panel and a center hole notched panel. For the center cracked panels the variation in the ratio of plastic zone size to crack length (r_p/a) that could be achieved was bounded below by the threshold and above by K_c, and was small (from .13 to .32). No difference in microcrack growth rate behavior was detected over this range of r_p/a. Because the crack tip plasticity is confined, only limited closure developed. This was verified using a wake removal technique. A short crack effect of at most a factor of 4 was observed for cracks less than 600 μm long.

For the center notched panels, a number of experiments were conducted to study free surface effects and initiation transients, three-dimensional crack geometry transient effects, and notch field effects. Natural initiation influenced results significantly because of free surface effects and crack geometry transients. Crack-growth rates more than an order of magnitude higher than long crack trends were observed in some cases. The influence of natural initiation · s observed to be accentuated by nearly elastic notch root deformation be vior. Elevated crack-growth rates were also observed when the crack was embedded in the plastic zone at a notch root.

The report pro/ides details of the experimental procedures used and a discussion of the experimental results including tabulations of the data. There is also a discussion of the implications of our findings relative to retirement for cause.

SUMMARY

This report presents results of an experimental program directed at assessment of the important aspects of the short-crack effect with regard to engine RFC analysis. Results of a first phase--a critical appraisal of the literature [4]--showed many factors have been viewed as possible sources of the short-crack effect. The purpose of the experiments was to identify and characterize key factors controlling the growth of small (short) cracks in engine applications. The desire was to make this assessment relative to LEFM--a deterministic continuum mechanics concept that assumes the existance of a dominant singularity. Accordingly, the study was also restricted to crack sizes that can be addressed as a dominant singularity in a continuum sense. Thus, the scope may be restricted by an implicit lower bound crack size on the order of 3- to 10-grain diameters.

The results of the literature survey indicated an absence of data that isolate or emphasize factors thought to promote a short-crack effect. This experimental study, therefore, set out to develop such information. Specifically, experiments were performed to isolate or emphasize r_p/a, closure, free surface effects and initiation transients, notch-field effects, stress-state effects, and 3D-crack geometry (transient) effects.

Analyses based on a pseudo plastic extension of LEFM have been developed to deal with values of r_p/a that exceed the LEFM confined flow situation (Appendix C). Analyses have also been developed to assess growth rate dependence on stress state and normalized stress level (Appendix A). The influence of 3D crack geometry effects have been addressed in a survey of available K solutions (Appendix B) and via experiments. The need for geometry specific K solutions that reflect the dependence of K on the near field (notch gradient) and the far-field boundaries has been demonstrated analytically (Appendix F). Also the fact that single term K expressions develop near infinite values of $d(K/S)/dc$ approaching the notch boundary has been analytically demonstrated. In this same context, the utility of K as a measure of crack driving force as $c \rightarrow 0$ has been questioned (Appendix F).

Exploratory experiments were performed to assess each of the above-noted factors in the finite growth-rate regime. The range of variations in

r_p/a that could be achieved were bounded below by the threshold and above by K_c, and were small. As expected, in view of the apparent effect of r_p/a in the literature, growth rates at small cracks were reasonably characterized by LEFM and long-crack data. Higher crack-growth rates of about a factor of 4 were observed for plane-fronted cracks growing from micro-preflaws. No applicable difference in microcrack-growth rate behavior was detected over the range of r_p/a considered. Finally, because plasticity was confined, only limited closure was expected to develop. This assertion was supported by results developed using the wake removal concept, over the range of r_p/a studied for net wakes as small as 40 μm.

A number of experiments were also committed to the study of free surface effects and initiation transients, 3D crack geometry transient effects, and notch-field effects. Results of these studies showed a significant influence of natural initiation developed, apparently through free surface effects and crack geometry transients. Short-crack effects of more than an order of magnitude were observed. The influence of natural initiation was observed to be accentuated by elastic (or nearly so) notch-root deformation behavior. A significant short-crack effect was also observed as a result of inelastic action at notch roots.

Given that specimen, notch, and crack geometry appear to control the mechanics factors noted as key drivers for a short-crack effect, it was emphasized that the incidence and extent of the short-crack effect observed depends on both the application of interest and the material. It was also noted that results generated to screen materials for a short-crack effect will depend on the test specimen geometry. Finally, it was emphasized that a lower bound exists below which deterministic continuum fracture mechanics cannot be applied. The implications of these considerations to polycrystalline DS and to SC materials of various strength levels were discussed for engine RFC analysis. Categories of behavior were identified based on the continuum limitation and r_p/a, and the specimen or component geometry regarding notch fields and crack shape.

FOREWORD

This technical report has been prepared by Battelle's Columbus Laboratories, Columbus, Ohio, under USAF Contract F33615-81-C-5051. The program has been administered by Mr. J. Larsen and Dr. T. Nicholas, AFWAL, Materials Laboratory.

Drs. M. F. Kanninen and B. N. Leis served as coprincipal investigators for this study. Dr. A. T. Hopper was the program manager.

Special acknowledgement is made to Mr. D. P. Goetz whose careful attention to detail was responsible for the successes in the laboratory. We would also like to acknowledge the substantial contributions of Mr. T. P. Forte and Mr. Dennis Rider of Battelle's Columbus Laboratories.

TABLE OF CONTENTS

TABLE OF CONTENTS

LIST OF TABLES

LIST OF FIGURES

LIST OF FIGURES
(Continued)

INTRODUCTION

Fatigue crack growth rate predictions based on linear elastic fracture mechanics (LEFM) have been widely and successfully used for many years. The electric utility industry is but one example of an industry that is relying increasingly on LEFM for run, retire, repair decisions on major components. Damage tolerance analyses have been developed by the Air Force and used in many Special Projects Offices to allow rational decisions to be made concerning inspectability and continued use of cracked components until the cracks are of near critical size. The success of LEFM in these and other applications has led to research to develop the technology to track the growth of defects in engine components. This work is part of the effort to ensure the integrity of expensive engine components undertaken by the Air Force Wright Aeronautical Laboratories.

There are sound reasons for not blindly applying damage tolerance analyses to engine components. A growing body of experimental observations support the conclusions that LEFM does not always consolidate crack-growth-rate data. Frost, Pook, and Denton [1], Ohuchida, Nishioka, and Usami [2], and Kitigawa and Takahaski [3] were among the first researchers to present data that did not conform to LEFM predictions at low- and near-threshold crack-growth rate conditions. Similar results have since been observed in many materials; the difficulties are particularly acute for physically short cracks. Data not consolidated by LEFM often indicate higher growth rates than expected thus implying some degree of nonconservatism in certain applications.

The Air Force (AFWAL/MLLN) undertook a study which had two ambitious objectives: identify the parameters that cause short cracks to behave differently than long cracks and develop a predictive model for short crack growth which included the effects of the governing parameters. The first undertaking of the program was a critical literature review which addressed the question of why small cracks apparently grow at rates that cannot be predicted using LEFM-based analysis methods that are successful for long cracks. The results were published in a report titled "A Critical Review of the Short-Crack Problem in Fatigue" [4]. It was concluded there that the reported short-crack

effect arose primarily because of crack tip plasticity, transients from initiation to microcracking, and incorrect or incomplete implementation of LEFM. Because the phenomenological data did not discriminate between the possible sources, it was not clear which were significant. Descriminating experiments were needed.

This report is concerned with the resulting test program. To provide continuity and background for the experiments, a summary of the findings of the literature review follows. It was from this data, that the test plan was devised.

Summary of the Literature Review

Considerable data was found that does not correlate when growth rate is plotted against the stress intensity factor [4]. It was observed that such failures may be due to the way LEFM has been implemented rather than to some inherent deficiency in the theory. For example, K has been used for short cracks where closure is a factor, even though it is well accepted that ΔK_{eff} is needed to account for stress ratio and closure effects for long cracks. There are also examples of data for which the underlying assumptions of LEFM were violated, making LEFM inapplicable.

Numerous miocro- and macro-mechanics of the flow and cracking processes which influence crack growth rate were identified in the literature. They include multiple growth modes, combinations of modes, and the three-dimensional nature of the fracture process; the length and configuration of the crack front involving dimensions of both the specimen and the microstructure; free surface effects on slip character including effects of surface treatment and crystallographic growth; multiple cracking processes including possible environmental effects; and transient effects due to inclusions, grain boundaries, and grain-to-grain misorientation. In addition to these materials-related factors, a number of mechanics-related factors were identified. These included the influence of the plastic zone to crack length ratio on LFM, anisotropic effects, surface residual stress and local closure effects due to plane stress surface flow confined by a plane strain field, crack

bifurcation and ill-defined crack fronts, stress redistribution due to notch root yielding and to material transient deformation behavior, and macroscopic closure due to residual stresses and deformations. All of these factors interrelate and need to be considered together.

The process of going from a situation in which there is not a crack on a scale on the order of the microstructure to a situation in which a crack exists is transient. The crack tends to a steady state condition, the limit of which is the long crack condition. The mechanism of initiation (brittle to ductile) will control the length that the crack will attain before a steady state develops at its tip.

Brittle initiation tends to form a crack which grows stably from the beginning, with limited flow at the crack tip. In contrast, ductile initiation would initially tend to violate the plastic zone to crack length limitation of LEFM. Ohuchida, Nishioka, and Usami [2] have presented results for several steels in which the active plastic zones in ductile cases are as large as 0.3 mm while those for brittle cases approach 10^{-3} mm. In this respect, a brittle steady state exists soon after inclusions crack, at crack lengths as small as can be consistently resolved using even highly sophisticated measurement systems. Ductile steady state, by contrast, develops only after extensive cracking. Significantly, LEFM criteria are satisfied for the lower extreme of brittle initiation at a crack length of about 10 μm--about the lower limit of detection. In contrast, LEFM criteria are violated at the upper limit of ductile initiation for cracks nearly 3 mm long.

Micromechanics is also a factor for short cracks for which the confined plasticity requirements of LEFM are met. In this case, local closure occurs due to plane stress flow on the surface that is contained within an unyielding plane strain field. For this reason, it is expected that cracks initiate naturally, in the absence of an overshadowing notch plastic field, will show a short-crack effect. Artificially induced cracks, such as those initiating at the end of a starter notch, will demonstrate it to a much lesser degree, or not at all. In the case of ductile initiation, both small and larger cracks may initially violate the LEFM confined plasticity requirement. Regardless of the reason for the existance of the plastic zone at the

initiation site which causes this violation, the crack cannot behave as a long crack until it has grown beyond the initiation zone and has developed its own steady state field. Again, both micromechanics and metallurgical features are important considerations in regard to the transient growth process. Equally important are multiple initiation and branching. Because artificial flaws would tend to concentrate deformation and tend to cause a more brittle initiation, natural cracks are expected to show the short crack effect much more than samples with starter notches. When the plastic zone is due to notch inelastic action, not only may the contained plasticity requirement be violated, but the K solution is inappropriate unless inelastic action in the notch field is taken into account.

Based on this information, experiments were designed to try to do two things:

- Isolate conditions under which physically small cracks exhibit anomalous growth when properly analyzed via LEFM.
- Define those factors which control such growth in both smooth and notched specimens.

The study has been performed on Inconel 718 in a heat-treatment condition found in current advanced engines. Nearly all of the tests were conducted at room temperature.

The experiments led to three major conclusions. These are:

1. In the absence of elevated temperature, corner cracking, and inelastic notch fields, LEFM analysis is appropriate for small cracks in Inconel 718 under engine service conditions.
2. Inability to measure and analyze corner-initiating cracks can cause LEFM to become practically invalid for short cracks of that type.
3. Notch root plasticity can elevate crack growth rates above those predicted by LEFM.

EXPERIMENTAL DETAILS

Experimental results which isolate or emphasize four factors are useful to identify mechanics factors controlling the growth of short cracks in fine-grained Inconel 718. These factors are (1) the transient behavior from initiation to the formation of a dominant singularity, (2) three-dimensional crack geometry and stress state effects, (3) the extent of plasticity, and (4) microcrack closure. The experiments performed to develop these results are explained in the following section.

Test Plan

Initiation Transients

The existence of a planar dominant singularity has been assumed in all analyses. Experiments with natural initiation (causing the associated transient initiation to microcrack), as well as experiments with flaw-induced initiation (which tends to minimize the microcrack transient), have been performed to explore the implications of this assumption.

From a fracture mechanics viewpoint, planar cracks longer or deeper than about 10 grains may be reasonably argued to be dominant singularities. Nonplanar (bifurcated) cracks greater than 10 grains long (in view of the LEFM analysis of Suresh [5]) can be expected to have lower stress intensities for the same effective length. Earlier experimental results of Schijve [6] also indirectly indicated a reduced stress intensity in that growth rates were reduced as compared to their planar counterparts as the same K level.

Three-Dimensional Effects

Three-dimensional effects due to crack geometry were investigated by comparing the results of tests using initial flaws to start cracks and tests in which cracks were initiated "naturally". Tests with initial flaws tend to minimize 3D crack-geometry effects, whereas those with natural initiation tend

to emphasize the 3D nature of the crack in that part-through-thickness cracks develop.

Tests in plates with holes were conducted. This introduces the added complexity of a 3D-stress-state effect at the notch root, which ranges from plane stress for geometries with thickness, t, to diameter, 2r, ratios approaching zero, to plane strain for geometries where t/2r exceeds about 2. (In this study all tests of plates with holes had t/2r = 0.18.) Plane stress tends to cause corner crack initiation; plane strain tends to cause mid-thickness initiation [7]. Both lead to the just noted 3D crack-geometry effects, particularly for the case of natural initiation. Also, notch root stress biaxiality may alter the rate of crack propagation versus that for the long crack stressed uniaxially in Mode I. Results in the literature suggest this subject remains a major research area with a wide variety of effects on growth rate depending on the material [8]. Results of a recent major symposium dealing with this subject, however, suggest that the varied dependence of growth rate on biaxial stress ratio, μ, could be correlated in terms of the ratio of maximum stress, S_{mx}, to the flow stress of the material, Y. The significance of this dependence for short cracks is alluded to in Appendix A along with free surface effects, and is discussed in more detail in the references cited there. The effect of biaxiality due to corner crack geometry is examined in the section on stress intensity factor solutions in the context of our experiments, as detailed in Appendix B.

Extent of Plasticity

Prior analysis [2,9] suggested that the confined-plasticity limitation of LEFM could be removed, at least in part, through the use of strip yield models. Discussion of this effort is presented in Appendix C. Experiments which emphasize this factor were performed by varying the ratio of the crack tip plastic zone size to crack length r_p/a; also, cracks were grown in both elastic and plastic notch zones.

Crack Closure

Discriminating experiments to sort out the role of plasticity induced closure were considered as the first priority, in view of the results of the review of the literature which formed the first phase of this program.

Analysis independently performed by Newman [10] during the course of the present study indicates that microcrack closure can simulate some of the crack growth tendencies referred to as short crack effects. To date, no conclusive studies have been performed to isolate the role of microcrack closure, although clear-cut evidence of macrocrack closure exists. For this reason experiments have been performed to isolate microcrack closure effects. The wake removal concept was used, as will be discussed later.

It should be remembered that closure can occur due to causes other than plasticity. Closure due to contacting asperities on nonplanar cracks and to oxide particles on planar or nonplanar cracks may be expected to reduce the effective stress intensity according to the work of Ritchie, et al [11,12]. This lowered ΔK_{eff} would reduce the growth rate. In general, nonplanar cracks are not expected to develop differently as a function of crack length for a given stress state and level of stress intensity factor. Thus, nonplanar cracks would be expected to have the same relative effect on growth rate independent of crack length for the same local stress intensity factor range. Oxide-induced closure, however, may vary according to crack length if the rate of oxide deposition relative to ΔCTOD differs as a function of crack length. In any event, if environmental accessibility controls the rate of oxide deposition, oxide-induced closure is expected to be greatest when the crack tip is most accessible to the environment. In this case, in the absence of very high deposition rates in systems developing hard oxides, the formation of a significant oxide layer would depress rates for short cracks more so than for long cracks.* However, if deposition rates were high and hard oxides

---

* It was noted in our earlier report that short cracks have been observed to grow at rates lower than LEFM long crack data would suggest. While academically of interest, this is not a safety problem in applications of RFC and thus is not of practical signifiance in the present study.

formed, the wedging action of the oxide would increase K_{mx} and da/dN and counteract any closure effect that tends to decrease ΔK_{eff} and da/dN. In the latter case, growth rate could either increase or decrease with increasing length depending on many factors, the study of which is beyond the present effort.

Plasticity-induced closure develops as a wake of plasticity forms behind the advancing crack. This crack closure decreases the range of the effective stress intensity factor, thus decreasing the crack-growth rate. Therefore, the role of closure should be evident by an increase in growth rate as wake is removed. This is illustrated schematically in Figure 1. This figure shows the results of a hypothetical test run with loading such that the stress intensity factor range ΔK is kept constant. First, a crack is nucleated from an electrical-discharge-machined (EDM) starter notch. As the microcrack grows to a length such that a steady-state wake of plasticity forms, a steady-state amount of closure also develops, and the crack growth rate takes on a constant value lower than the initial "short crack" rate. This constant rate is the long crack LEFM behavior. The wake is then removed by the EDM process, but the crack tip is left undisturbed. The crack tip now is affected by a minimum amount of wake. Although the crack has grown during the test, the situation is essentially the same as just after crack nucleation. The resumption of fatigue loading causes crack growth at an accelerated rate until a steady-state wake (and thus steady-state closure and effective ΔK) is developed again.

What is the upper bound on the increment of crack growth after wake removal for which the transient behavior can be seen? It is the crack length when the microcrack first grows at the long-crack rate. Unfortunately, data documenting the growth of short cracks in Inconel 718 are sparse. In the absence of such data, estimates of the length of crack below which a short crack effect can be expected follow from the threshold and endurance characteristics of the material [2,3,13,14]. But published data for Inconel 718 documenting threshold crack growth behavior and fatigue endurance behavior for the fine-grained microstructure of interest in this study are also sparse. In the absence of such results, estimates of these variables can

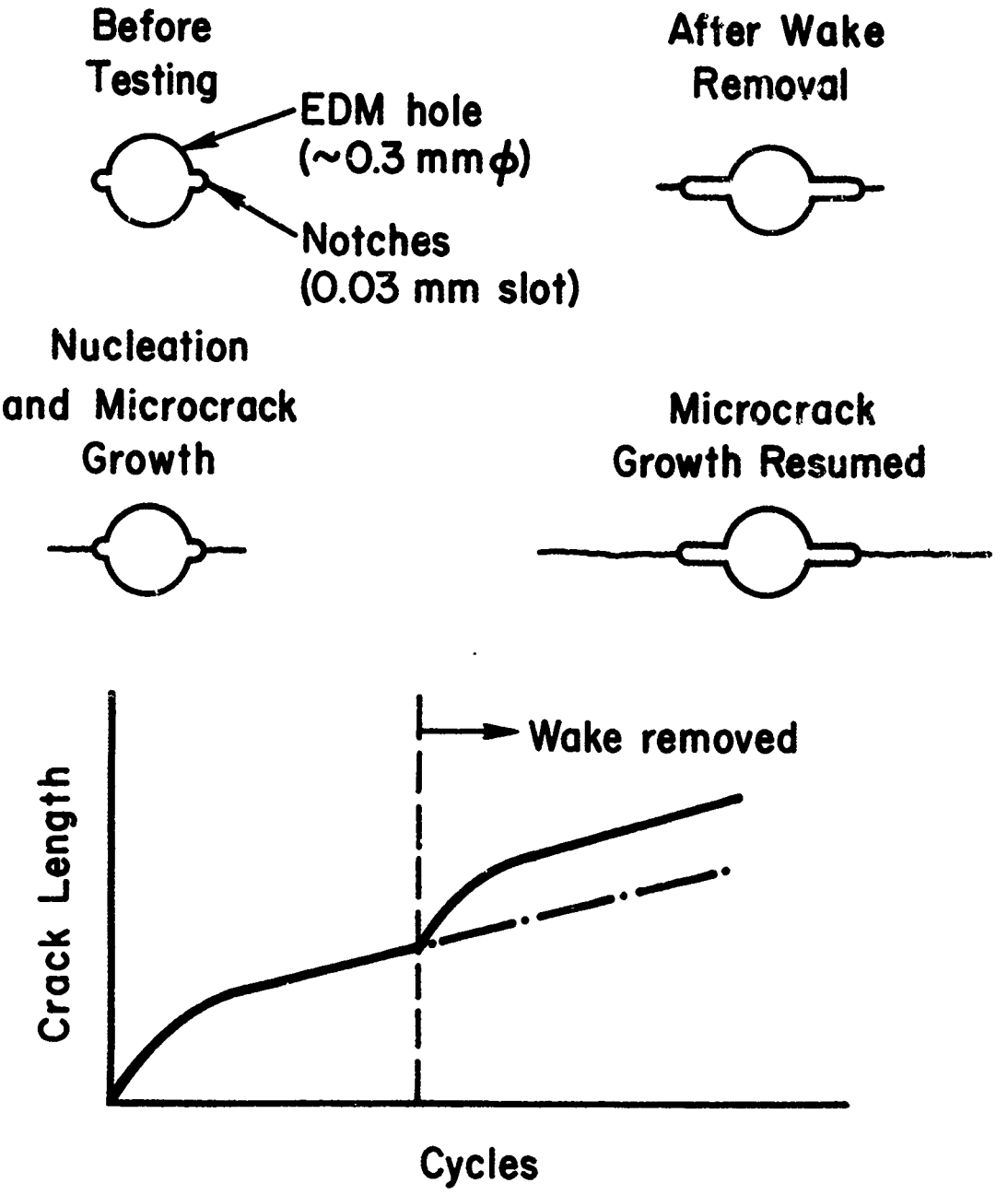

FIGURE 1. SCHEMATIC DESCRIBING A DISCRIMINATING TEST OF CRACK CLOSURE EFFECTS BASED ON THE WAKE REMOVAL CONCEPT

be made from very limited unpublished data made available by General Electric Co., Aircraft Engine Group, late in 1982. These estimates are plotted in Figure 2, reproduced from Reference 4. They indicate that aberrant growth trends based on LEFM will develop only at very small crack lengths. Depending on grain size, this figure indicates the short crack effect will be confined to semicrack lengths less than 0.25-0.5 mm at 540 C. Therefore wake removal experiments with the material used in this study require measurement of very short crack lengths.

Other factors also suggest that difficulties may be met in successfully determining the role of closure using the wake removal concept. First, it should be noted that, prior to wake removal, the closure forces are distributed over some crack face area. Removal of that wake may simply decrease this area thus increasing the closure stress, unless sufficient material is removed to cause compression yield over the crack region remaining in contact. Secondly and alternatively, if closure is confined to the near-tip region (say 25 μm), then wake removal becomes practically impossible because short cracks are seldom straight within 25 μm over their entire front. Thirdly, the scale of plasticity also has practical implications. The larger the plastic zone, the larger the region of closure. In order to keep the test conditions similar to the service conditions of interest (i.e., typical engine conditions), only stress levels representative of service were used in testing.

Two factors can be expected to help in conducting the wake removal experiments. The behavior of short cracks related to closure may be accentuated by the dominance of plane stress behavior (e.g., [10,15]). To this end, the study focused on thin sheet behavior. (However, difficulties are to be anticipated regarding the rotation of Mode I cracks from preflaws to stable Mode II cracks, as is often observed in thin sheets, e.g., [15-17].) Closure effects are also expected to be accentuated at low values of stress ratio, R. Given the range of behavior of concern in engines, the scope of the study embraced $-1 \leq R \leq 0.1$.

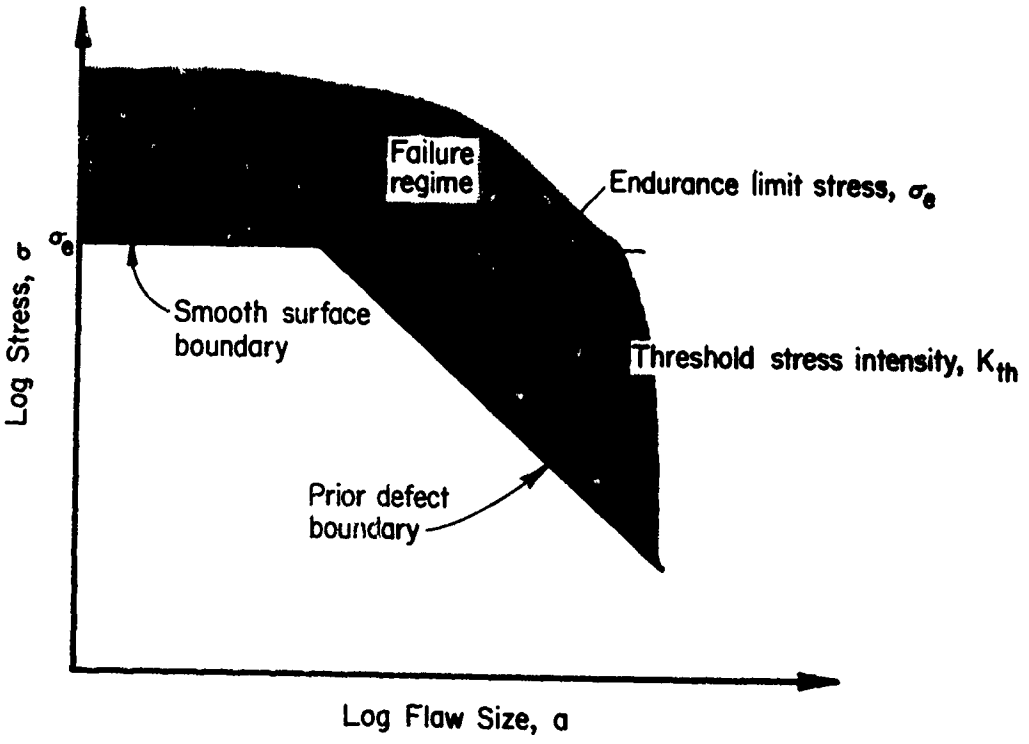

a. schematic, after Staehle [12]

FIGURE 2. BEHAVIOR OF STRESS AMPLITUDE AS A FUNCTION OF SEMICRACK SIZE

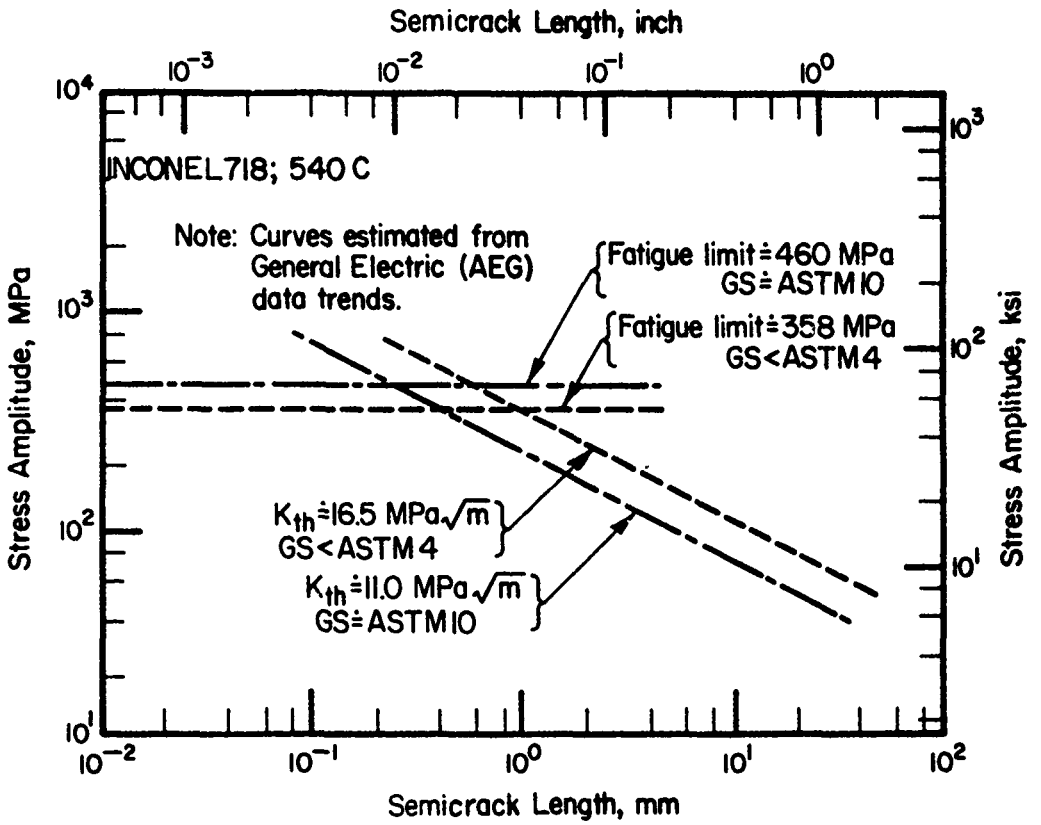

b. results for Inconel 718 at 540 C, based on GE/AEG data

FIGURE 2. (Concluded)

Test Plan Summary

The test plan and parameters of interest are set forth in Table 1. Thirty-three specimens have been employed to characterize the microcrack growth rate process embracing the effects of closure, initiation transients, notch stress fields, 3D crack geometry, stress level and R, net wake, and temperature. Cross correlation to isolate or emphasize these effects follows the plan laid out in Table 2 and includes useful results from completely successful tests on 18 specimens.

Crack Tracking--Techniques and Practical Implications

Obtaining crack growth behavior for cracks $\sim$0.5 mm long (deep) requires tracking procedures other than typically used methods. ASTM standards require a minimum increment of crack growth between measurements of 0.25 mm or 10 times the crack length measurement precision, whichever is greater. The precision of the measurement techinque is defined as the standard deviation on the mean value of crack length determined for a set of replicate measurements. Obviously, the requirement of 0.25 mm growth cannot be satisfied. Therefore, the ASTM standard cannot be applied to the study of cracks of lengths of interest to the present study. But guidance can be taken from the requirement that the minimum increment be 10 times the standard deviation, $\bar{\sigma}$. Insight as to the required tracking scheme also follows from the desire to obtain multiple readings during the anticipated interval of the short crack behavior. Adopting a minimum increment of Δa = 50 μm meets this need and in turn requires a standard deviation (i.e., measurement precision) of 5 μm to meet the alternative ASTM requirement. (The effect of using $1\bar{\sigma}$ or $2\bar{\sigma}$ versus $10\bar{\sigma}$ on the analysis of data for short cracks is examined later in this report.)

Study of available tracking schemes such as traveling microscope and KRAK gages indicates these may not provide the required precision. But more importantly--most provide only a voltage analog rather than a direct image. Data generated using a photographic technique developed in earlier studies

TABLE 1. SUMMARY OF TEST PARAMETERS
(Center Cracked Panels)

Specimen	Temp. C	Freq. (Hz)	R	S_{mx} (MPa)	$\frac{S_{mx}(a)}{\gamma}$	r_p/a(b)	Crack Length, mm Before Wake Removal Side 1	Side 2	Average Net Wake, mm	Comments
CC-1	20	1	0.01	676	0.56	0.21				entire crack cut out in attempt to remove wake
CC-2	20	1	0.01	676	0.56	0.21				film record of poor quality
CC-5	20	1	0.1	630	0.56	0.19				film record of poor quality
CC-8	20	1	0.1	690	0.57	0.22				film record of poor quality
CC-7	20	1	0.01	690	0.57	0.22				non-cylindrical hole; corner cracks
CC-4	20	5	0.01	690	0.57	0.22				crack too long after precracking
CC-6	20	5	0.01	690	0.57	0.22				crack too long after precracking
CC-9	20	5	0.01	690	0.57	0.22	0.434	0.465	0.076	
CC-10	20	5	0.01	820	0.68	0.31	0.381	0.363	0.041	
CC-11	20	5	0.01	740	0.61	0.26	0.389	0.523	0.102	
CC-12	20	5	0.01	820	0.68	0.31	0.417	0.389	0.117	
CC-13	20	5	0.01	820	0.68	0.31	0.452	0.478	0.041	
CC-14	20	10	0.01	580	0.48	0.16	0.411	0.376	0.071	
CC-15	20	2	-1.0	522	0.43	0.13	0.579	0.566	0.061	
CC-17	643	5	0.01	820	0.84	0.23	2.957	2.27	--	gross section yielding; test abandoned
CC-3	643	5	0.01	662	0.55	0.32	0.744	0.729	0.010	
CC-18	20	5	-1.0	524	0.43	0.13	0.457	0.478	0.058	
CC-19	20	5	-0.6	814	0.67	0.31	0.569	0.897	0.213	

(a) Flow stress γ = (ultimate stress + yield stress)/2
(b) Plane stress value calculated at wake removal.

TABLE 1. SUMMARY OF TEST PARAMETERS (Center Notched Panels)

Specimen	Temp. C	Freq. (Hz)	R	S_{mx} (MPa)	$\frac{S_{mx}}{Y}$(1)	r_p/a(2)	x_p(c) (mm)	Crack Length c Before Wake Removal (mm) / Net Wake after Wire Cutting (mm) Side 1 Crack 1	Side 1 Crack 2	Side 2 Crack 1	Side 2 Crack 2	Comments
2024 T351 Al	20	0.5	0.01	186	0.44	1.41	2.0					-validation test for strip yield model.
CH-2	20	1.0	-1.0	293	0.24	0.31	0.0					-benchmark: [illegible] crack efect [illegible]
CH-10	20	1/.5	-1.0	483	0.40	0.85	0.46					-film record lost in processing
CH-14	20	0.5	-1.0	483	0.40	0.85	0.46					-film record lost in processing
CH-9	20	0.5	-1.0	483	0.40	0.85	0.46					-film record lost in processing
CH-15	20	2/.5	-1.0	483	0.40	0.85	0.46					-film record lost in processing
CH-8	643	0.33	0.01	362	0.38	0.73	0.20					-film record lost in processing
CH-12	643	0.33	0.01	362	0.38	0.73	0.20					-film record lost in processing
CH-1	20	1.0	-1.0	483	0.40	0.85	0.46	1.039 0.102	0.0 0.0	1.971 1.041	0.0 0.0	corner cracking for crack 2
CH-16	20	1.0	-1.0	483	0.40	0.85	0.46	0.032 *	0.411 0.142	0.0 0.0	0.0 0.0	*wire cut notch longer than surface crack
CH-4	20	1.0	-1.0	483	0.40	0.85	0.46	0.160 *	0.871 *	0.231 0.094	1.171 0.356	*wire cut notch longer than surface crack
CH-5	20	1.0	-1.0	483	0.40	0.85	0.46					accidentially overstressed-test not completed
CH-3	20	1.0	-1.0	483	0.40	0.85	0.46	0.373 0.058	0.104 0.069	0.391 0.081	0.074 0.036	
CH-20	20	2.0	-1.0	310	0.26	0.35	0.0					no wake removal
CH-6	20	4.0	-1.0	241	0.2	0.21	0.0					no wake removal

(1) Flow stress, Y = (yield stress + ultimate stress)/2
(2) For $c \leq .89$ mm
(3) Notch plastic zone size estimated by determining distance at which the local stress based on a width corrected elastic stress distribution equals yield stress.

TABLE 2. COMPARISONS USED TO ISOLATE OR EMPHASIZE SPECIFIC PARAMETERS

Parameter	Specimens to be Compared
Unnotched Specimens (intended initial $K_{max} \doteq 193$ MPa$\sqrt{m}$)	
• net wake	CC12 (long) vs. CC10 (short)
• stress level	CC13 (high) vs. CC11 (mod.) vs. CC9 (mod.-low) vs. CC14 (low)
• stress ratio	CC19 (R=-.6) vs. CC12 (R=.01) vs. CC15, CC18 (R=-1)
• temperature	CC3 (643 C) vs. CC12 (20 C)
Notched Specimens	
• short cracks	CH2, preliminary test - does the material show a short crack effect
• initiation transients, corner vs. plane fronted cracking	CH1, CH16 (natural, corner) vs. CH3, CH4 (preflawed)
• stress level	CH3, CH4 (high) vs. CH20 (mod.) vs. CH6 (low)
• notch field	CH3, CH4, CH20, CH6 (notched) vs. CC15, CC18 (unnotched)
• temperature	CH3 (643 C) vs. CH20 (20 C)

[18] indicated that precisions on the order of that required could be achieved. And, a photographic procedure would develop a permanent record of the crack (at least as it appears on the surface). Refinement of the photographic technique via increased magnification and changes in triggering the shutter produced precisions on the order of 5 μm as summarized in Appendix D. Because the permanent record and the precision of the photographic technique suited the needs of this study, it was adopted with adaptations of the scheme used in Reference 18, as follows.

As is shown in Figure 3, the photographic method of crack tracking used standard 35 mm single lens reflex (SLR) cameras to monitor surface crack tips on both faces of the specimen. To maximize the region of the specimen inspected without too much loss of detail, the film record was made at about five times magnification at the film plane. Subsequent interpretation was performed at an additional 16 times magnification or more, a factor of two greater than used previously. The triggering was also changed. The prior study used peak load to trigger the shutter and flash. However, it was found that the camera's internal shutter triggering systems were not uniform enough to consistently catch the crack at maximum load when it is most open and the crack tip could most easily be located. This introduced scatter into the measurements. For this reason, shutters were triggered early in the rising portion of selected cycles. The film record was made by triggering flash units, mounted to produce incident (glare) lighting across the crack, at the peak load in that cycle. Counter devices were developed to trigger film advance, shutter, and flash at preset intervals.

The cameras were equipped with 250-exposure film backs. This was done to minimize changing rolls of film. Such long rolls of film required special processing, including drying in a warm forced air dryer built specially for these long rolls.

Although this crack tracking technique was desirable for the present study, the tremendous amount of film generated during testing was formidable. The main objective of the experiments involving wake removal was to record the crack growth just after initiation and again just before and after wake removal. Because the number of cycles to crack initiation could only be

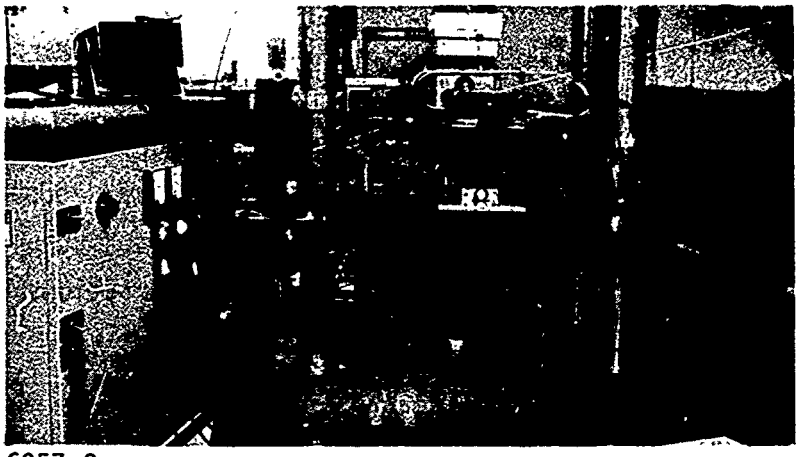

6057-2

a. overview

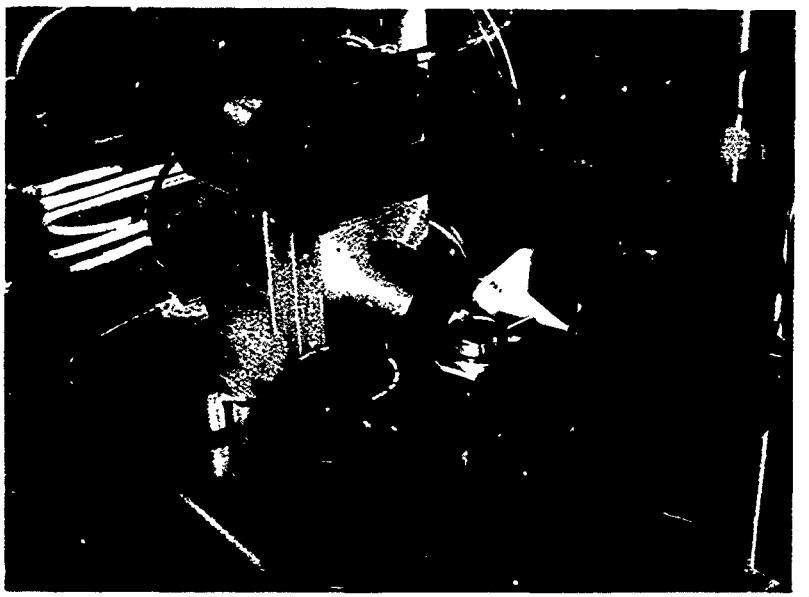

6049-2

b. closeup

FIGURE 3. THE EXPERIMENTAL SETUP FOR CRACK TRACKING USING THE PHOTOGRAPHIC TECHNIQUE (AS USED AT 643 C)

estimated, much film was expended before it occurred. The period of crack growth over which elevated growth rates could be seen was expected to be small. This necessitated allowing a small number of cycles between photographs. Generally 1000-2000 exposures were taken per test. Fortunately, much of this film did not need to be reduced. It was only used to verify that a crack had not initiated.

At the beginning and end of each roll of film, pictures were taken of labels giving the specimen number, which camera, and the current number of cycles. This was essential in keeping track of all the film through processing and data reduction. A picture was also taken of a scale object. Because resolution is lost when the film is projected during crack measuring, a rule with scribed lines did not work. The end of a narrow strip of thin plastic was eventually found to work well. The distance between the corners was measured carefully using a microscope and micrometer-driven specimen table.

The processing of so much film would be prohibitive if prints were made of each frame. Instead, the negatives were projected onto a large (4' x 5') digitizing table using a standard film strip projector. The positions of the crack tips were entered by means of a cursor equipped with crosshairs; cartesian coordinates of the points were stored on magnetic tape. The scales of the reference axes were entered using measurements on the scale at the ends of each roll. Points giving crack tip positions were paired with their respective cycle counts by entering them on the magnetic tape when digitizing each point. A simple computer program translated the digitized data into crack lengths.

Projection greatly increased the magnification, but it also decreased the picture resolution somewhat. Small errors in focusing at 5X magnification were multiplied in the process. Thus, careful camera setup was essential.

Various flash unit arrangements were tried. It was found that the positioning of the flash units was very important. The most effective setup used one unit on each side of the specimen as shown in Figure 3.

Appendix D presents a study of the accuracy and precision of this measurement and data analysis procedure.

Material and Specimens

The Inconel 718 material used in this investigation was 0.093 inch thick sheet with the following chemistry (in weight percent):

C	Mn	P	S	Si	Cr	Cb/Ta	Cu
0.04	0.07	0.012	0.006	0.13	18.42	5.14	0.03
Mo	Fe	Co	Ti	Al	B	Ni	
3.07	18.14	0.3	1.06	0.48	0.004	bal.	

The as-received material was cut into specimen blanks and then heat treated in batches of 10 using a duplex heat treatment including:

Anneal in vacuum 954 C/Air Quench
Heat 704 C/8 hours
to 621 C/8 hours
then air cool.

The heat-treated material exhibited a fine grain size (ASTM 10 to 10.6), as evident in Figure 4, a microstructure typical of this alloy for the indicated heat treatment. Metallographic study did not disclose any significant alloy depletion or any other undesirable surface condition as a result of any of these treatments. Grains were uniform, and there were no significant microstructural features on the order of the upper bound crack size associated with the short crack effect expected in view of Figure 2.

The grain size of this material is about 10 μm. Thus, on the average, increments of crack advance measured on the surface separated by less than 5 μm will represent growth steps within surface grains. However, the crack tip observed on the surface is tied to a subsurface front that on the average crosses about 225 grains. Therefore, while on the surface the crack tip may be tied up by grain and subgrain features, this tip will be dragged along by the subsurface crack front.

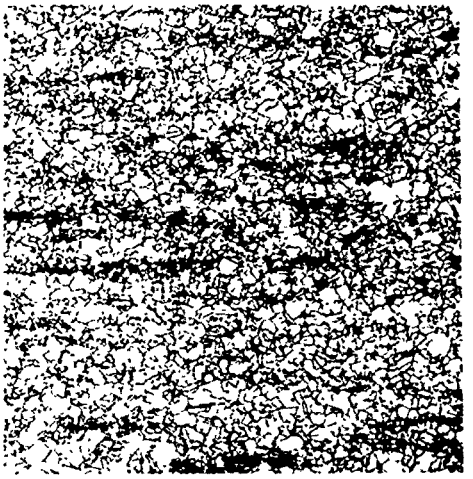

2L976 100X

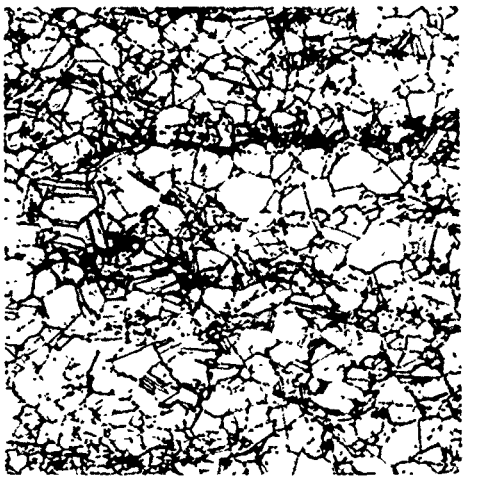

2L978 250X

(Etch: 97 HCl, 3 HNO_3 with ½ gm CuCl)

2L980 750X

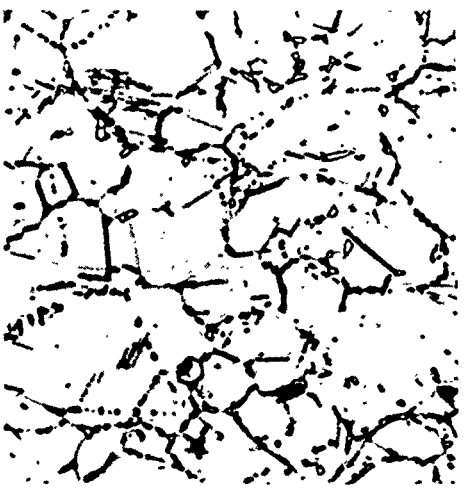

2L981 1000X

(Etch: 42 Glycol, 29 Hcl, 29 HNO_3)

FIGURE 4. PHOTOMICROGRAPHS OF MICROSTRUCTURE TYPICAL OF THE MATERIAL INVESTIGATED

The material used in this study had room temperature mechanical properties as follows:

Ultimate tensile stress 1378.7 MPa
0.2 percent offset yield 1027.3 MPa
21.4 percent elongation, and
a modulus of 194.6 GPa.

These properties were obtained from a single 5.1-cm-gage-length sheet, tensile coupon tested at 20 C at a displacement rate of 0.063 mm sec^{-1}. The average hardness was measured to be about R_C42.

Two types of specimens have been used in this investigation. In both, the long axis of the specimen was aligned with the rolling direction of the sheet. For the study of microcrack closure, a center-crack panel (CCP) was used because (1) the stress field is symmetric and the K solution simple, and (2) both active surface crack tips on one side of the sample could be tracked with a single camera. Local access to numerically controlled EDM machining facilities meant suitable preflaws could be developed within the range of sizes anticipated to produce the short crack effect (see Figure 1). The specific CCP geometry used is shown in Figure 5(a). The remainder of the study has made use of the center-hole-notched panel (CNP) shown in Figure 5(b). A notched geometry was selected to achieve the program's plan to examine microcrack growth through notch fields. A center circular notch is preferred over other notch configurations because holes are commonly found in engine components. It is also preferred because a center notch facilitates tracking four surface cracks through the use of dioptric lenses which cut out the center of the camera's field of view to bring diametrically opposite cracks together; then they could be photographed at one time by the same camera.

Apparatus and Procedure

All tests were performed in a commercially available servo-controlled test system under axial load control using a sinusoidal forcing

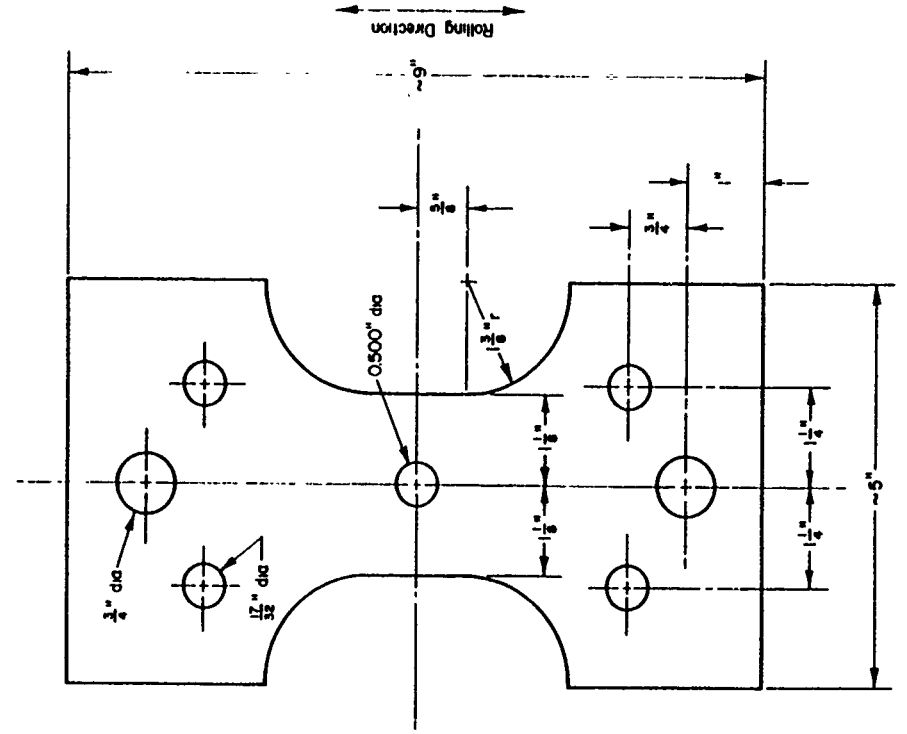

(b) CNP sample

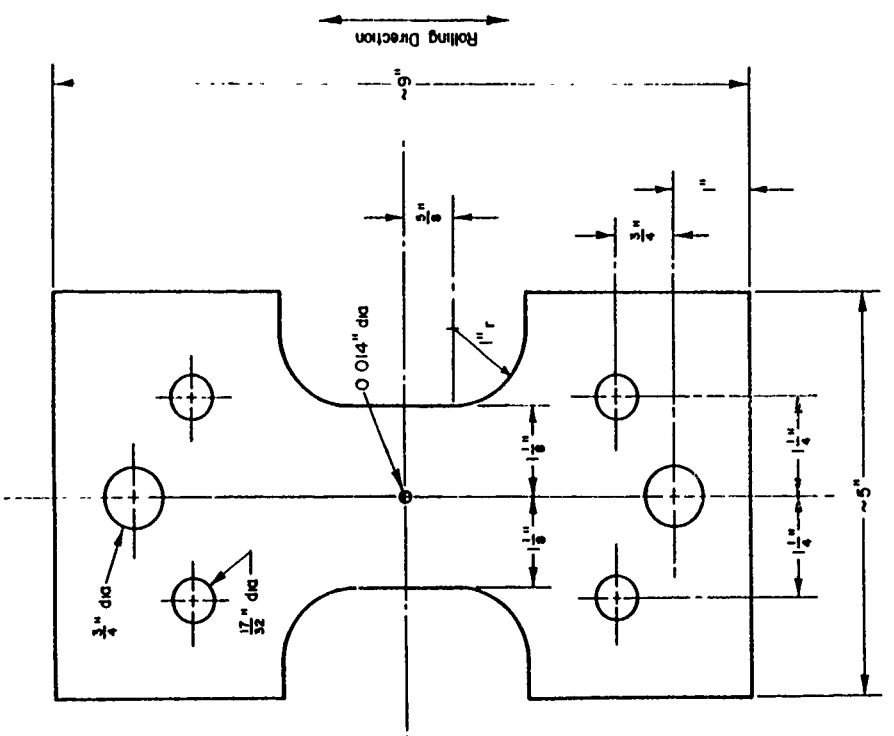

(a) CCP sample

FIGURE 5. DETAILS OF THE CCP AND THE CNP SAMPLES USED

function. The load was measured via a load cell mounted in series with the specimen. The load cell was calibrated prior to the testing program to within ±1 percent accuracy.

The camera system used was built using commercially available optics and flash units, adapted to present focal length and magnification requirements. (During the program, several unusual failures occurred in the photographic equipment because they were rapidly subjected to several lifetimes of service.) Shutter and flash triggering electronics were designed and built to match requirements of this and other similar studies. Cameras were mounted on X-Y slide translation mechanisms attached to the test frame to permit coarse focus and to center the camera with respect to the line of crack extension assuming symmetric growth.

Setup of each experiment involved the usual specimen installation and setting of the command function. Prior to testing, the anticipated area of crack advance was polished on each specimen with successively finer grades of paper and polishing compound, in some cases down to 0.5 μ diamond paste. (While this developed a near mirror image, the roughness of the surface and the presence of localized microstructural perturbations left randomly distributed dark spots on the otherwise polished surface.) Cycle interval and initial delay for the cameras were then programmed and the test initiated. For tests involving wake removal, crack position was monitored and growth was permitted until a preset increment of crack advance occurred. Judging the time to stop the test was often difficult. The surface crack tips were often at varying lengths. Thereafter specimens were removed and the surface crack lengths were measured at about 35X magnification using an optical microscope and a micrometer-driven translating specimen table. Decisions as to the amount of wake removal were then made based on the nature of the cracks and purpose of the test. Wake was removed using a numerically controlled wire cutting machine equipped with 50 μm wire. Specimens were then reinstalled in the loading frame and testing resumed. Experiments not involving wake removal followed this same procedure, except that the specimen was not removed for wake removal prior to separation.

Numerically controlled electrical discharge wire cutting was the key to using the wake removal concept. It was found that conventional electrical discharge machining was not sufficiently controllable to cut out a preexisting crack while leaving the tips untouched. Generally, the wire cutting process could be controlled as closely as $\pm$ 25-50 μm during wake removal. This is remarkable, given that the machinist had to relocate the starter notch and then remove a crack he could not see. Still, some risk was involved in wirecutting each specimen. The desired results were not always obtained. Perhaps the main complicating factors were the irregularities of the crack front, especially when the crack twisted through the thickness of the plate, and relating the crack measurements to a reference location on the specimen. A reference hole was EDMed near the grip area of each specimen. Using this, the orientation of the specimen could be determined very accurately.

DATA REDUCTION

Nomenclature

The raw data generated in this study consist of surface crack length and the corresponding number of cycles, N, for a given crack†. For each specimen containing preflaws, as many as four crack tips may be active. However, for natural initiation, multiple cracks have been found to be active at a site anticipated to generate one crack. In these cases, many more than four crack tips could be active*. For the sake of crack identification, each crack is labeled as follows: specimen number, specimen face, crack location, as detailed in Figure 6. CCP specimens are prefixed with CC while the CNP specimens are prefixed with CH. As an example, consider the crack identified as CH6, crack 1,2. The specimen number is CH6. The crack is located at the left-hand notch root, designated as 2, with respect to the front face, designated 1. Discussion of this crack in comparison to others in CH6 would refer to crack 1,2.

Editing Procedure**

Several factors made editing of the raw crack growth data necessary. The automatic measurement system used did not allow decisions to be made about the admissibility of each reading as the test was in progress. Therefore, such decisions had to be made after the complete crack length versus cycles record was produced. "Admissible" in this study means meeting the criterion

---

† Raw data are tabulated in Appendix E.

* In all but one case in which multiple initiations were observed, the crack growth data reported here is for the crack which eventually grew until specimen separation. Data for one crack which did not grow to cause failure is reported for specimen CH6.

** Comments here apply to surface crack length measurements made for both CCP and CNP samples, although the nomenclature relates specifically to the CNP geometry.

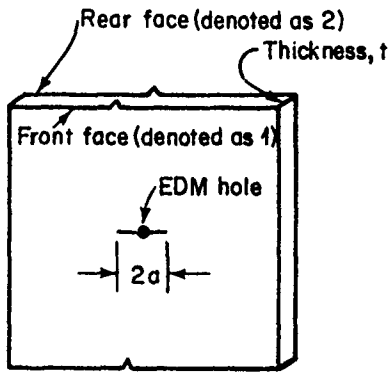

Crack 1 is on the front face
Crack 2 is on the rear face
All cracks symmetric, to within a few percent

(a) CCP sample, denoted CC

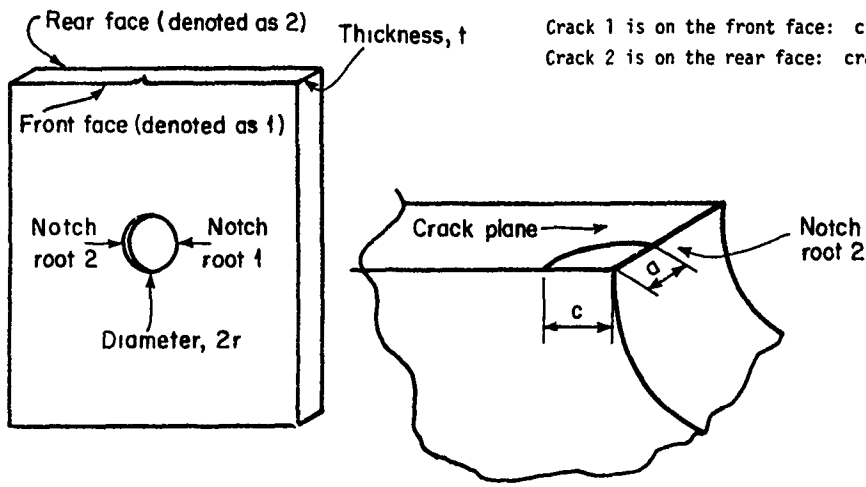

Crack 1 is on the front face: crack 1,2 left notch; crack 1,1 right notch
Crack 2 is on the rear face: crack 2,2 left notch; crack 2,1 right notch

(b) CNP sample, denoted CH

FIGURE 6. ILLUSTRATION OF SPECIMEN NUMBERING SCHEME AND CRACK NOMENCLATURE

explained below. The purpose of this criterion is to ensure that the increment in crack extension between successive readings was greater than the precision of the measurement system used--enough so that unreasonable scatter would not present a problem. As described below, a criterion based on a multiple of the standard deviation in repeat measurements, $\bar{\sigma}$, was chosen. As mentioned in a previous section, the ASTM standard requires a minimum crack growth increment of 0.25 mm or 10 $\bar{\sigma}$, whichever is larger. Guidance was taken from the second requirement. Still, because the editing criterion might have an effect on the data trends, a study was made on its effect.

To establish a reasonable value of Δc between successive readings, results from several specimens were edited using $\Delta c = 1\ \bar{\sigma}$, $2\ \bar{\sigma}$, and $10\ \bar{\sigma}$. Very little difference was observed in the resulting data trends for unedited data and the results for edits using $\Delta c = 1\ \bar{\sigma}$, $2\ \bar{\sigma}$. But, in cases where data trends showed changing slopes on the c-N plots for small values of c, editing using $\Delta c = 10\ \bar{\sigma}$ significantly altered these trends. This is, of course, to be expected because such large values of Δc effectively skip the region of the short crack effect. Given the results of this survey, $\Delta c = 2\ \bar{\sigma}$ has been chosen as the standard editing increment. In all cases, editing began after the first data point. Comparison of different choices for Δc between readings is given in the next section as we consider calculation of crack growth rates.

Evaluation of dc/dN**

It remains to decide upon analysis procedures to translate raw c-N data into a format that admits comparison of data for long and short cracks and other stress levels and specimen geometries. To this end, dc/dN must be calculated as a function of the stress intensity factor, K.

Calculating the crack growth rate dc/dN is complicated by the nature of the short crack problem. Because dc/dN may vary significantly for only small changes in N, values of dc/dN for prior or successive cycles may bias the computed "average" value found in smoothing procedures. On the other

---

**Ibid.

hand, simple slope calculations may lead to excessive scatter. With these considerations in mind, dc/dN has been calculated for a range of results using unedited data and data edited using $\Delta c = 1\ \bar{\sigma}$ and $10\ \bar{\sigma}$.

Results of one comparative study are presented in Figure 7, for the case of a plate with a central hole and plastic behavior at the notch root. Note from Figure 7(a) that simple slope analysis (SSA) for unedited data and data edited at $\Delta c = 1\ \bar{\sigma}$ produce comparable trends showing a large amount of scatter. The only difference between results edited at $\Delta c = 1\ \bar{\sigma}$ and the unedited data is a reduction in scatter for smaller lengths. However, if $\Delta c = 10\ \bar{\sigma}$ is used, the editing eliminated most of the detail for short crack lengths. Unedited results for a three-point-divided difference analysis (3PDDA)* show essentially the same trend as observed for the corresponding simple slope calculation of dc/dN. Using 3PDDA, results for $\Delta c = 1\ \bar{\sigma}$ show a decreasing then increasing trend--i.e., an apparent "short crack effect". But when edited at $\Delta c = 10\ \bar{\sigma}$, the initial slightly decreasing trend for SSA is now moderated to an increasing tendency by 3PDDA, as shown in Figure 7(b). When dc/dN is calculated using a seven-point incremental polynomial analysis (7PIPA)†, the unedited data and data edited at $\Delta c = 1\ \bar{\sigma}$ show an increasing, then decreasing, then increasing tendency, as shown in Figure 7(c). With still further smoothing of the data by editing at $\Delta c = 10\ \bar{\sigma}$, this aberrant growth rate trend disappears.

The example trends presented in Figure 7 and other similar results show that the growth rate calculation procedure can accentuate or camouflage possible short crack effects. Experience with this analysis and the analyses of other short crack data suggests that SSA introduces the least analysis bias but is prone to high scatter. On the other hand, 7PIPA tends to reduce

---

* The three-point-divided difference is a weighted average of crack growth rates:

$$\left(\frac{dc}{dN_i}\right) = \left(\frac{c_i - c_{i-1}}{N_i - N_{i-1}}\right) + \left(\frac{N_i - N_{i-1}}{N_{i+1} - N_{i-1}}\right)\left[\left(\frac{c_{i+1} - c_i}{N_{i+1} - N_i}\right) - \left(\frac{c_i - c_{i-1}}{N_i - N_{i-1}}\right)\right] .$$

†This analysis is explained in ASTM Standard E647.

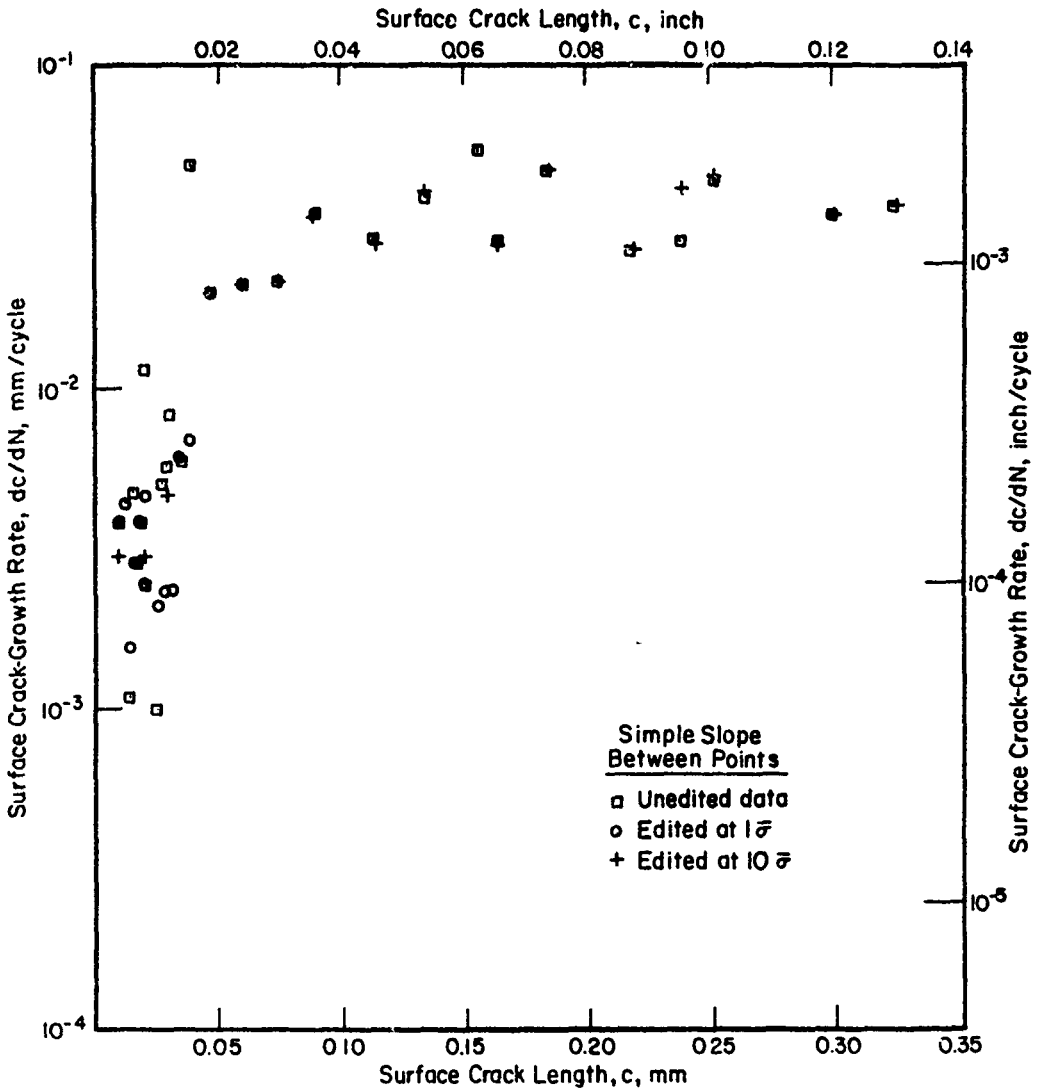

a. simple slope analysis

FIGURE 7. COMPARISON OF CRACK-GROWTH RATE CALCULATION PROCEDURES WITH VARIOUS LEVELS OF EDITING

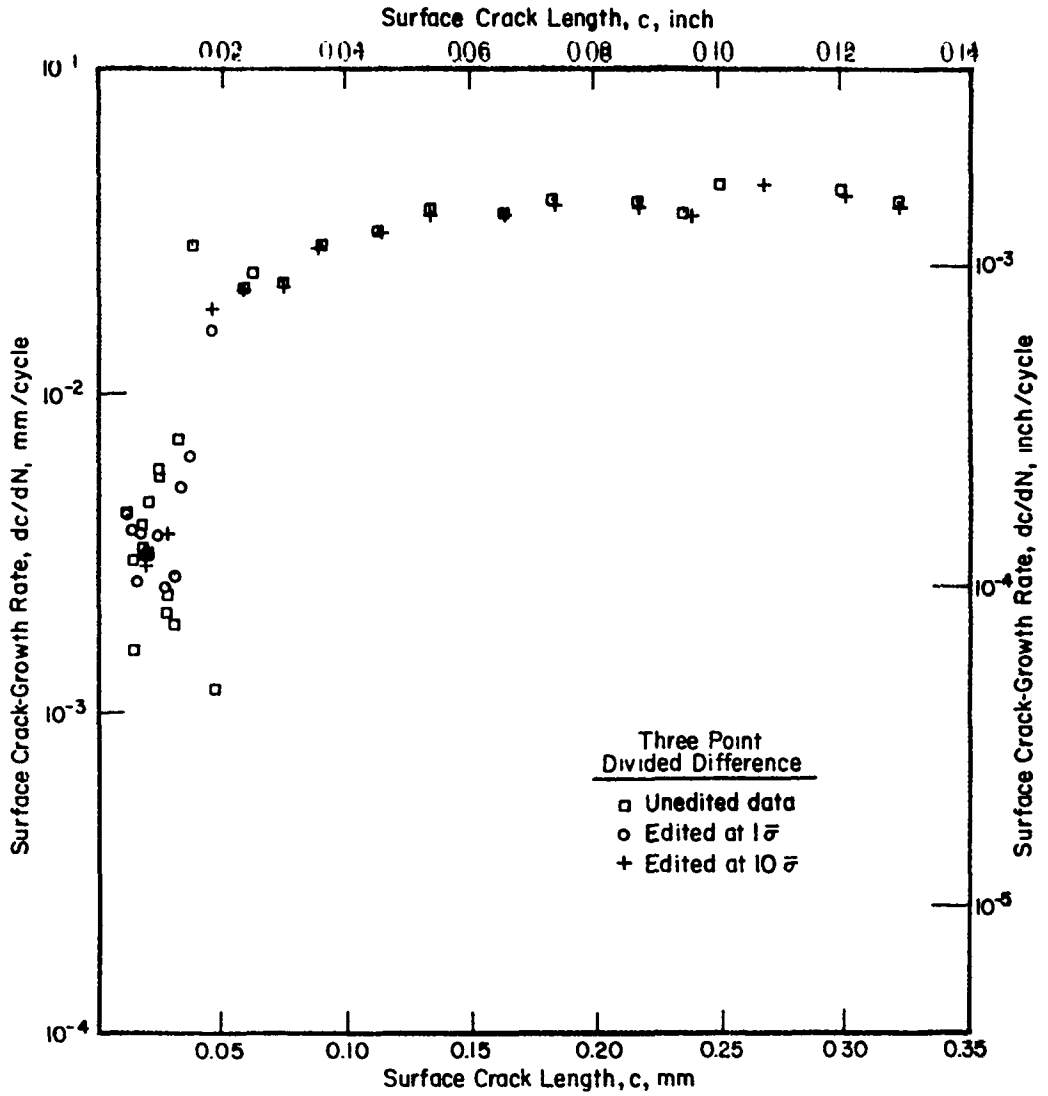

b. three-point-divided difference analysis

FIGURE 7. (Continued)

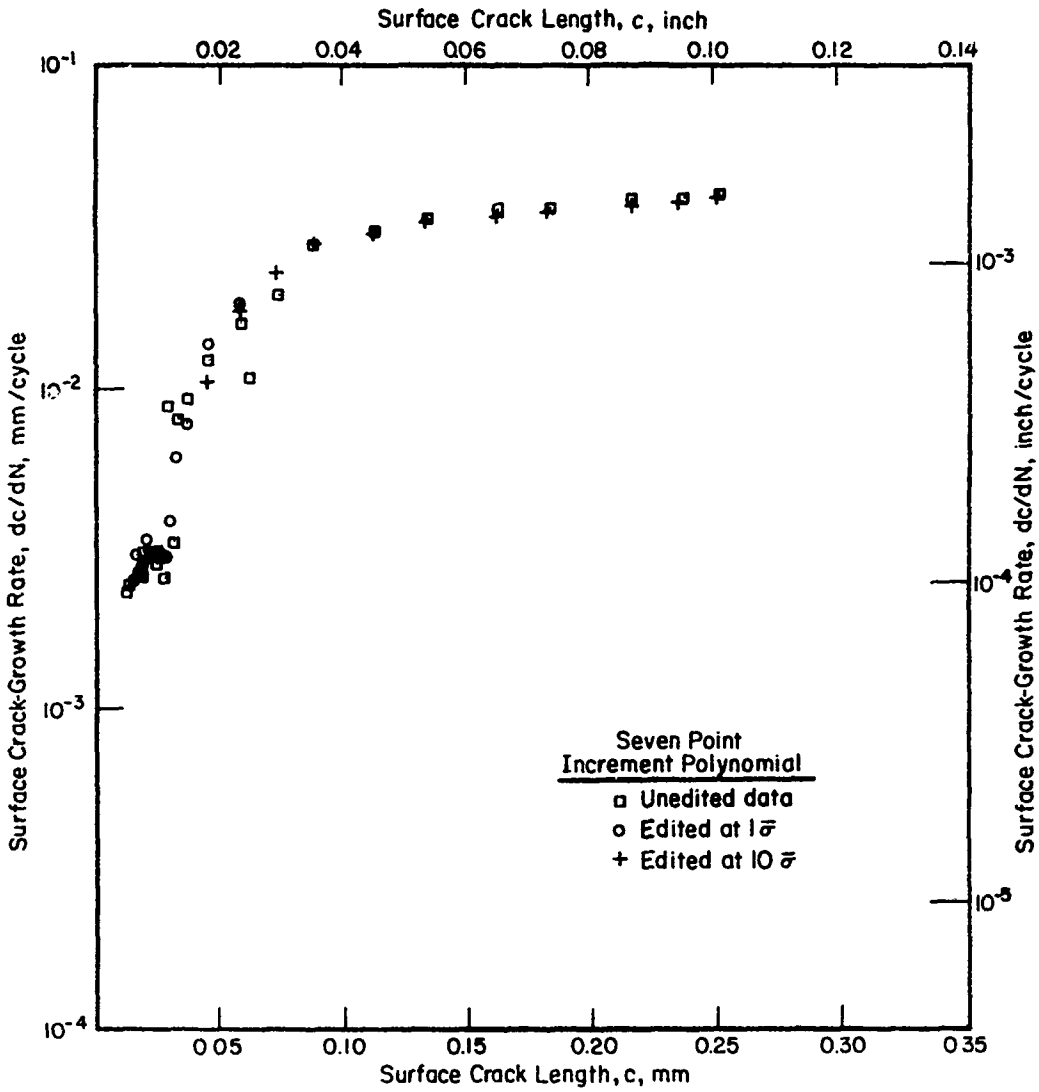

c. seven-point incremental polynomial

FIGURE 7. (Concluded)

SSA scatter but in so doing may smooth out what are real short crack effects. The 3PDDA lies between the extremes of SSA and 7PIPA and suffers (to a lesser extent) the same drawbacks of these extremes. But it provides a middle ground--more scatter (less smoothing) than 7PIPA (vice versa for SSA)--and thus seems best suited for present purposes. For this reason, the 3PDDA is used to calculate dc/dN throughout the remainder of this report, except for the long crack reference data, for which the 7PIPA was used.

Stress Intensity Factor Solutions

Consider now measures of the driving force for cracking. Portions of this study have addressed analyses of the crack driving force when the crack tip plastic zone is large compared to the crack length. As alluded to in Appendix C and discussed in detail in References 9 and 19, this situation can be dealt with using ΔCTOD calculated via pseudoplastic strip yield models (e.g., [20]) or elastic-plastic numerical analysis. For other situations where the plasticity is confined, LEFM is appropriate. However, the finite size of test specimens and the development of local biaxial stress states and corner cracking precludes the use of the simpler and therefore more popular stress intensity factor (K) solutions.

Through Cracks

The K solution for the CCP (Figure 5(a)) of finite width, W, containing through cracks, subjected to axial tension with Mode I cracking used in this study is represented by the result for the infinite plate,

$$K = S\sqrt{\pi a} \quad , \tag{1}$$

where S is the far field stress and a is the surface semicrack length. The influence of the edge of the plate is provided in this study by the secant correction, so that

$$K = S\sqrt{\pi a}\ \sec\frac{\pi a}{W}^{\frac{1}{2}} \quad . \tag{1a}$$

The K solution for the finite width CNP (Figure 5(b) with symmetric through cracks of length c has a comparable form to that for the CCP

$$K = S\sqrt{\pi c}\ F(\frac{c}{W}) \quad , \tag{2}$$

where c is the surface length of the crack measured from the edge of the notch.

Values of F(c/W) must include the influence of the notch root free surface, the notch gradient, and the finite width of the specimen. For physically very small cracks, K is reasonably approximated by

$$K \doteq 1.12\ K_t\ S_N\sqrt{\pi c} \quad . \tag{2a}$$

Here K_t is the net section stress concentration factor, equal to the ratio of the maximum principal stress, denoted as σ, to the net section stress denoted as S_N. S_N is related to S by the ratio of far field (gross) section area, A, to net section area, A_N:

$$S_N = S(A/A_N) = S(W/(W-2r)) \quad , \tag{3}$$

and r denotes the radius of the hole.

For two physically short cracks in notched plates, if the K_t's are the same and the gradient in σ as a function of distance across each plate is geometrically similar, K will provide similitude in the crack driving force for the same degree of through thickness constraint (same t/2r). In the absence of the same constraint, K will not provide similitude based on numerical results generated for cracks in the absence of the notch gradient [21], for values of c measured on the plate's surface. Likewise, if the diameter of the hole is the same but the width varies, Equation (2a) indicates K will not provide similitude unless (F(c/W)) is geometry specific. That is, solutions for K (F(c/W)) that represent the geometry in Figure 5(b) are required. A number of different forms of F(c/W) have been considered for present purposes. Included are numerical solutions for similar geometries,

solutions adapted to the geometry considered (e.g., [22-25]), and others (as outlined in Appendix B).

Because the interest here is in short cracks and Equation (2a) is exact in the limit as $c \to 0$, the suitability of the various functions F(c/W) have been judged by comparing them to the trend for Equation (2a) for crack sizes 25 μm $\leq c \leq$ 490 μm. These bounds are the limits of the validity and accuracy of Equation (2a) as developed in Appendix F. They have been chosen with regard to matching the peak stress and the stress gradient in the K solution adapted to that in the CNP of Figure 5(b). The upper bound has been chosen by consideration of related work done by Schijve [26], Novack and Barsom [27], Smith and Miller [28], Broek [29], Karlsson and Backlund [30], and others who developed analysis for or discussed control of the notch field on the crack driving force via LEFM analyses. Results catalogued by Tada, et al [25] have also been considered.

Note that, within the noted crack lengths, Equation (2a) estimates K within 5 percent (at c = 490 μm). (Also, redistribution due to cracking is ignored.) Thus, it is expected that the optimum F(c/W) should match that for Equation (2a) at c = 490 μm within about 5 percent. Of the solutions considered, several do not approach the anticipated result as $c \to 0$. That of Newman [24] developed numerically for an almost identical plan form comes closest to the anticipated limit. It also matches closely the solution discussed by Karlsson and Backlund [30] which is similar to Equation (2a), but valid for somewhat longer cracks (see Appendix F). Therefore, this function, which is plotted in Figure 8, will be used in subsequent analysis of the CNP for symmetric cracking. Correction for asymmetric cracking follows from factors developed for infinite plates normalized with respect to crack length for the approximate degree of asymmetry developed. Such corrections are discussed in the work of Newman [31].

Part Through Cracks

The K solutions discussed above are valid only for through cracks. If surface or corner cracks develop, the solutions must be modified to account

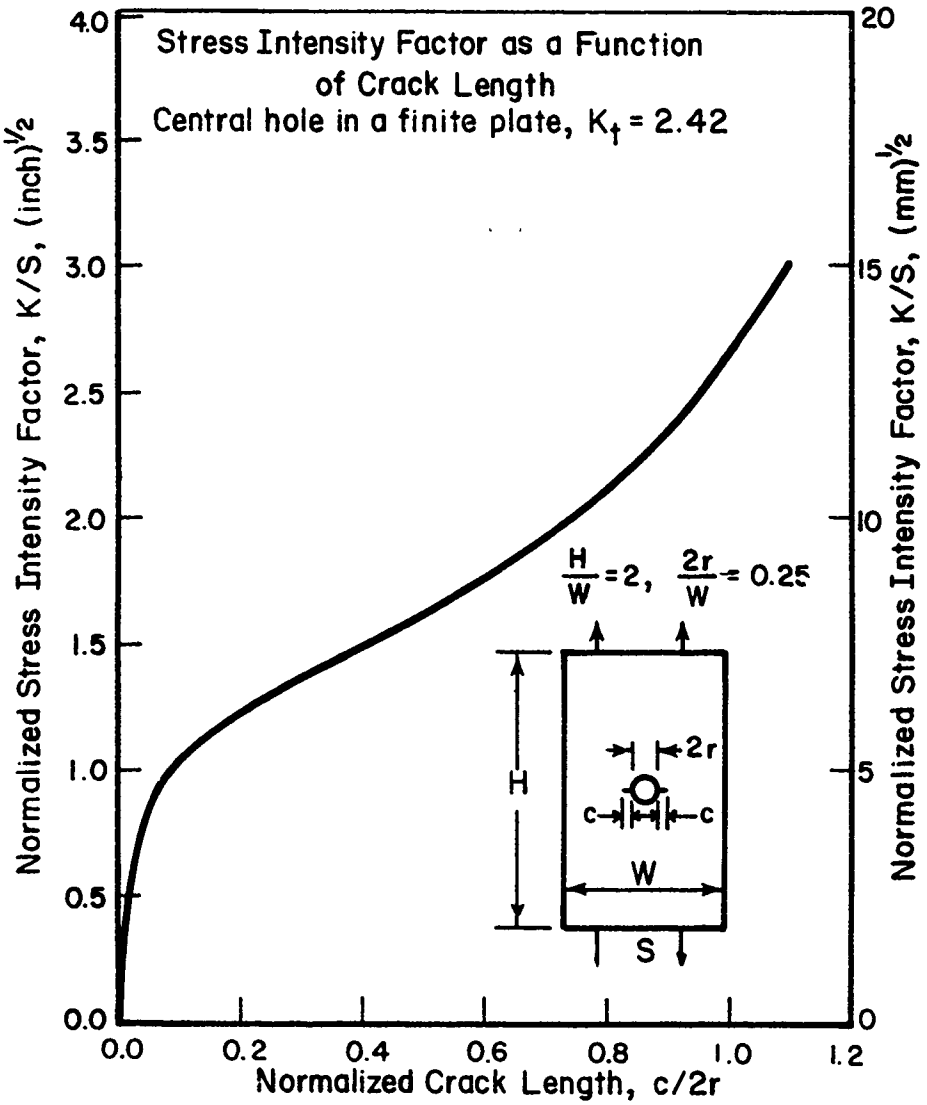

FIGURE 8. STRESS INTENSITY FACTOR SOLUTION ADOPTED FOR CNP SPECIMENS [24]

for the 3D effects of crack shape for both CCP and CNP--Equations (1) and (2)--and for the biaxial, through-thickness stress that develops as a function of t/2r in the CNP--Equation (2).

A number of stress intensity factor solutions now exist for part through cracks. Several good reviews present or compare these solutions (e.g., [31-35]. There is little agreement in the available solutions; this is illustrated, for example, by the wide range of solutions for surface cracks in Figure 9(a). The analyst has a broad range of K values to choose from for a given crack size and aspect ratio. Given the spread of K solutions available and no clear-cut basis by which to choose the correct result, uncertainty in the reduction of growth-rate data is almost unavoidable for physically short cracks that have not started the transition to through thickness. Once the through thickness transition begins, the choice of K and its implementation becomes even more complex because actual crack shapes are not always "part elliptical". However, once the transition is complete and a steady-state crack configuration develops, the uncertainty in K disappears in the absence of other factors.* Crack growth trends, by definition, follow long-crack trends associated with through-thickness cracks, once a steady-state through crack develops.

There are many analyses of the corresponding problem for various cracked CNP specimens. These solutions range from somewhat general empirical equations to geometry specific trends generated via 3D finite element analyses. A broad range of K/S values are observed for quarter circular cracks, the extent to which is shown, for example, in Figure 9(b), reproduced from [36]. True 3D solutions (stress field and crack configuration) also exhibit a t/2r dependence. These trends are apparent in results presented in detailed summaries and reviews of 3D K solutions (e.g., [31-35,37]).

---

* One complicating factor is the transition to a tongue-shaped long crack such as is typically observed in thin sheet prior to the transition from Mode I to stable Mode II cracking (e.g., 16, 65). The influence of the tongue shape and the ensuing Mode II growth has been ignored in the present study because their analysis is complex--and, more importantly, their influence on fatigue growth rates is small in an absolute sense (based on observations in an aluminum alloy [65]).

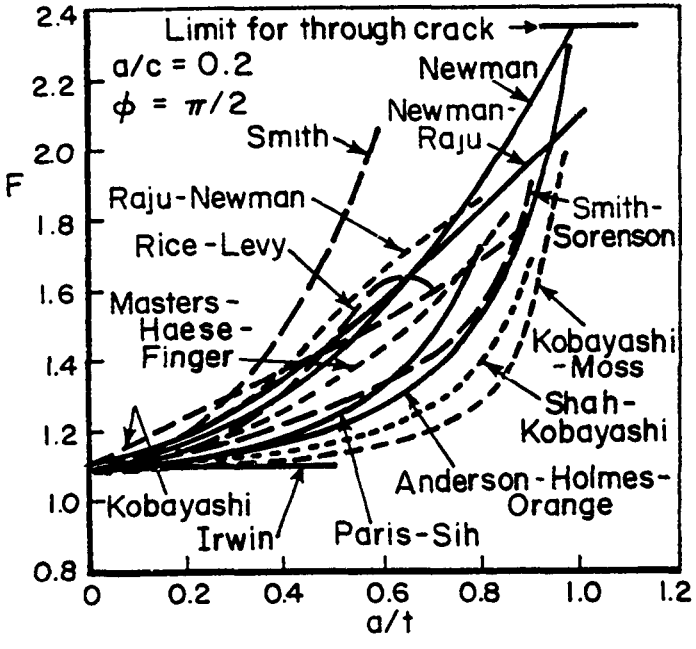

(a) Part through semi-elliptical surface crack; after [33], for point of maximum depth, at depth/length = 0.2

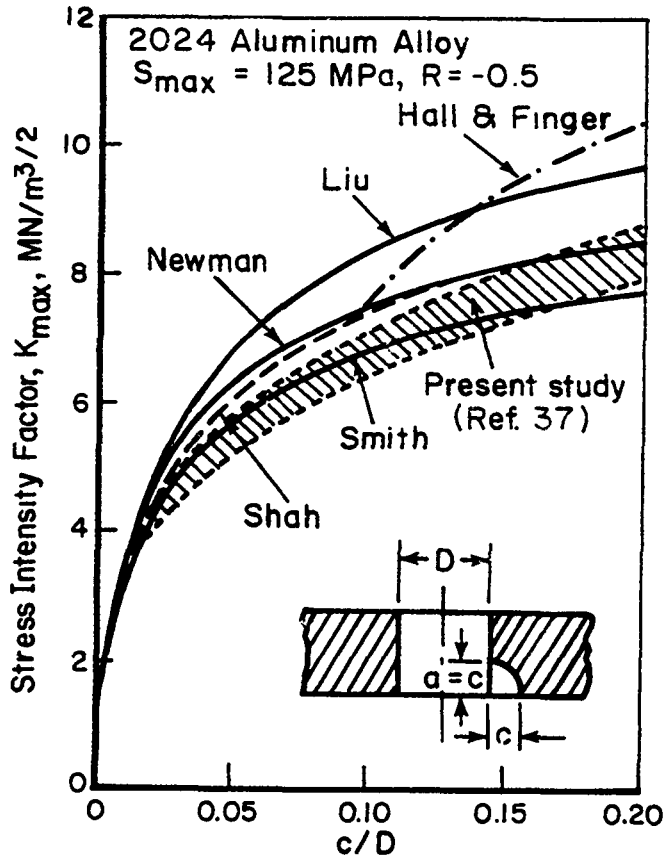

(b) Circular corner cracks at a notch root; after [36], for a specific test situation

FIGURE 9. STRESS INTENSITY FACTOR SOLUTIONS FOR PART THROUGH CRACK SITUATIONS

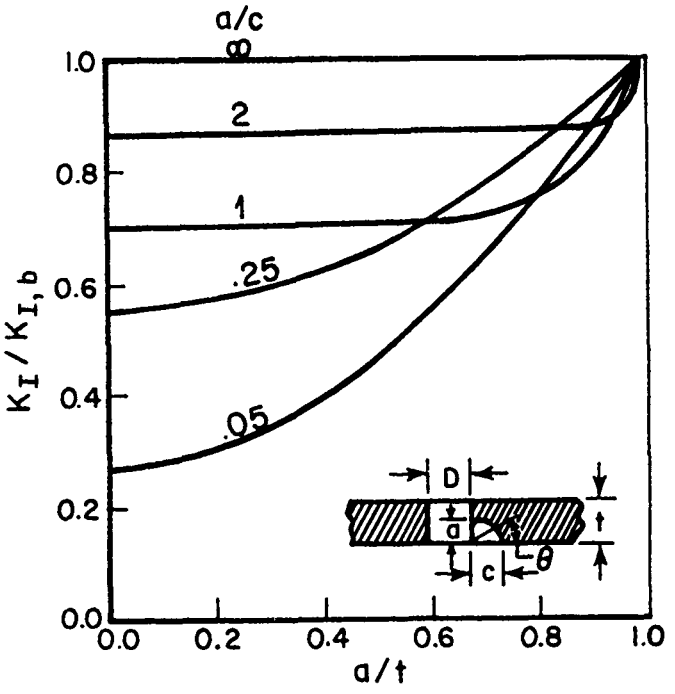

(c) Predicted stress intensity (with respect to surface crack) normalized by the Bowie solution for an infinite plate of finite thickness with D/t = 1, after [37]

FIGURE 9. (CONCLUDED)

Newman [37] has compared results of numerical 3D solutions (near the hole) for otherwise infinite plates to the Bowie [38] result*. Examination of this comparison reproduced in Figure 9(c) shows that the 3D value of K/S, for the same surface crack length, is less than that for a through crack the extent to which strongly depends on the aspect ratio, a/c. Values of a/c > 1 are of interest for the present analysis. In this case, Figure 9(c) indicates K_{3D} (the 3D value of K) is bounded above by the through-crack value and below by about 0.7K, depending on a/t. Results considered in the process of the survey reported in Appendix B also showed that K_{3D} is less than the corresponding through-crack value. In view of Figure 9(c) and the general trends in the literature, the driving force for growth of physically small cracks is reduced by as much as 30 percent (i.e., to about 0.7K) in the presence of circular corner cracks. As the crack propagates across the thickness, the aspect ratio tends toward a plane-fronted through crack, and the surface length increases so that $K_{3D} \rightarrow K$ as evident in Figure 9(c).

It is apparent that 3D effects reduce the driving force for crack growth on the surface at crack sizes small as compared to the diameter of the hole. Further, they act to counter any short-crack effects that tend to increase growth rate. For typical crack-growth rate behavior, this could increase the apparent threshold K by as much as 30 percent (in the absence of correctly computed 3D values of K). These same considerations taken in the finite life regime indicate 3D crack-shape effects can suppress growth rates tracked on the surface by more than an order of magnitude. Likewise, during the formation of small cracks at near threshold stress intensity levels, the reduction in dc/dN due to 3D crack-shape effects may be significant. But once growing at finite rates, 3D crack-shape effect diminishes as the crack gets longer, and (in view of Figure 9(b)) disappear after break-through on the second face. Fortunately, for the most part, this study has used through preflawed CNP specimens and, as evident in Figure 10, these preflaws grew as

---

* Tweed and Rooke [39] have been quite critical of the accuracy of the Bowie solution. Nevertheless, it remains popular (e.g., [35,37]) and is widely used in comparing results for infinite plates.

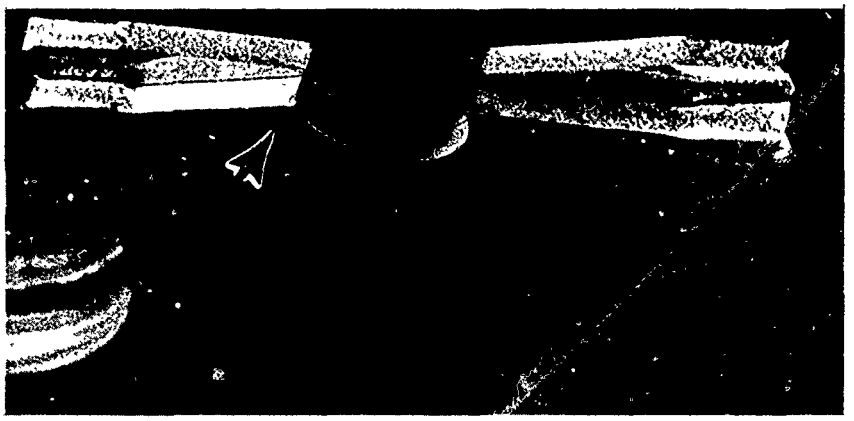

(a) Overview at low magnification (2X)

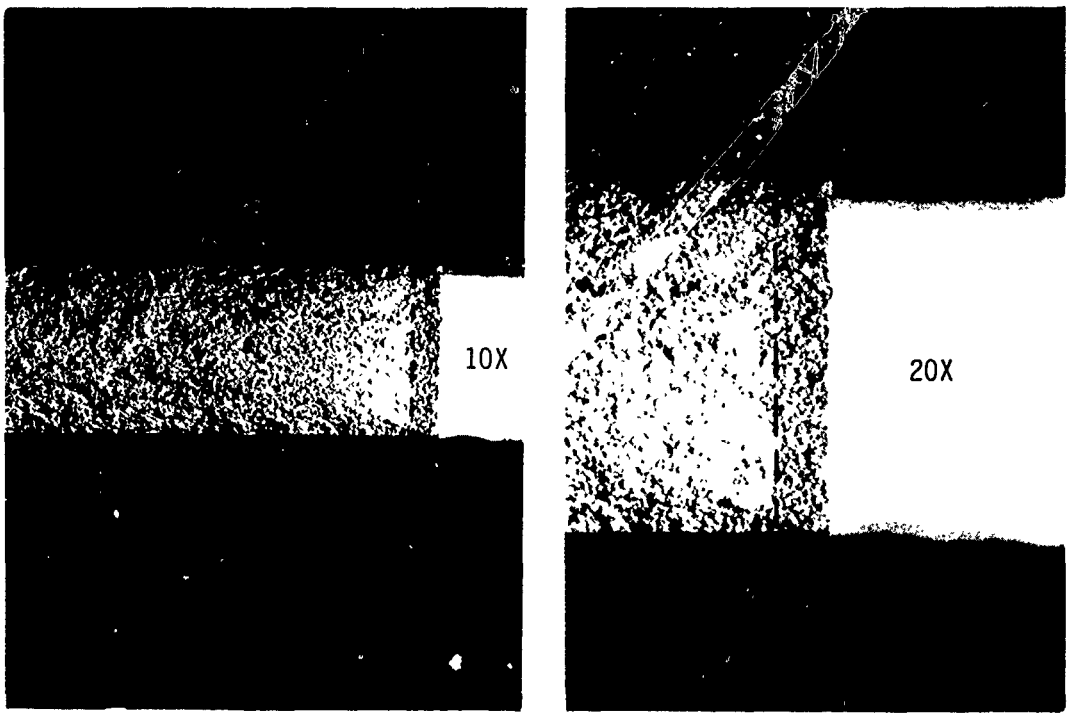

(b) Detail of the region in part (a), near the origin (10X;20X)

FIGURE 10. MACROFRACTOGRAPHIC VIEWS OF CRACK FRONTS IN PREFLAWED CNP SAMPLES

plane-fronted short cracks. Where corner cracks developed, the results presented in Figure 9(c) have been used to modify K/S in Figure 8, in accordance with the aspect ratios observed until transition. Thereafter, Equation (2) (Figure 8) has been used.

It should be noted that the K solution only embodies part of the mechanics of the 3D situation. However, it is established that crack growth rate also depends on stress state (e.g., [8]). Analysis performed to assess the significance of this aspect is alluded to in Appendix A and leads to the results reproduced in Figure 11. For the CNP geometry examined, the value of t/2r is 0.18. Three-dimensional elasticity analysis [40] indicates the local biaxiality ratio $\mu \equiv \sigma_2/\sigma_1$, corresponding to t/2r = 0.18, is $\mu \doteq 0.012$, for Poisson's ratio of 0.3. For fatigue crack initiation, the literature [7] indicates the influence of local biaxiality is significant. For the CNP used in this investigation, the literature suggests that local biaxiality results in a slightly decreased life to develop small cracks and indicates there is a preference to form corner cracks in the absence of artificial preflaws. Figure 11 indicates that the limited local biaxiality developed in the CNP used (μ = 0.012) causes an almost negligible decrease (<2%) in growth rate over the entire range of stress levels imposed in this study.

Consequently, when the preflawed samples tested in this study develop through plane-fronted cracks, it is concluded that the 3D stress state effect of the notch does not contribute to the observed growth rate behavior. Likewise, it can be concluded that notch induced stress state effects do not affect the growth rate of corner cracks as compared to that observed in the usual long crack uniaxial geometries, beyond the effect already embedded in K as function of crack geometry.

Results

Thirty-three crack growth specimens were tested in this study, as listed in Table 1. Results from several of these specimens have been used to develop a long-crack reference data base for this study. Specifically, raw data have been analyzed using the 7PIPA with a view to reduce data scatter as

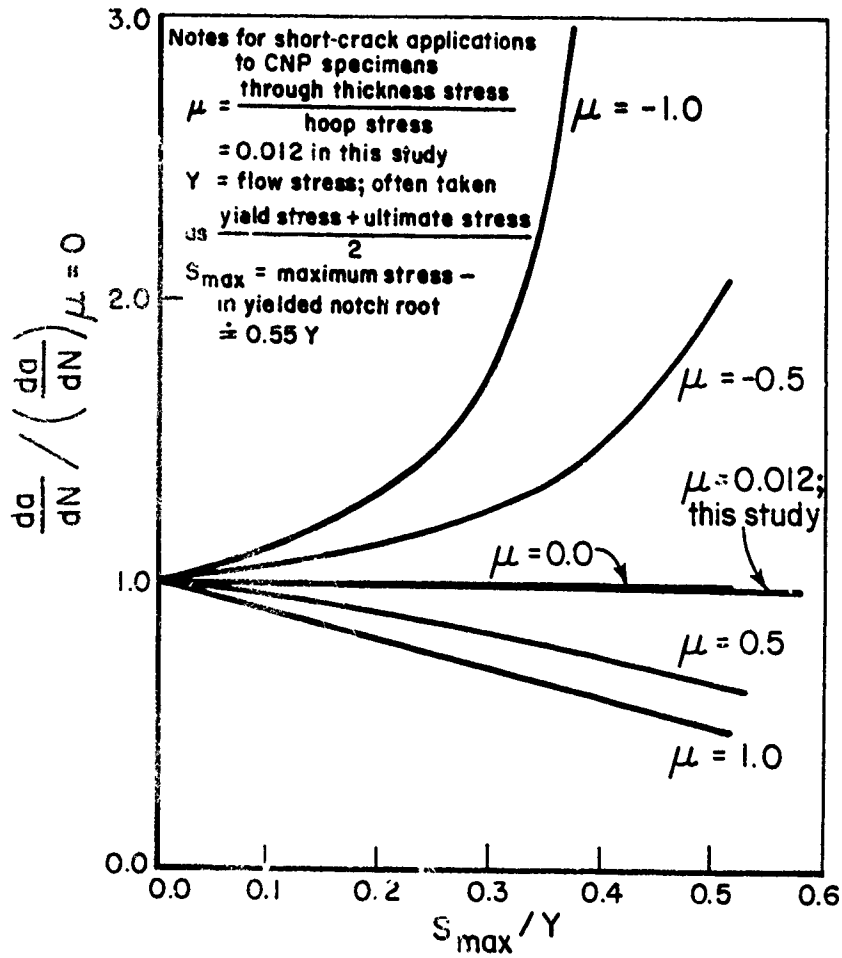

FIGURE 11. DEPENDENCE OF CRACK-GROWTH RATE ON BIAXIALITY RATIO, AS A FUNCTION OF NORMALIZED STRESS (From Appendix A)

much as possible. Results representative of the long crack finite-crack-growth rate behavior of this material have been developed from five separate cracks for R = 0.01, from two cracks for R = -0.6, and from three cracks for R = -1.0. Raw data typical of the scatter encountered are shown for the R = 0.01 case in Figure 12(a), on coordinates of dc/dN and K_{mx}. Trends shown for R = 0.01 and R = -1.0 in Figure 12(b) form the long crack reference data base used in the next section titled "Discussion of the Results".

The long-crack trend for R = 0.01 of Figure 12(b) for the present material matches unpublished data independently developed by GE for a fine-grained Inconel 718 under otherwise identical loading conditions (except T = 148 C). This match is evident in Figure 12(c), whereas Figure 12(d) contrasts results for coarse and fine grained material. Other GE data indicative of long crack trends at 538 C and 643 C are shown in Figures 12(e) and (f). Note that all GE data have been developed for surface-cracked geometries.

Results of 18 specimens provide information useful in the study of small cracks in Inconel 718. Crack length versus cycles data edited as detailed earlier are presented in Appendix E. Table 2 provided a matrix of these specimens and identified comparison results which serve to isolate or emphasize a particular parameter considered to cause short crack effects. Table 3 extracts the salient features of Table 2 and presents the various direct comparisons along with the appropriate figure numbers keyed to plots of data analyzed as just detailed. Generally, Part (a) of a given figure presents edited data points on coordinates of c and N for each specimen and Part (b) presents data on coordinates of log dc/dN and log K_{mx}. When helpful, relevant fractography is included. Where reference is made to the long crack trend, the results presented in Figure 12(b) for the appropriate stress ratio have been used for the 20 C comparisons. Finally note that many figures consist of several graphs that are compared to each other or to graphs in other figures. While there are obvious reasons to make all of the scales identical in such cases, it was felt that loss of detail was a more compelling consideration. Thus, scales have been chosen to retain detail, and caution must be exercised to avoid confusion in making comparisons for cases where the scales differ.

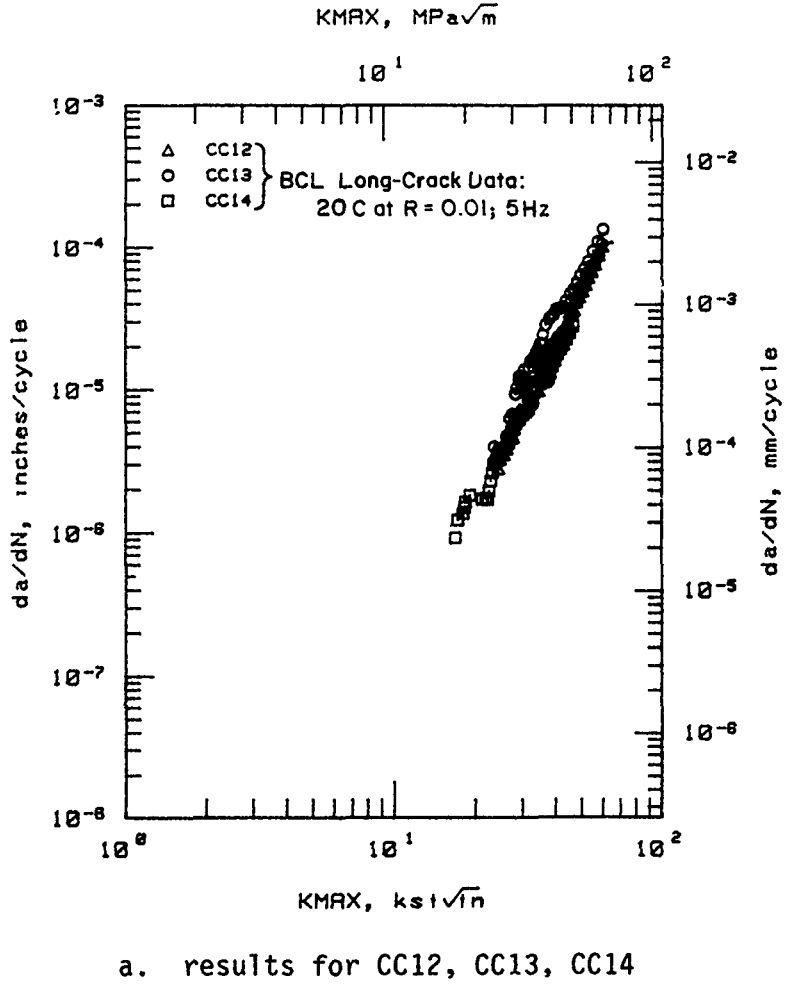

a. results for CC12, CC13, CC14

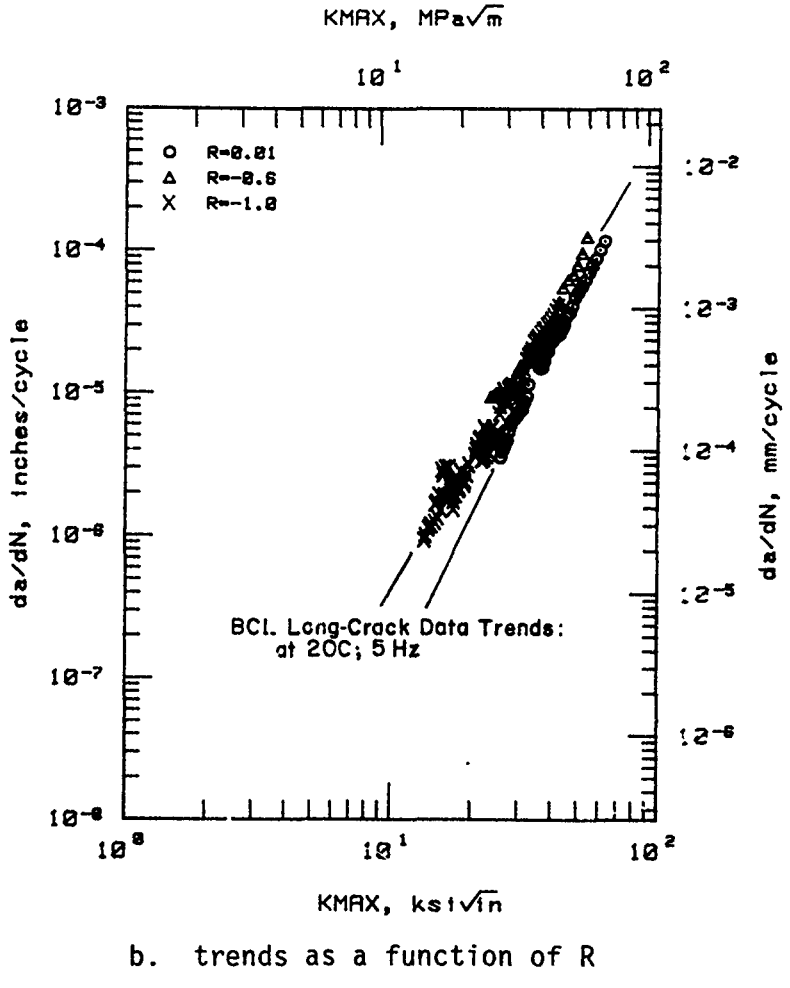

b. trends as a function of R

FIGURE 12. LONG-CRACK REFERENCE CRACK-GROWTH RATE DATA FOR INCONEL 718

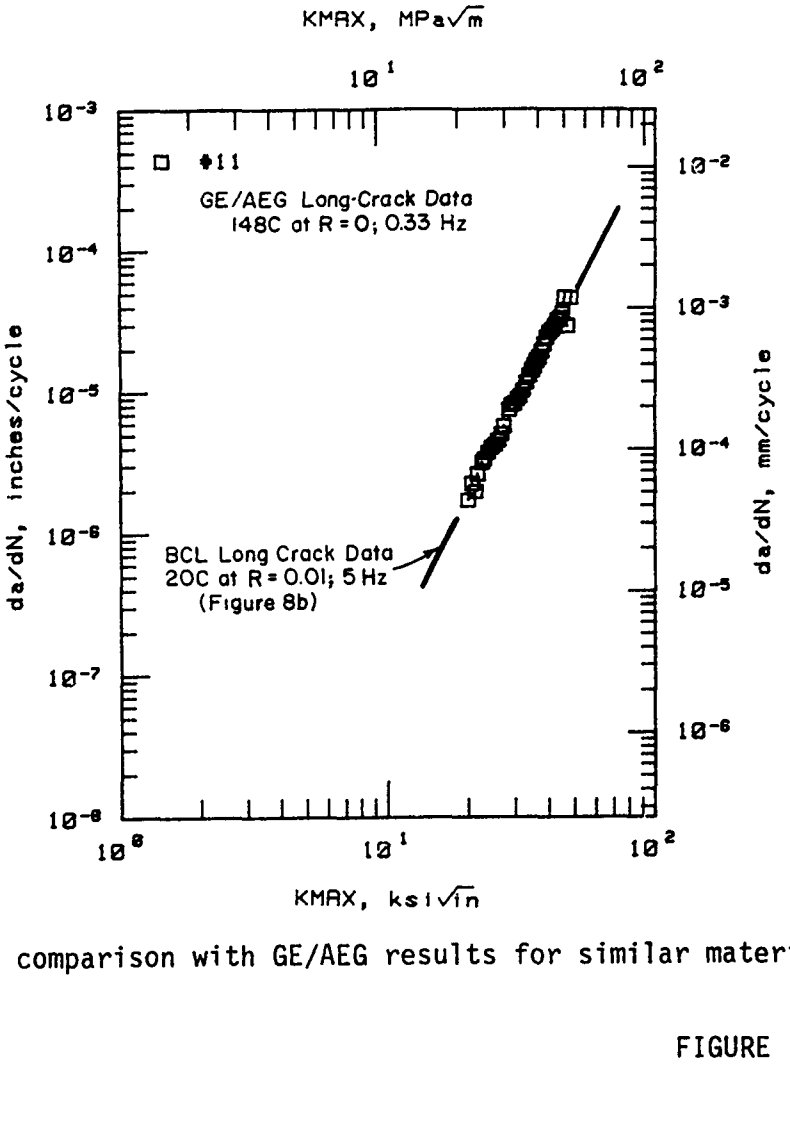

c. comparison with GE/AEG results for similar material

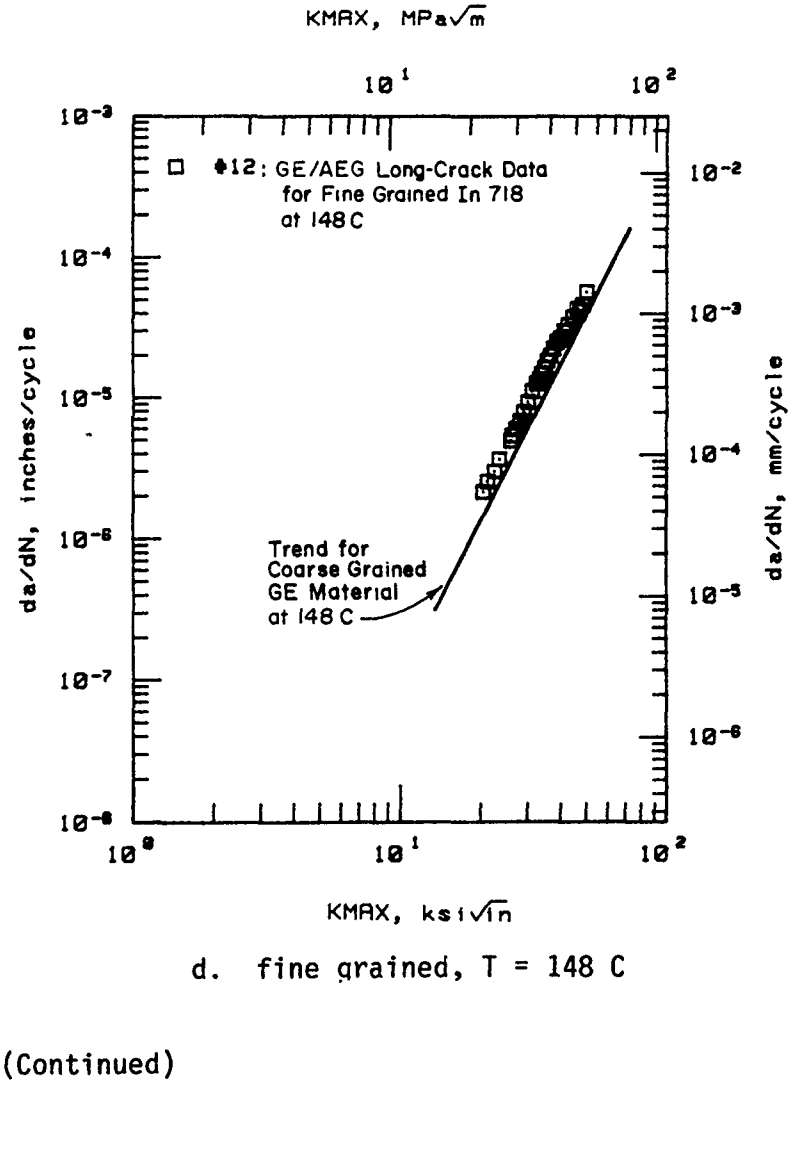

d. fine grained, T = 148 C

FIGURE 12. (Continued)

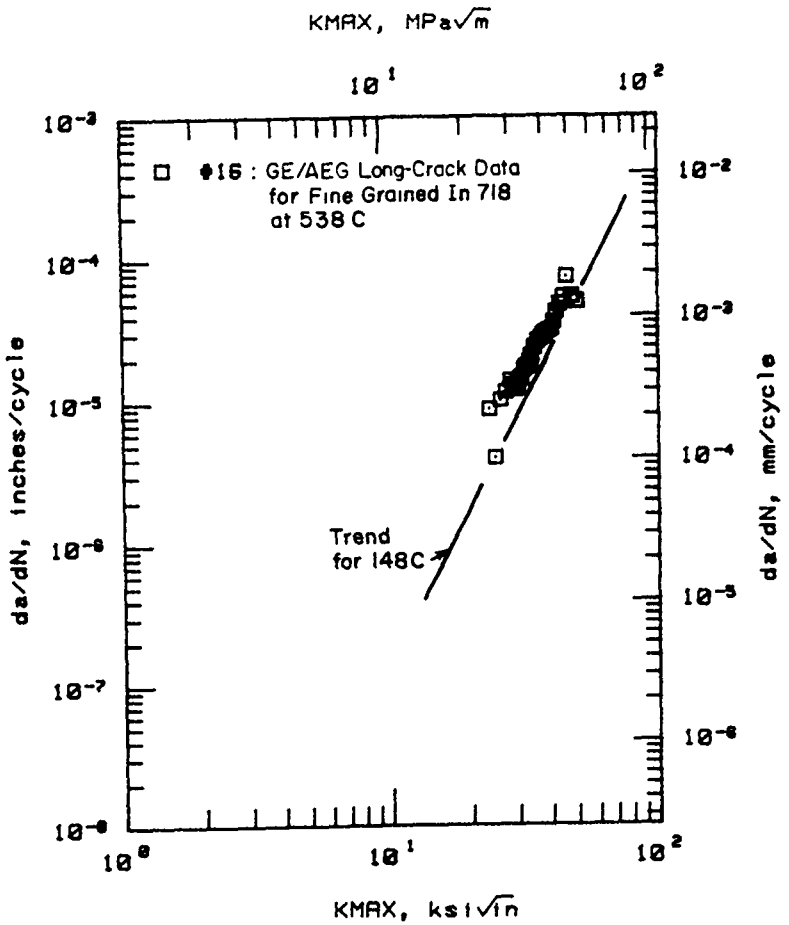

e. fine grained, T = 538 C

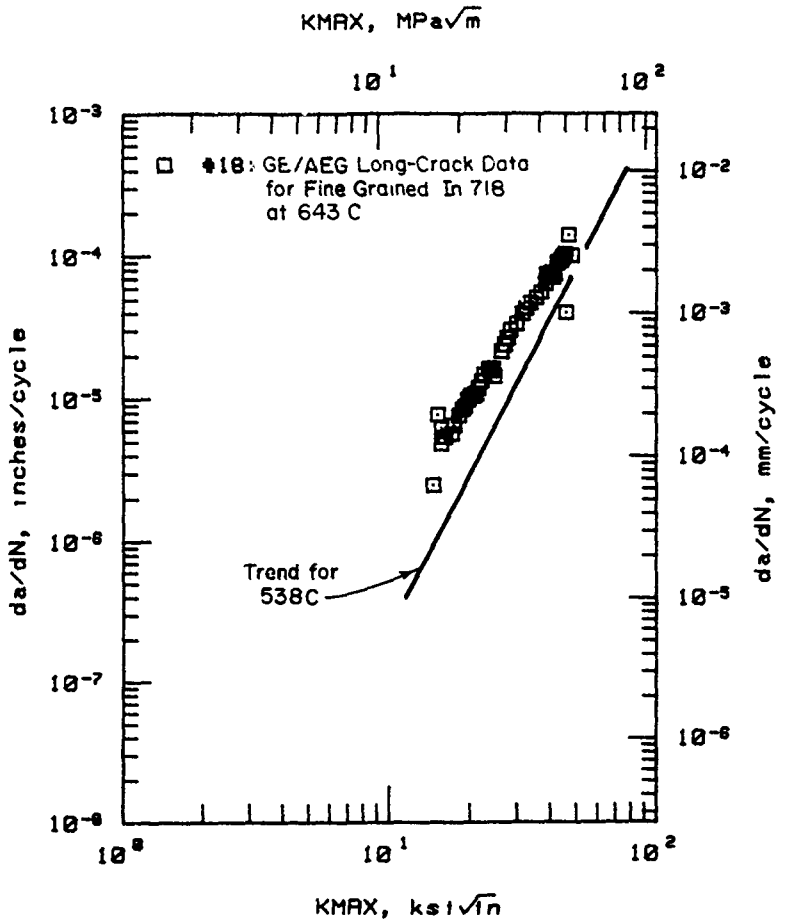

f. fine grained, T = 643 C

FIGURE 12. (Concluded)

TABLE 3. KEY TO DATA INTERPRETATIONS

Parameter	Figure Number	Compare Results for Specimens
	Center Cracked Panel Specimens	
• stress level	13	CC13 (high) vs. CC11 (mod.) vs. CC9 (mod.-low) vs. CC14 (low)
• net wake	14	CC12 (long) vs. CC10 (short)
• stress ratio	15	CC19 (R=-.6) vs. CC12 (R=.01) vs. CC15, CC18 (R=-1)
• temperature	16	CC3 (643 C) vs. CC12 (20 C)
	Center Notched Panel Specimens	
• short cracks	17	CH2, preliminary test - does the material show a short-crack effect
• stress level	18	CH3, CH4 (high) vs. CH20 (moderate) vs. CH6 (low)
• notch field	18	CH3, CH4, CH20, CH6 (notched) vs. CC15, CC18 (unnotched)
• initiation transients, corner vs. plane fronted cracking	19 (see also 18)	CH1, CH16 (natural corner) vs. CH3, CH4 (preflawed)
• temperature	20	CH8 (643 C) vs. CH20, CH3 (20 C)

Figures 13, 14, 15, and 16 present results for CCP specimens, as laid out in Table 3. Figure 13 includes results showing the influence of nominal stress. Since crack lengths are comparable, this figure also examines the influence of plastic zone size, r_p, normalized by crack length. In conjunction with data from Figures 13 and 15, Figure 14 shows the influence of closure and net wake. Figure 15, in conjunction with data for CC13 from Figure 13 presents the influence of $R = S_{mn}/S_{mx}$ under conditions of high stress, or at different stress levels. With a backdrop from Figure 12 and taken with Figure 14, Figure 16 presents the effect of temperature for continuous cycling.

Table 3 indicates that results for notched specimens are plotted in Figures 17 through 20. Figure 17 presents the results of a preliminary test designed to verify that the fine-grained Inconel 718 did indeed show evidence of a short-crack effect. Figure 18 includes results that compare growth rates at different gross section stress levels and in elastic and plastic notch fields. Figure 18, using data from Figures 13 and 16, along with data from CH1 and CH16, also characterizes the influence of the notch stress field. Figure 19, using results from Figure 18, indicates the significance of the initiation transient and corner cracking. Finally, Figure 20 shows fractographs of room and elevated temperature fracture surfaces at comparable K.

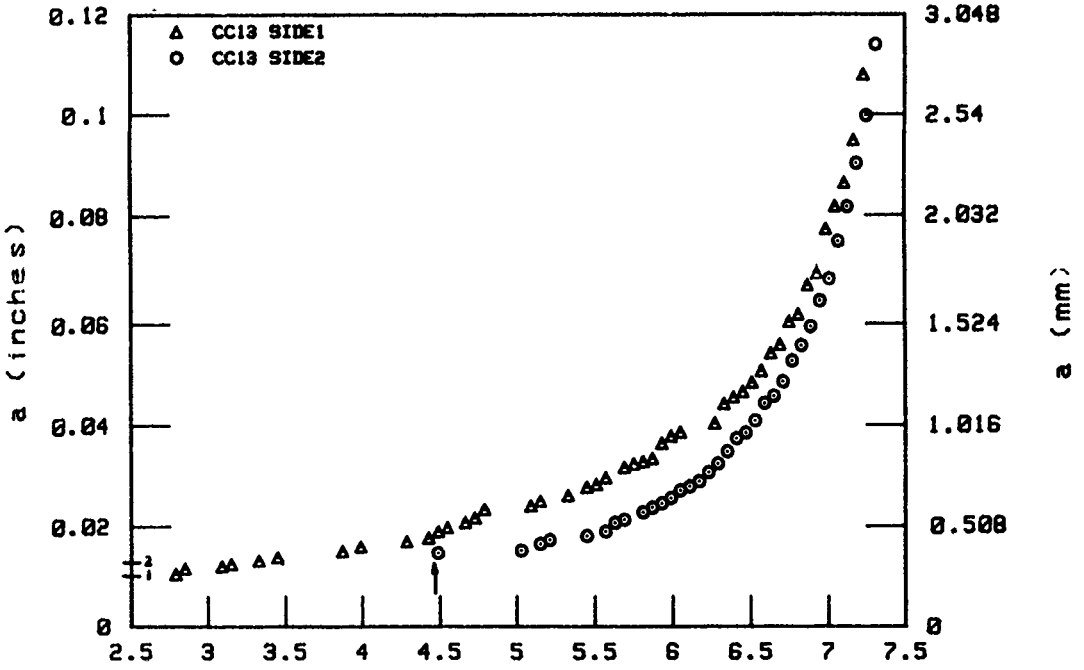

CC13; high stress, $S_{mx}/Y = 0.67$

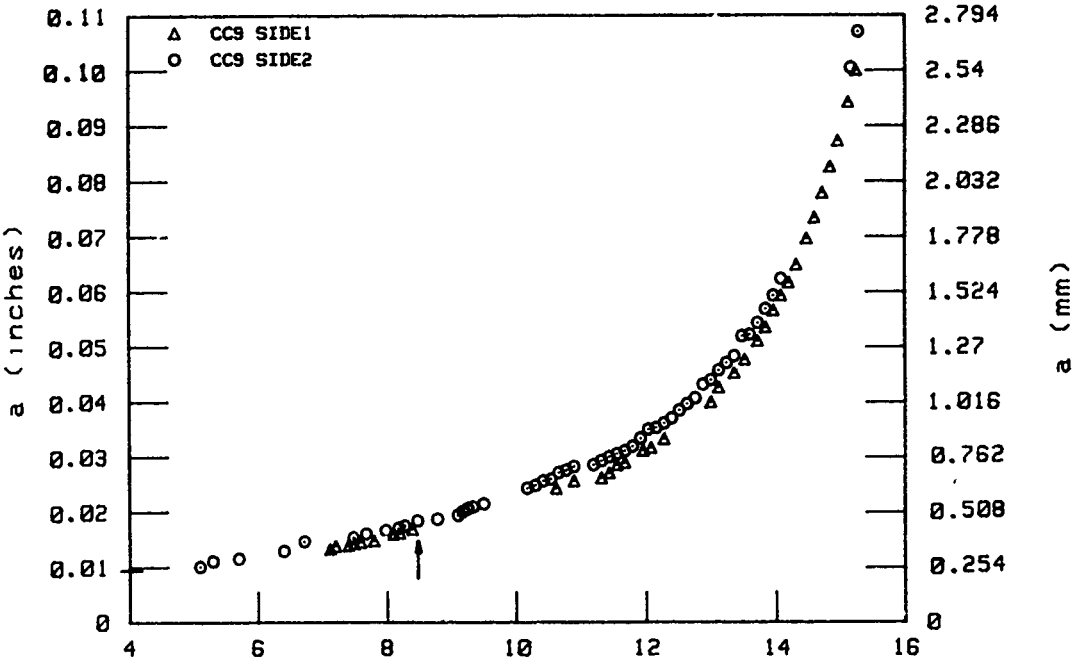

CC9; moderate/low stress, $S_{mx}/Y = 0.57$

a. crack length versus cycles

FIGURE 13. INFLUENCE OF STRESS LEVEL ON CRACK-GROWTH BEHAVIOR IN CCP SAMPLES FOR R = 0.01 AT 20 C

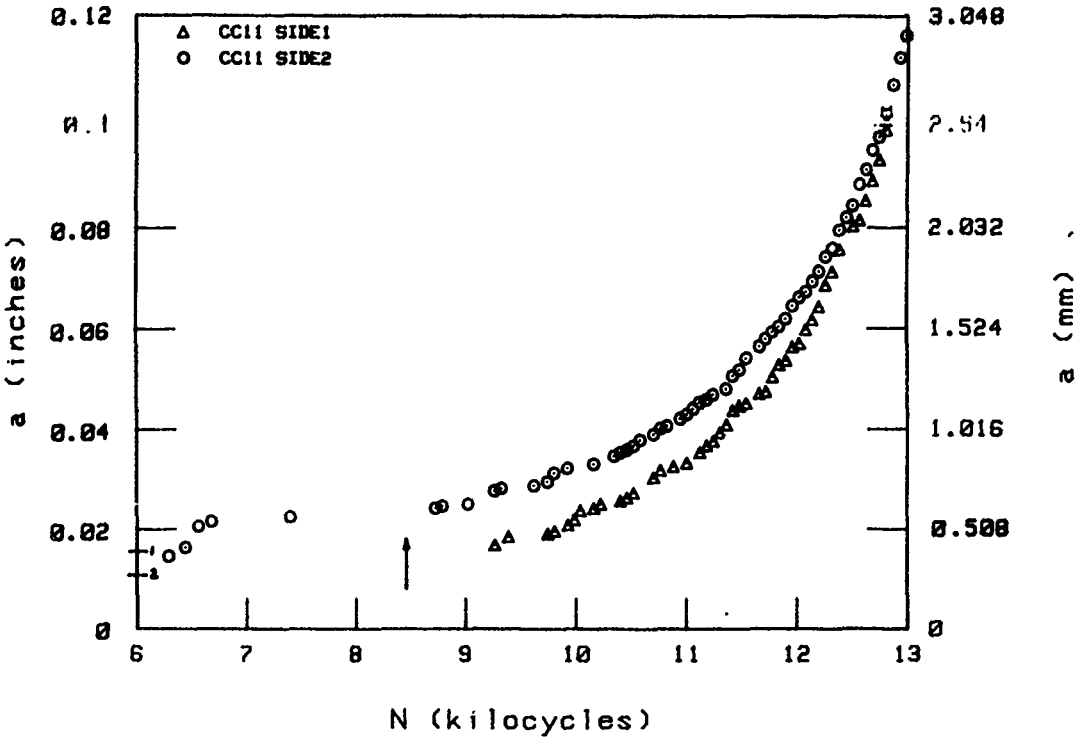

CC11; moderate stress, $S_{mx}/Y = 0.61$

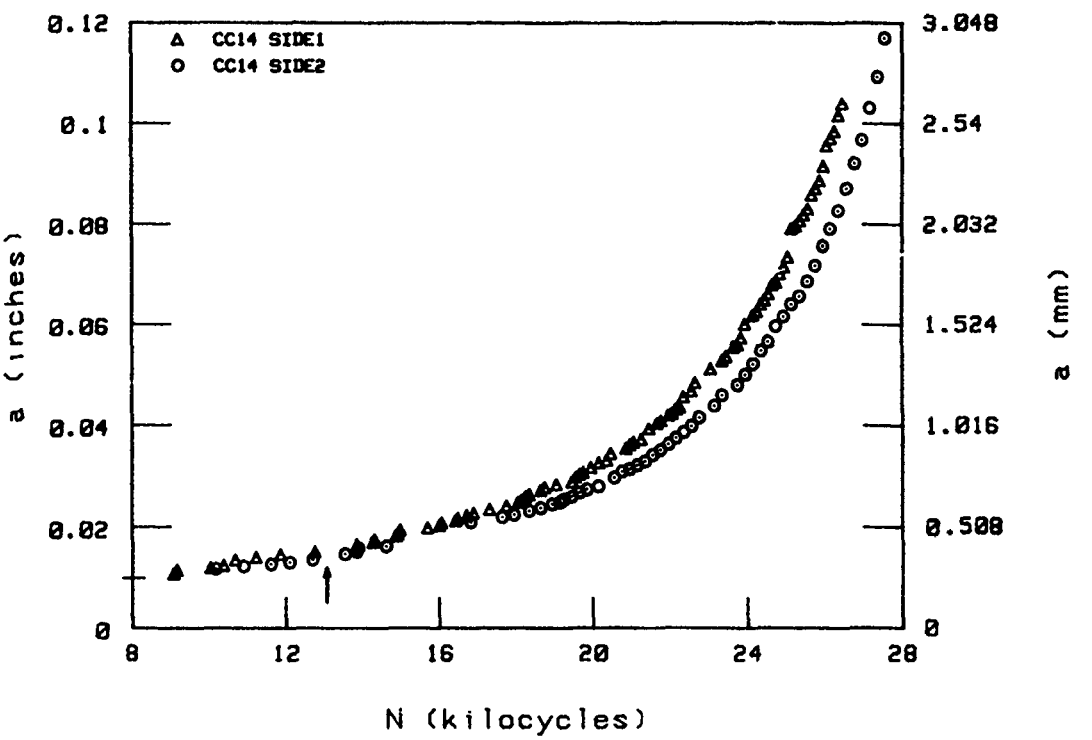

CC14; low stress $S_{mx}/Y = 0.48$

a. (concluded)

FIGURE 13. (Continued)

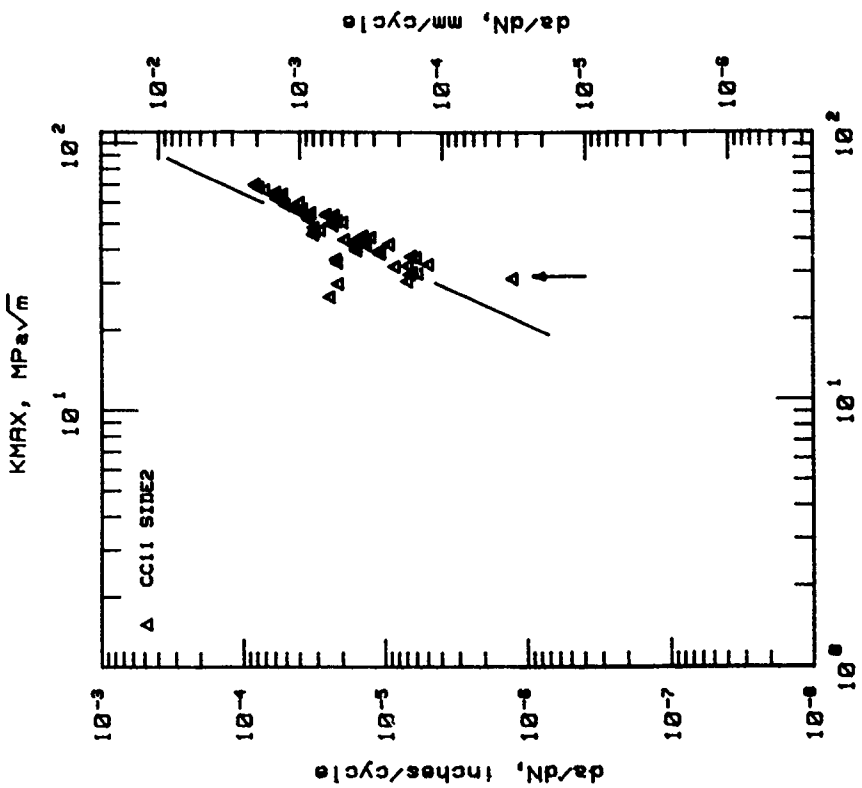

CC11/crack 2; $S_{mx}/Y = 0.61$

b. crack growth versus K_{mx} at moderate stress

FIGURE 13. (Concluded)

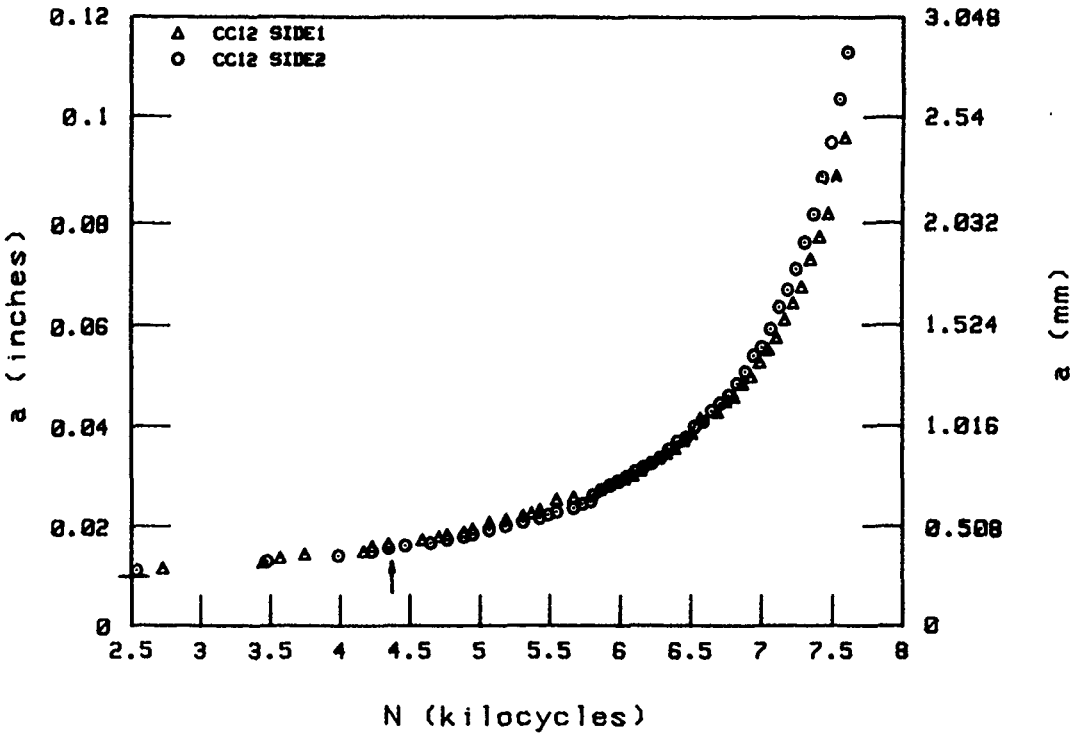

CC12; long net wake, 115 μm

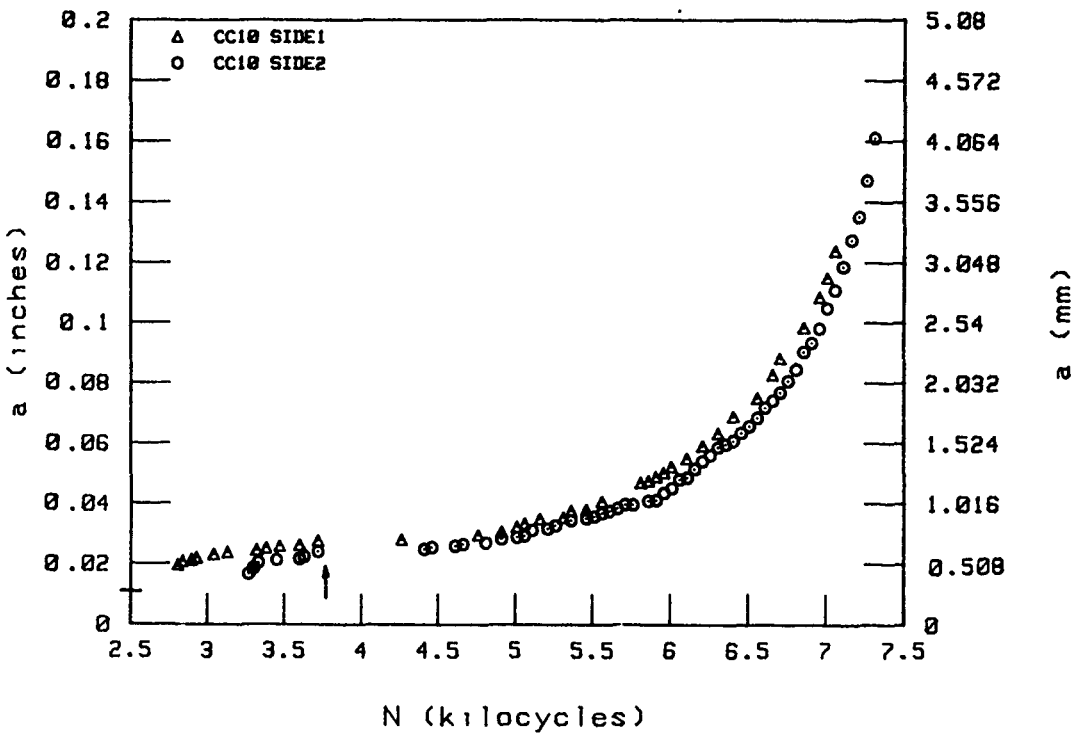

CC10; short net wake, 40 μm

a. crack length versus cycles

FIGURE 14. INFLUENCE OF NET WAKE/CLOSURE ON CRACK GROWTH OF CCP SPECIMENS AT R = 0.01 AND 20 C

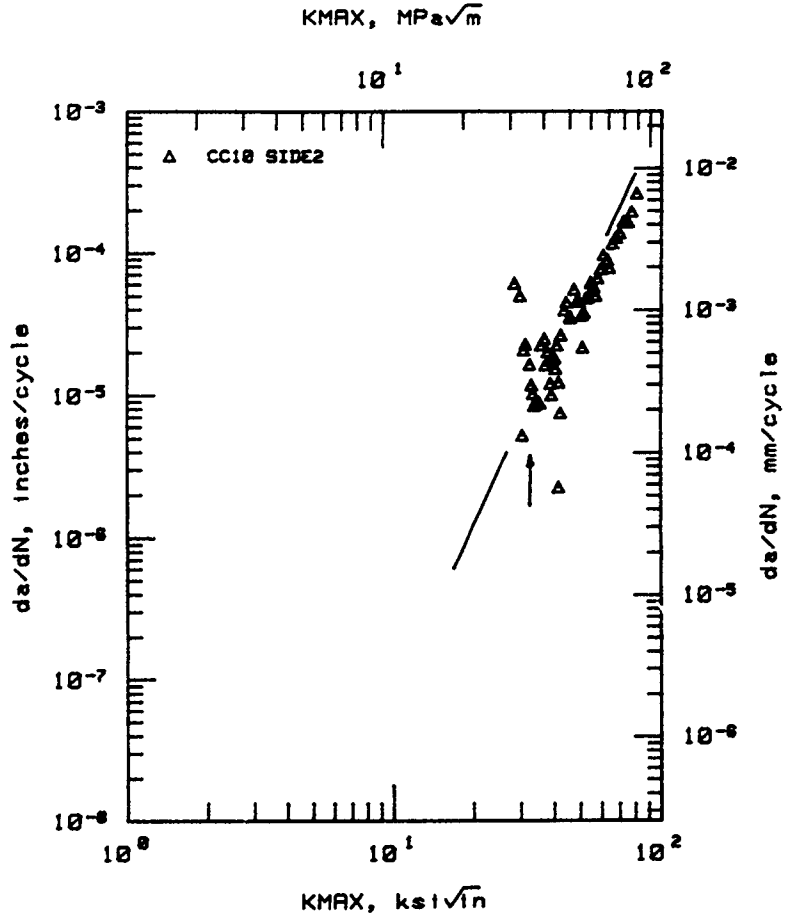

CC10/crack 2; short-net wake

b. crack-growth rate versus K_{mx}

FIGURE 14. (Concluded)

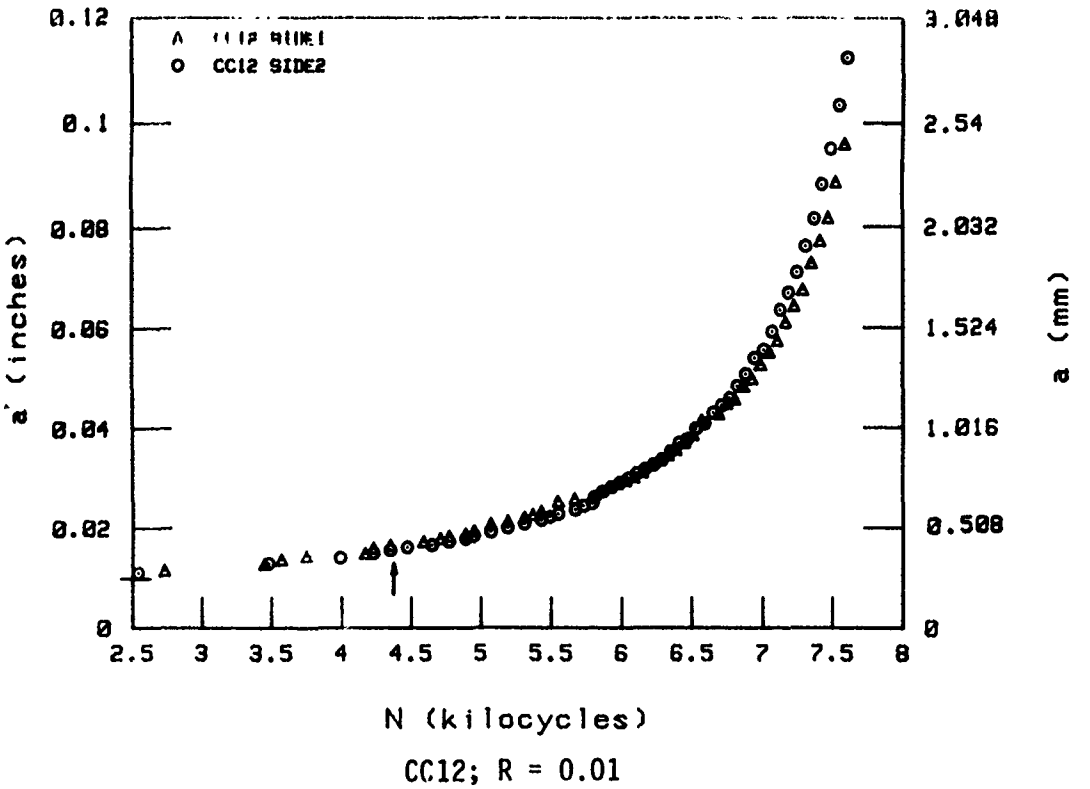

CC12; R = 0.01

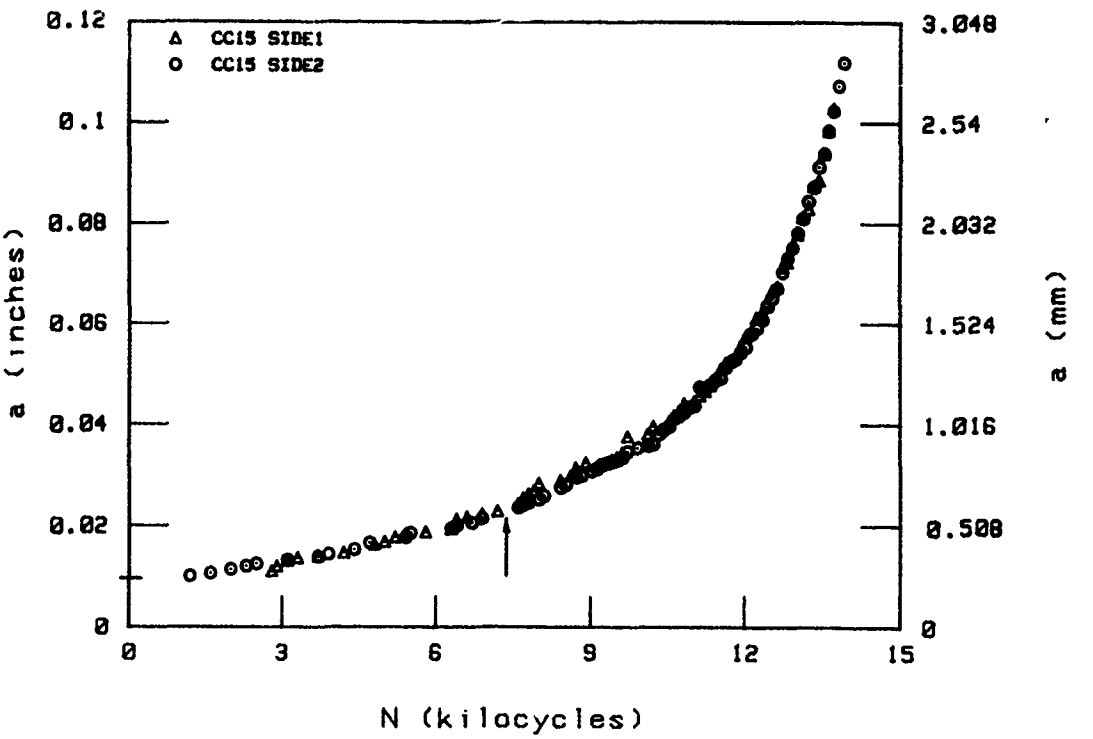

CC15; R = -1.0

a. crack length versus cycles

FIGURE 15. INFLUENCE OF STRESS RATIO ON CRACK-GROWTH BEHAVIOR OF CCP SPECIMENS AT 20 C

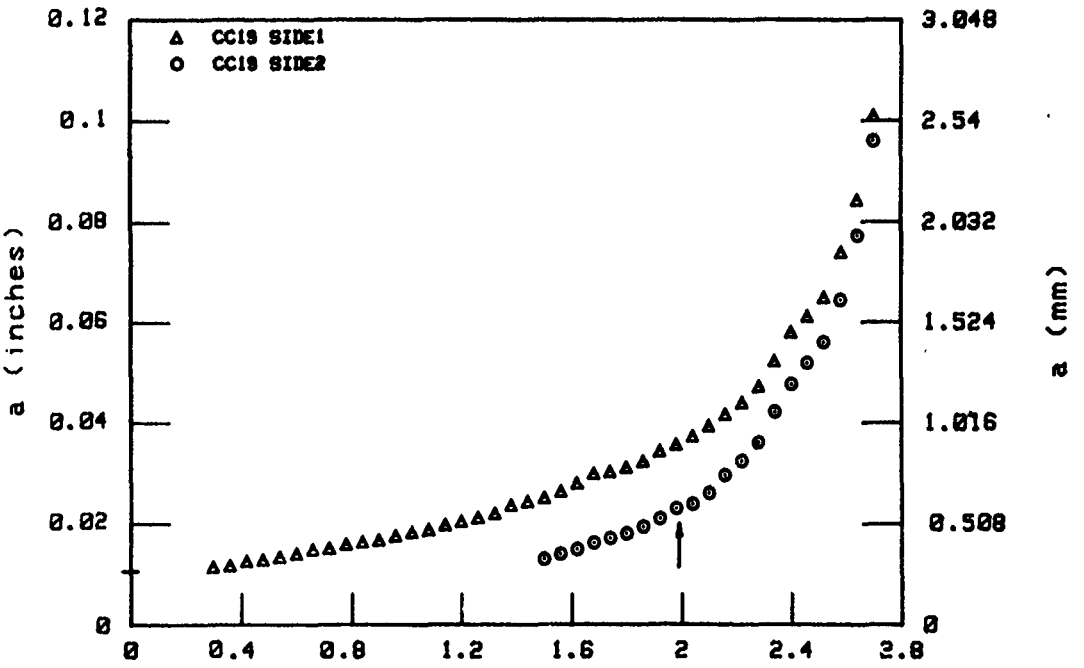

CC19; R = -0.6

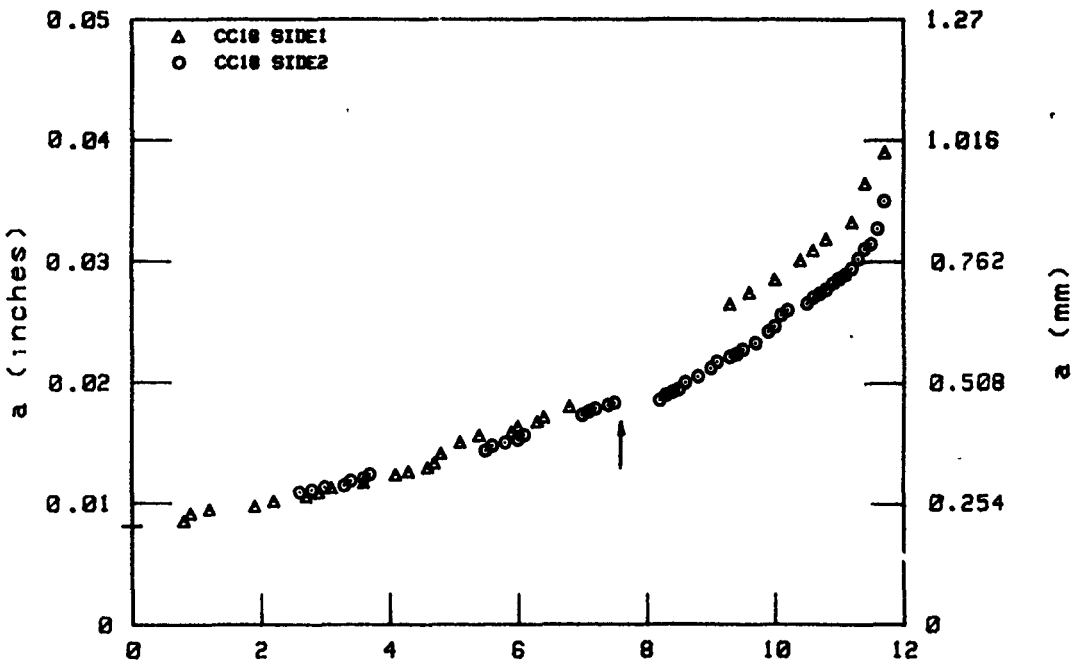

CC18; R = -1.0

a. (concluded)

FIGURE 15. (Continued)

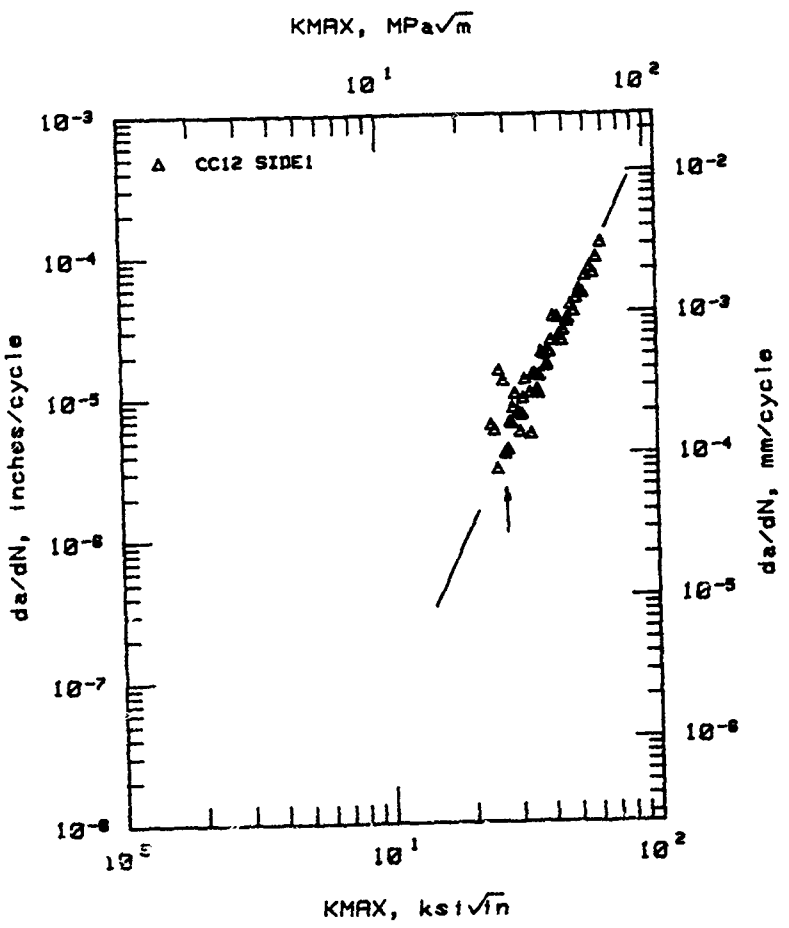

CC12/crack 1; R = 0.01

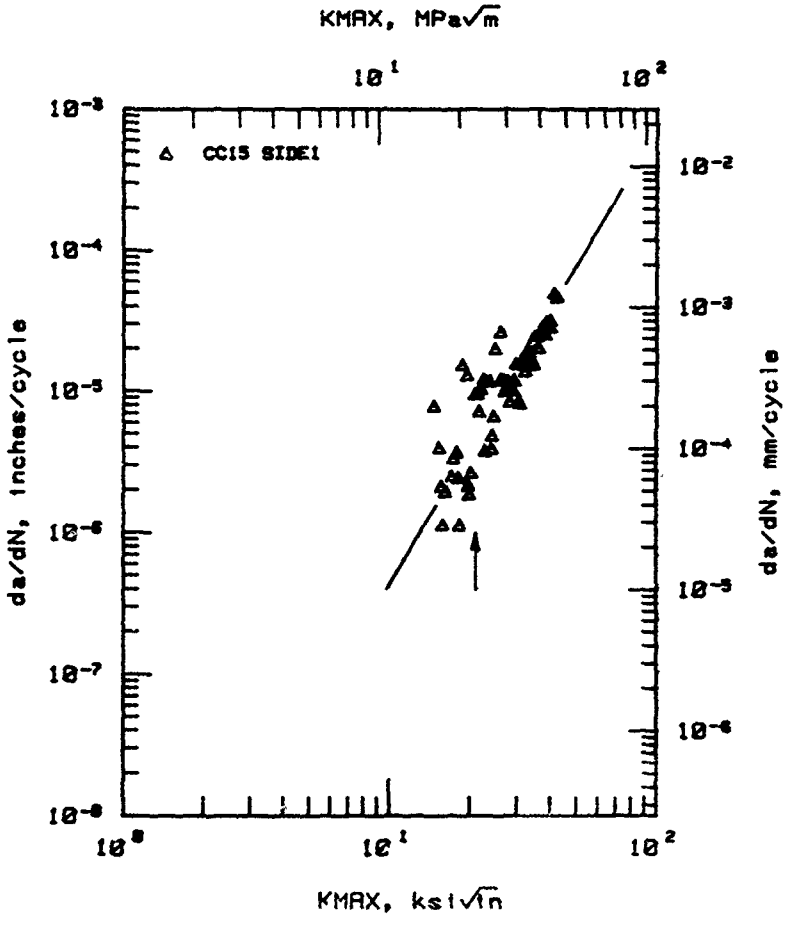

CC15/crack 1; R = -1

b. crack-growth rate versus K_{mx}

FIGURE 15. (Concluded)

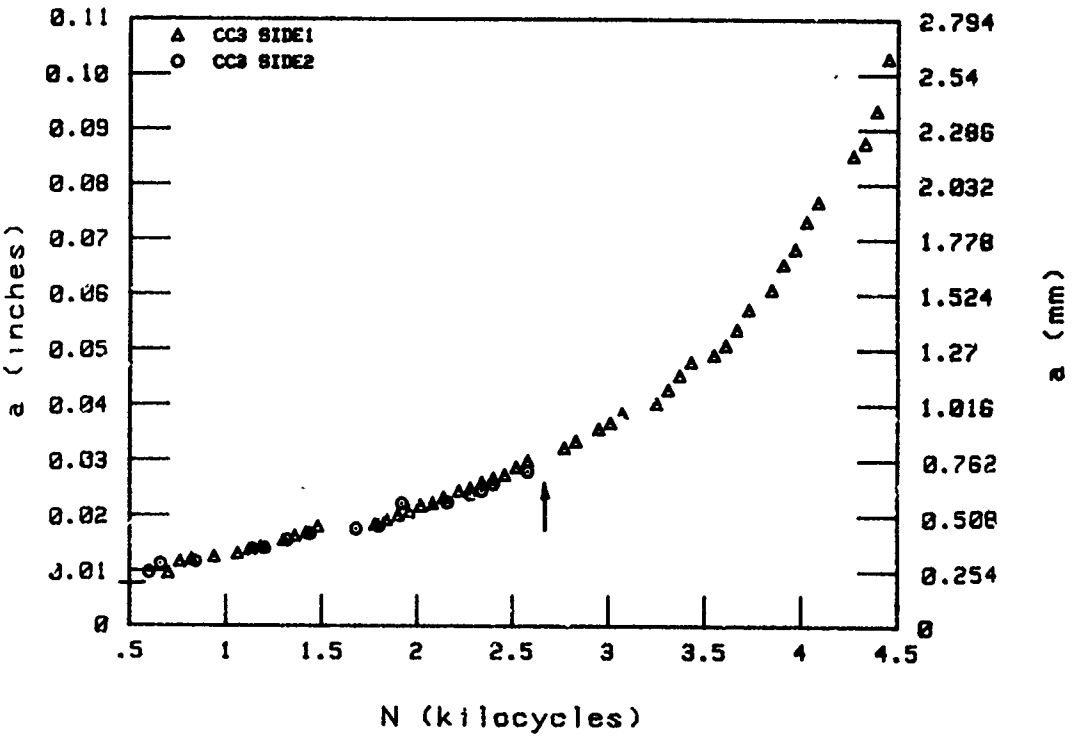

CC3, T = 643 C

a. crack length versus cycles

FIGURE 16. CRACK-GROWTH DATA DEVELOPED FOR A CCP SPECIMEN FOR R = 0.01 AT 643 C AND 5.0 HZ

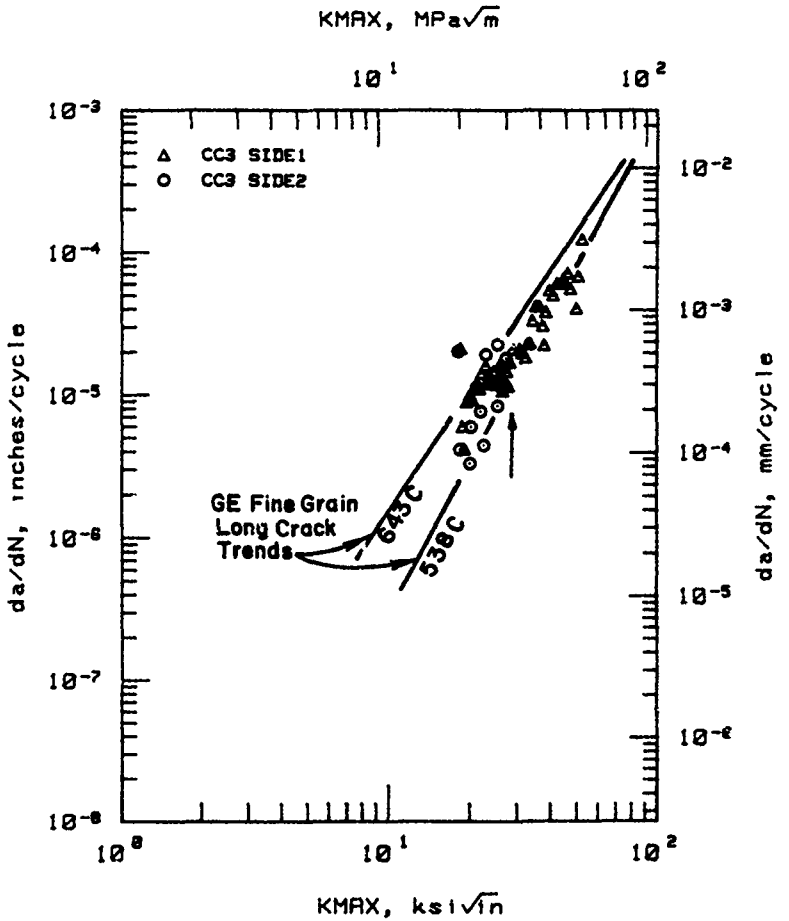

CC3, T = 643 C

b. crack-growth rate versus K_{mx}

FIGURE 16. (Concluded)

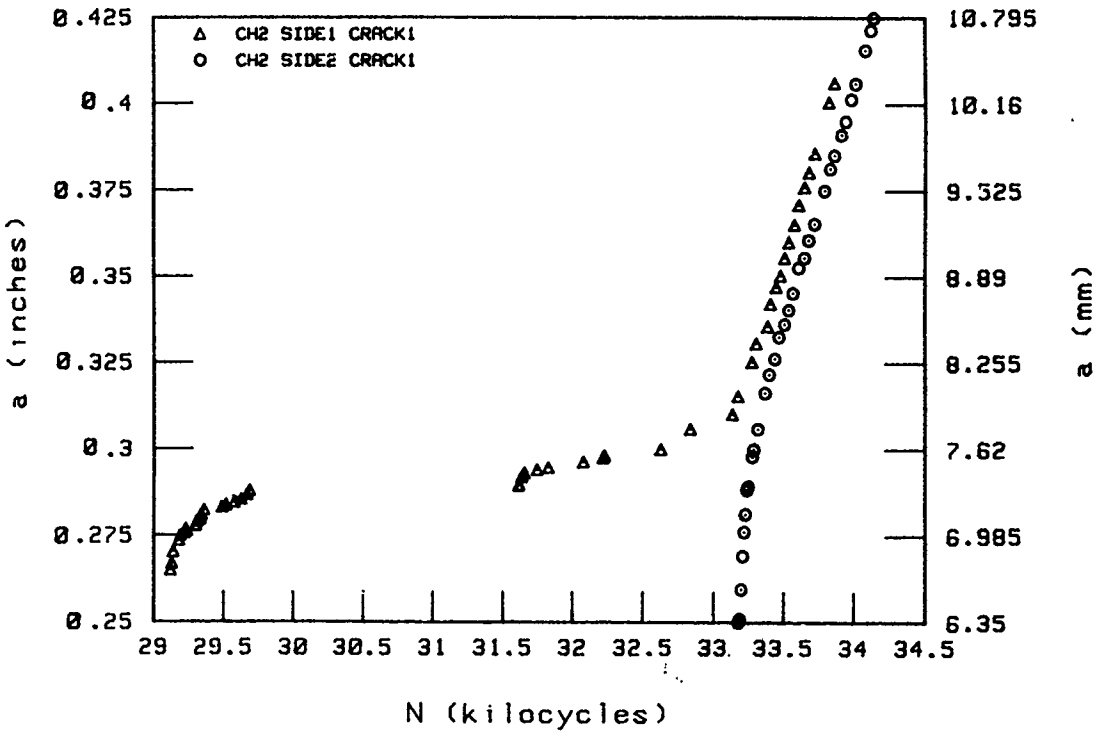

CH2/crack 1,1; corner crack in elastic field

a. crack-growth rate versus cycles

FIGURE 17. PRELIMINARY TEST DEVELOPING CORNER CRACKS VIA NATURAL INITIATION IN AN ELASTIC NOTCH FIELD AT R = -1 AND 20 C

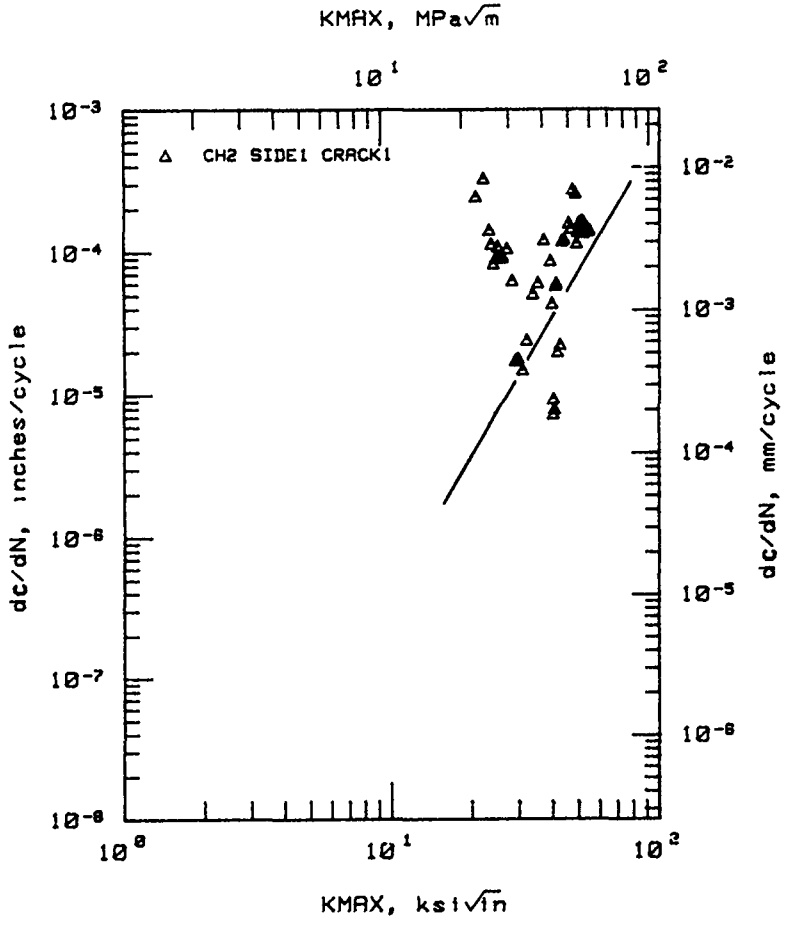

CH2/crack 1,1; analyzed as a through crack

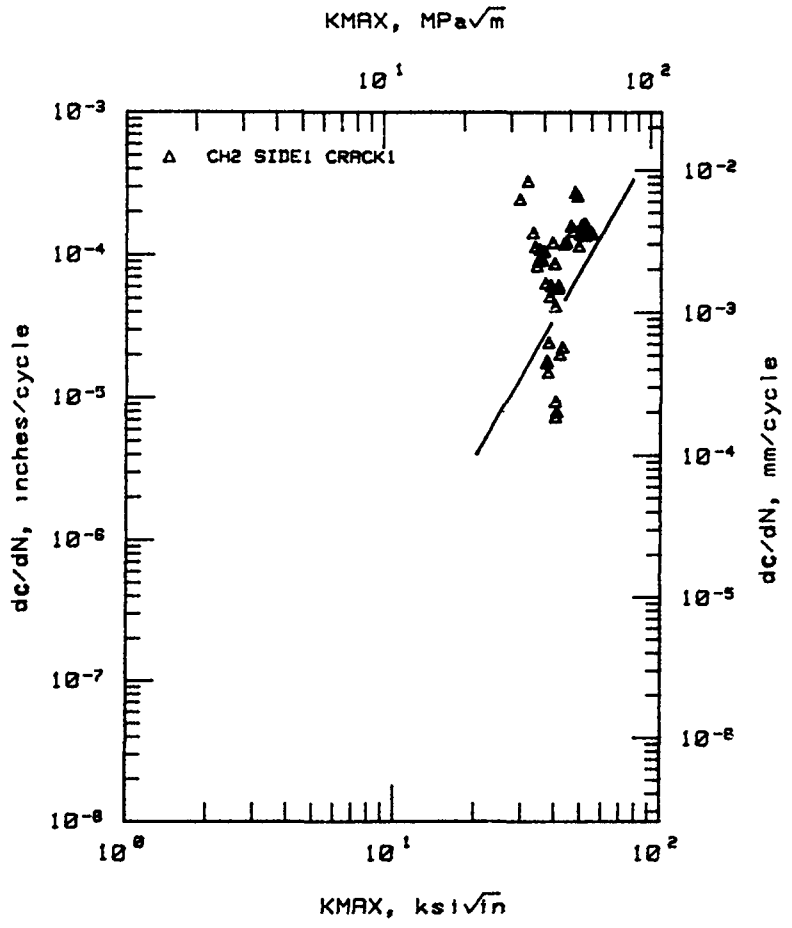

CH2/crack 1,1; analyzed as a corner crack

b. crack-growth rate versus K_{mx}

FIGURE 17. (Concluded)

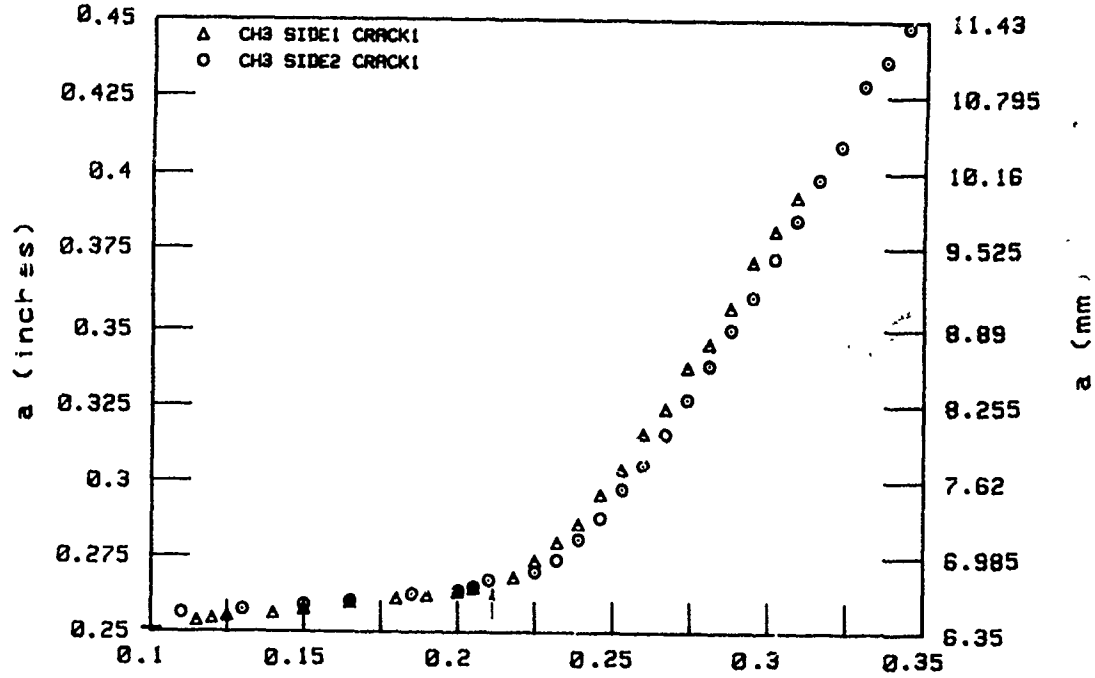

CH3/crack 1; high stress, $S_{mx}/Y = 0.40$

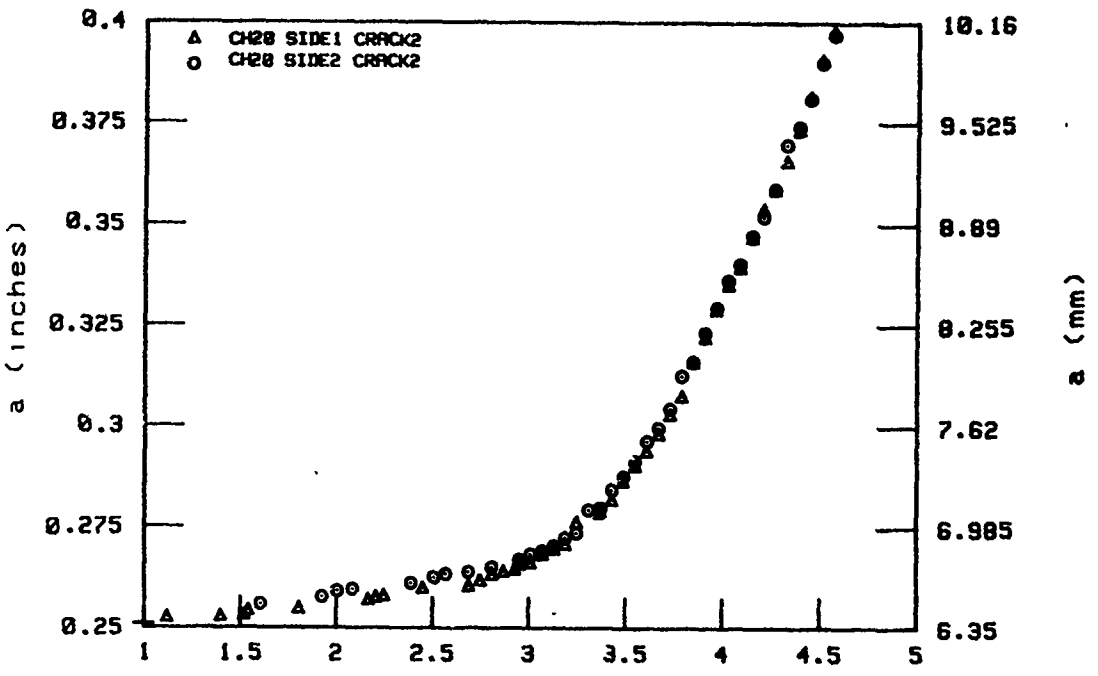

CH20/crack 2; moderate stress, $S_{mx}/Y = 0.26$

a. crack length versus cycles

FIGURE 18. INFLUENCE OF STRESS LEVEL AND CRACK GROWTH THROUGH NOTCH FIELDS FOR R = -1 AT 20 C

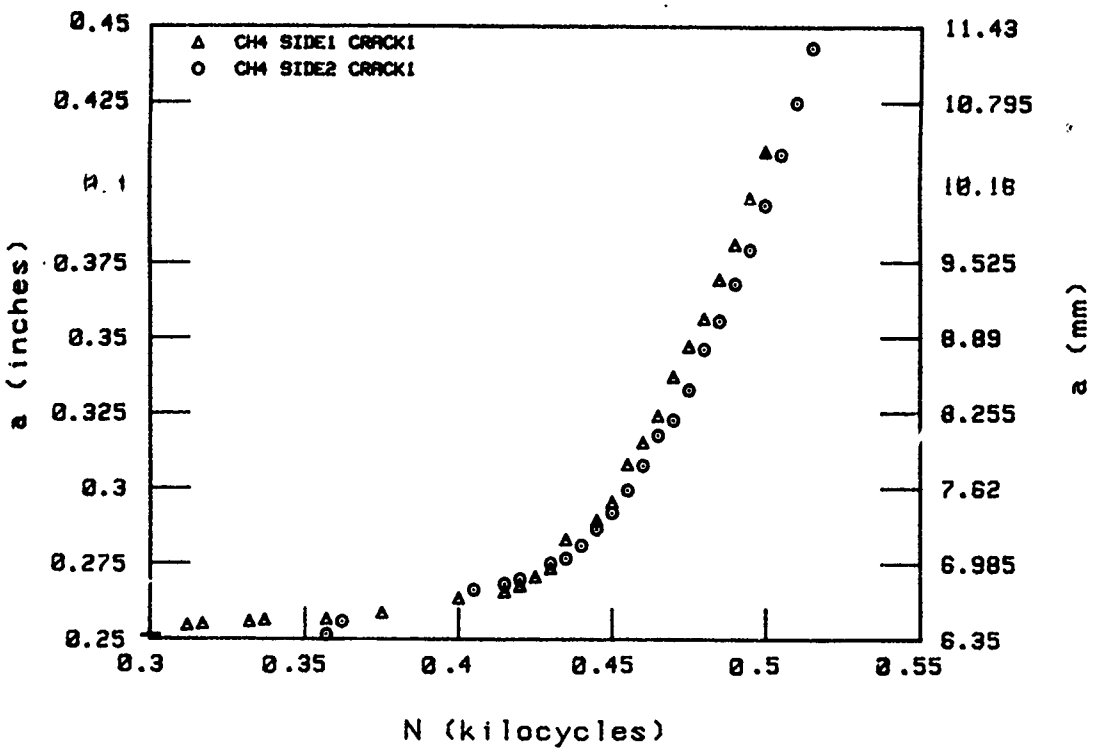

CH4/crack 1; high stress, $S_{mx}/Y = 0.40$

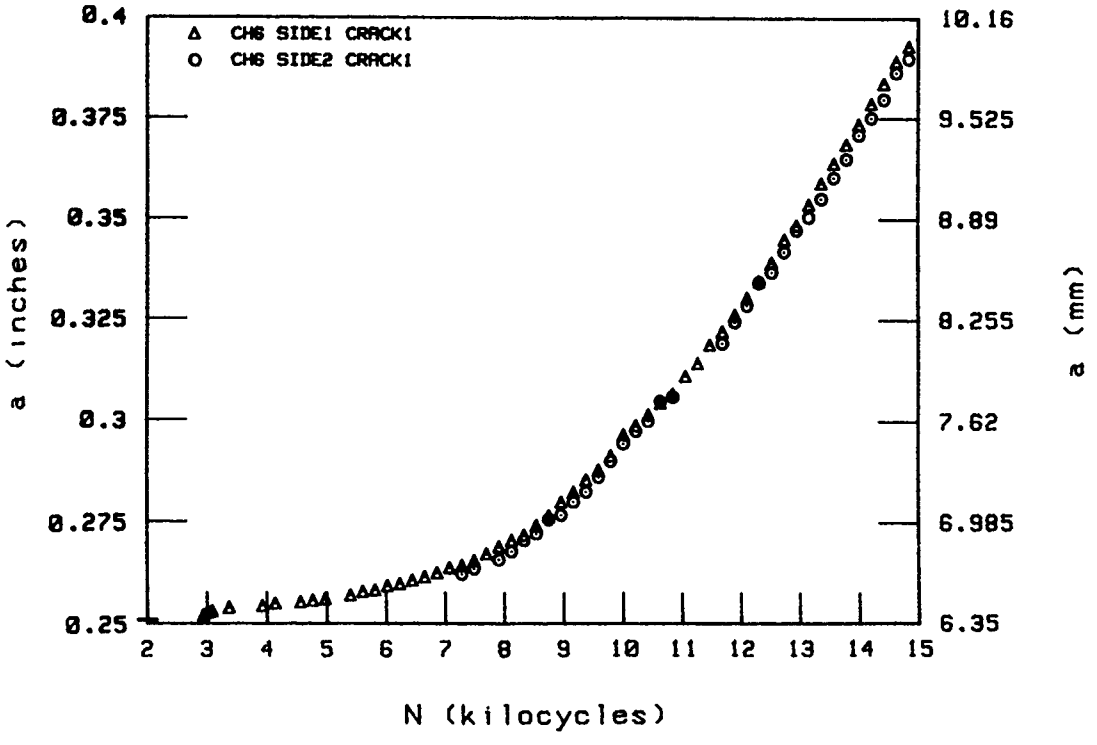

CH6/crack 1; low stress, $S_{mx}/Y = 0.20$

a. (concluded)

FIGURE 18. (Continued)

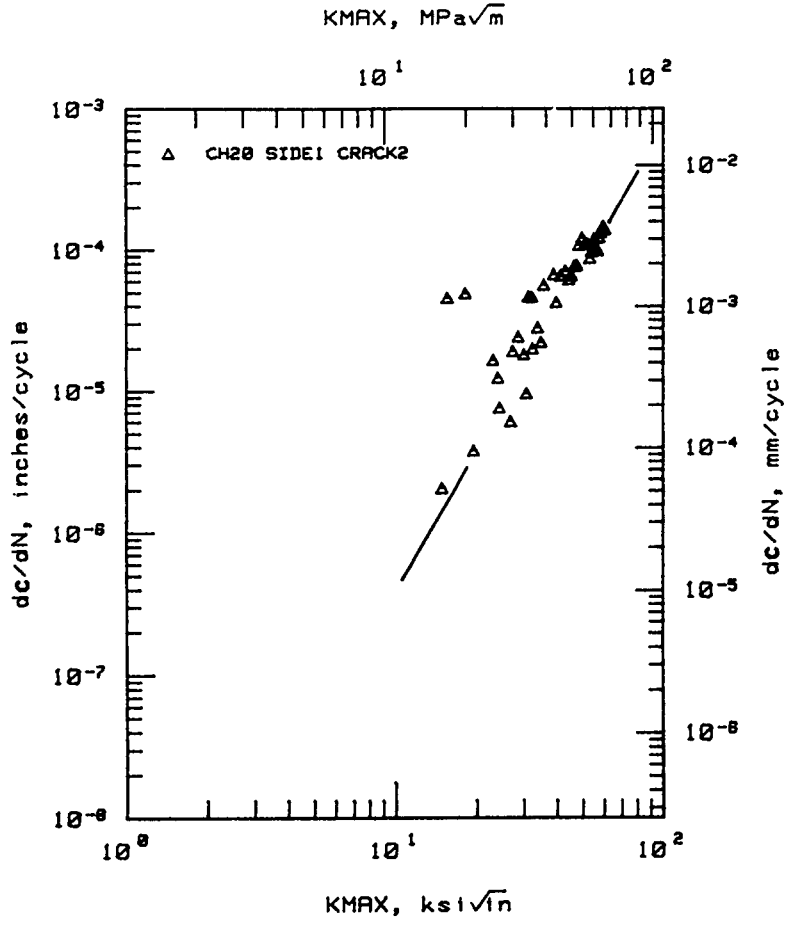

CH20/crack 1,2; elastic

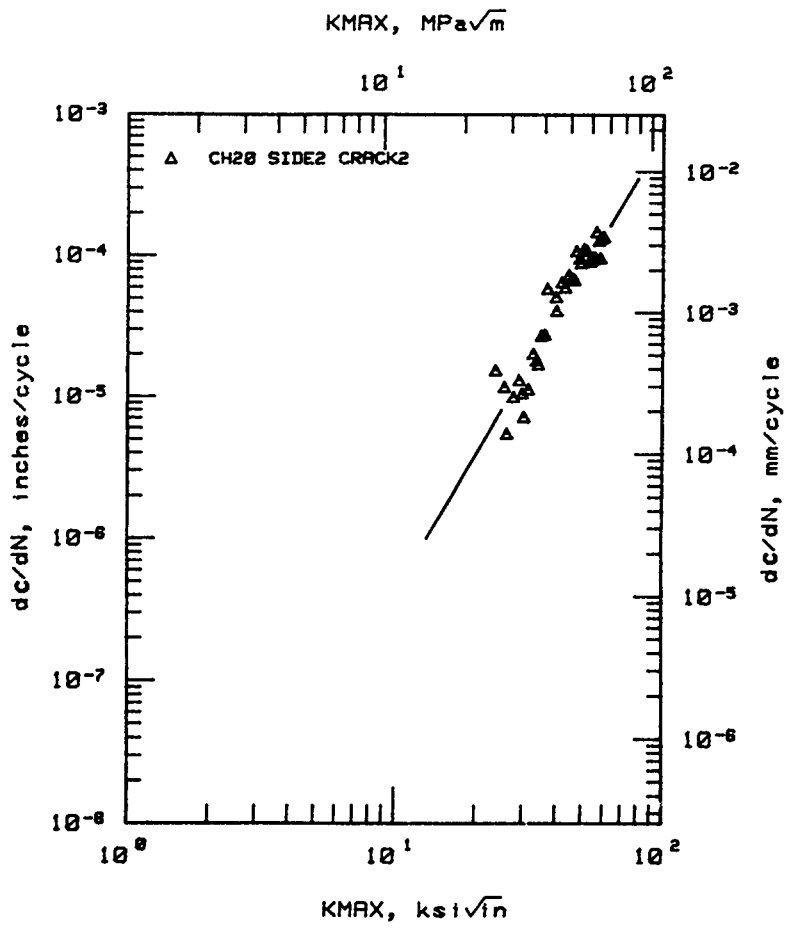

CH20/crack 2,2; elastic

b. crack-growth rate versus K_{mx}

FIGURE 18. (Continued)

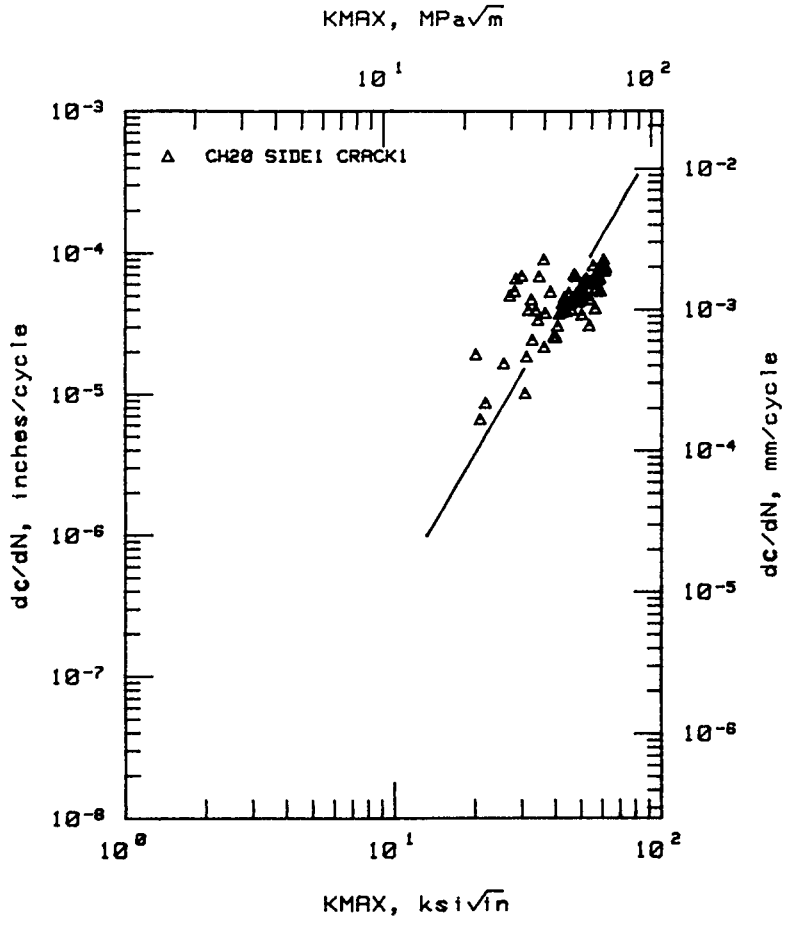

CH20/crack 1,1; elastic

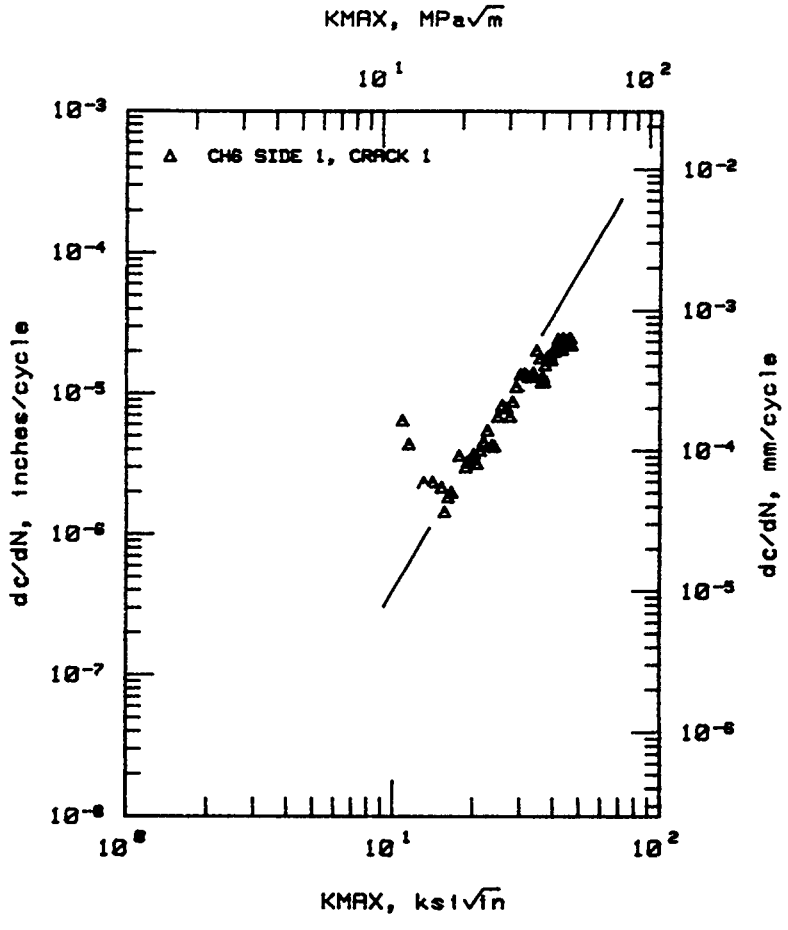

CH6/crack 1,1; elastic

b. (continued)

FIGURE 18. (Continued)

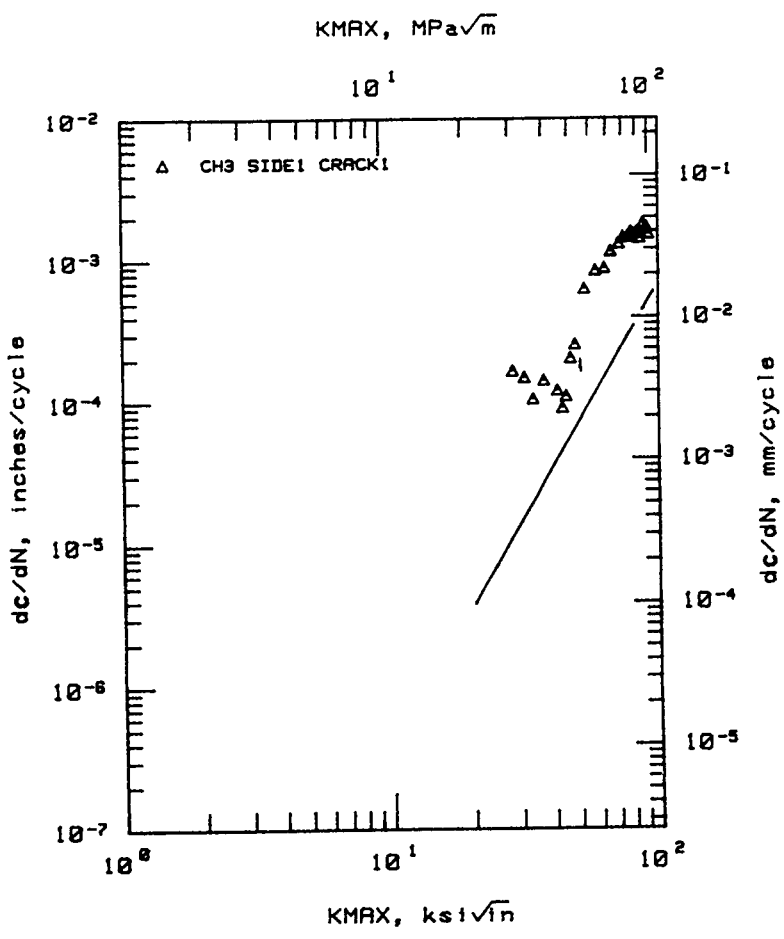

CH3/crack 1,1; inelastic

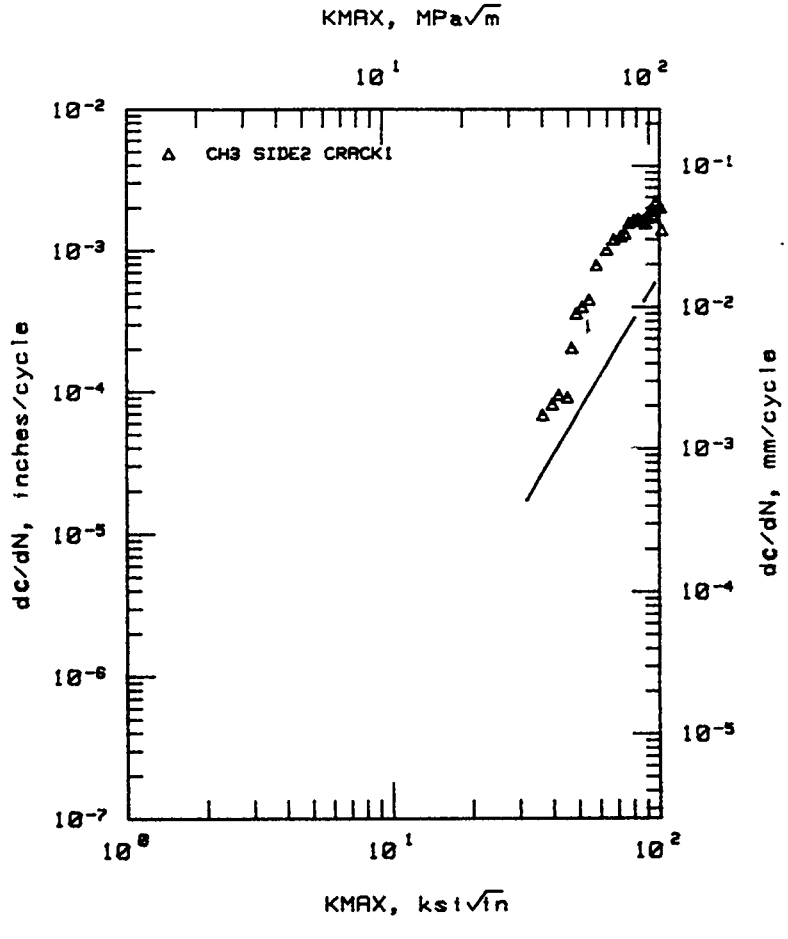

CH3/crack 2,1; inelastic

b. (continued)

FIGURE 18. (Continued)

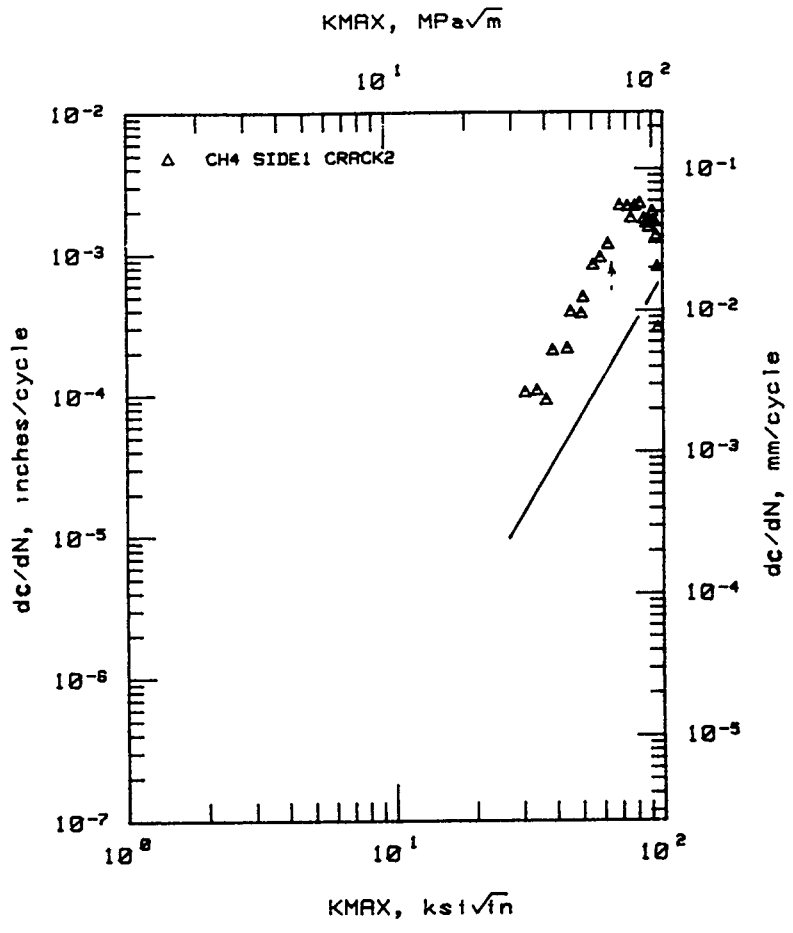

CH4/crack 1,2; inelastic

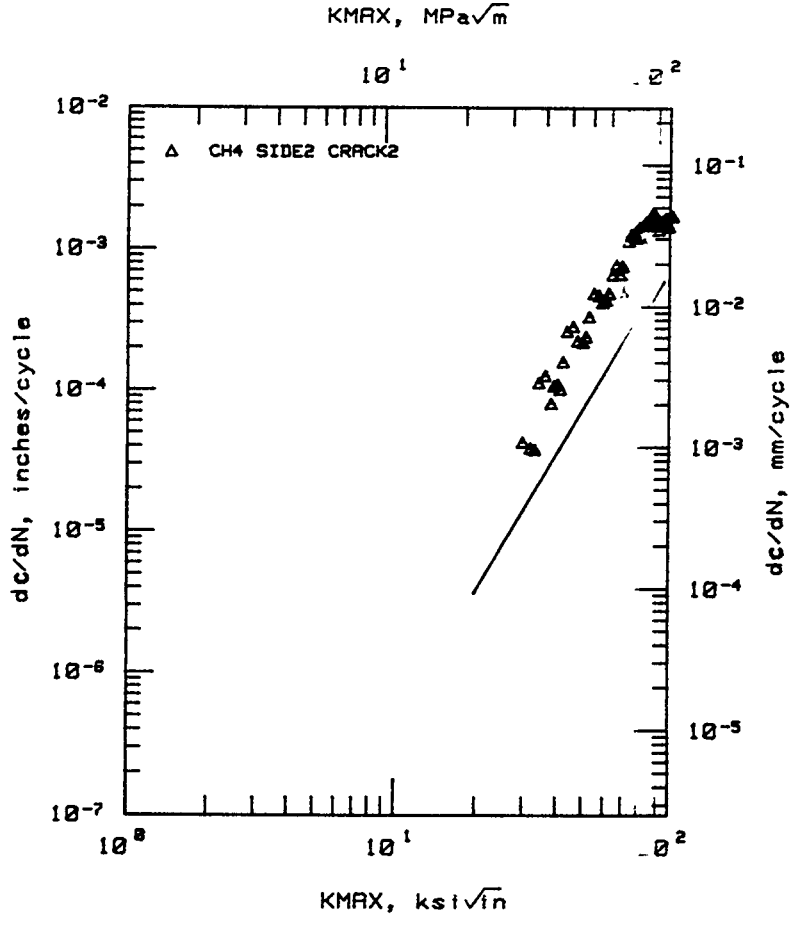

CH4/crack 2,2; inelastic

b. (concluded)

FIGURE 18. (Concluded)

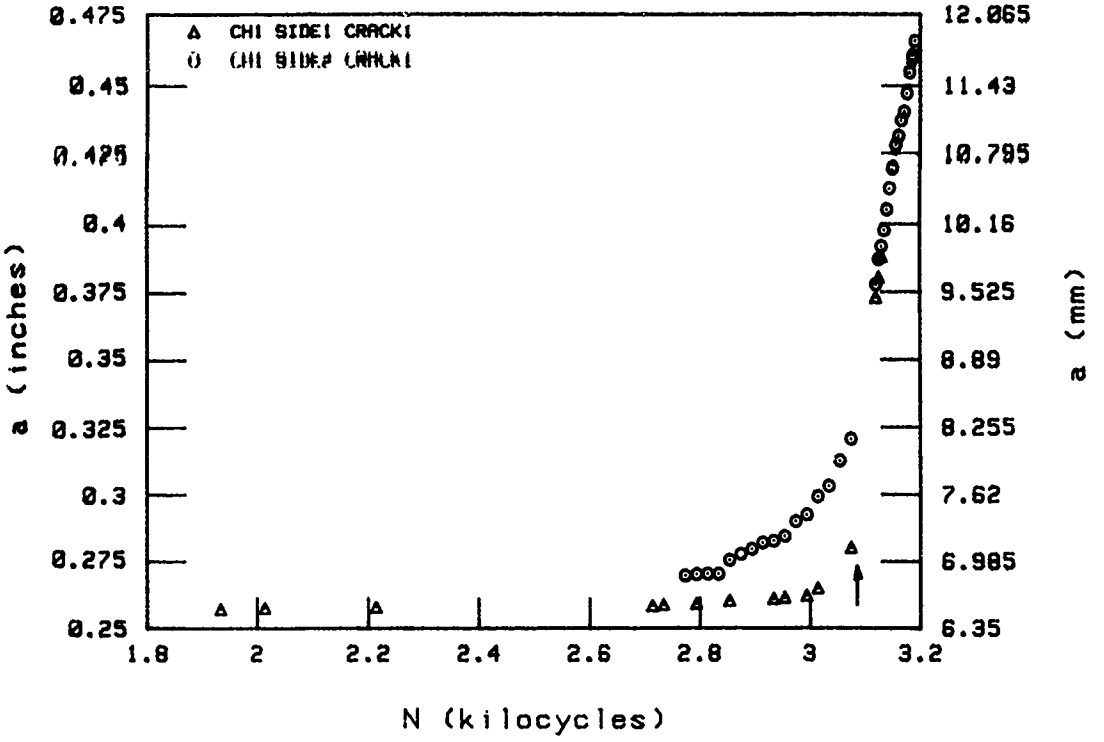

CH1/crack 1

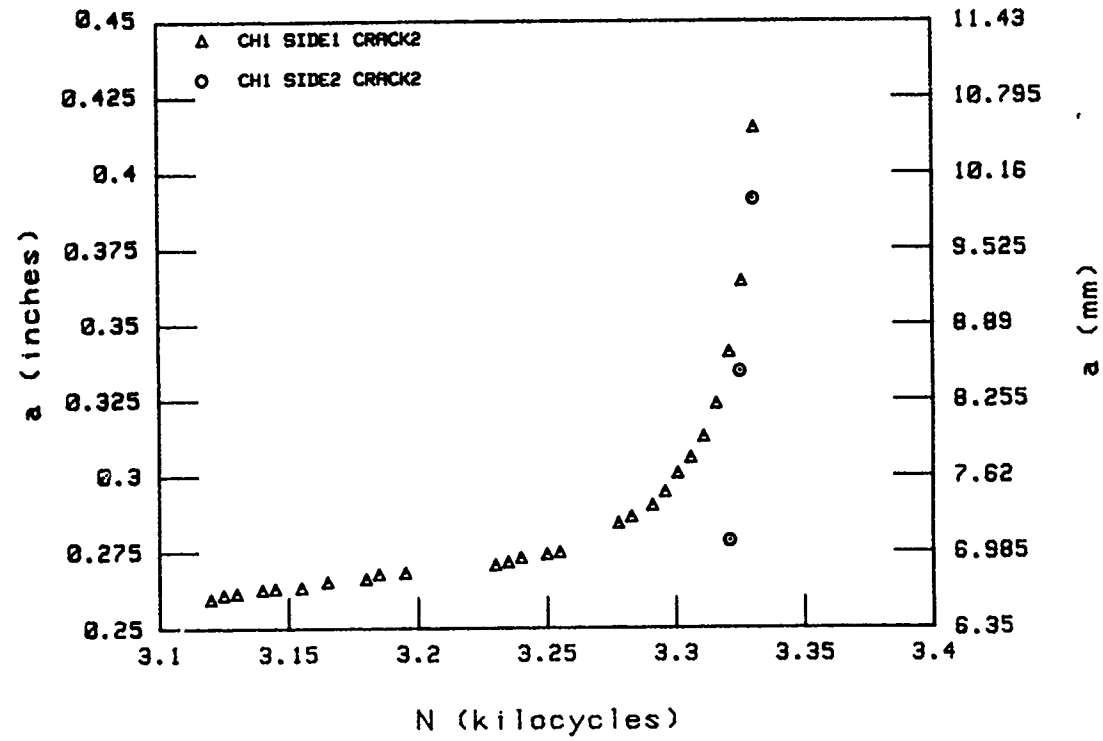

CH1/crack 2

a. crack length versus cycles for corner cracks in an inelastic field

FIGURE 19. INFLUENCE OF NATURAL INITIATION (INITIATION TRANSIENT), FREE SURFACE, AND 3D CRACK CONFIGURATION ON CRACK GROWTH IN AN INELASTIC NOTCH FIELD AT R = -1 AND 20 C

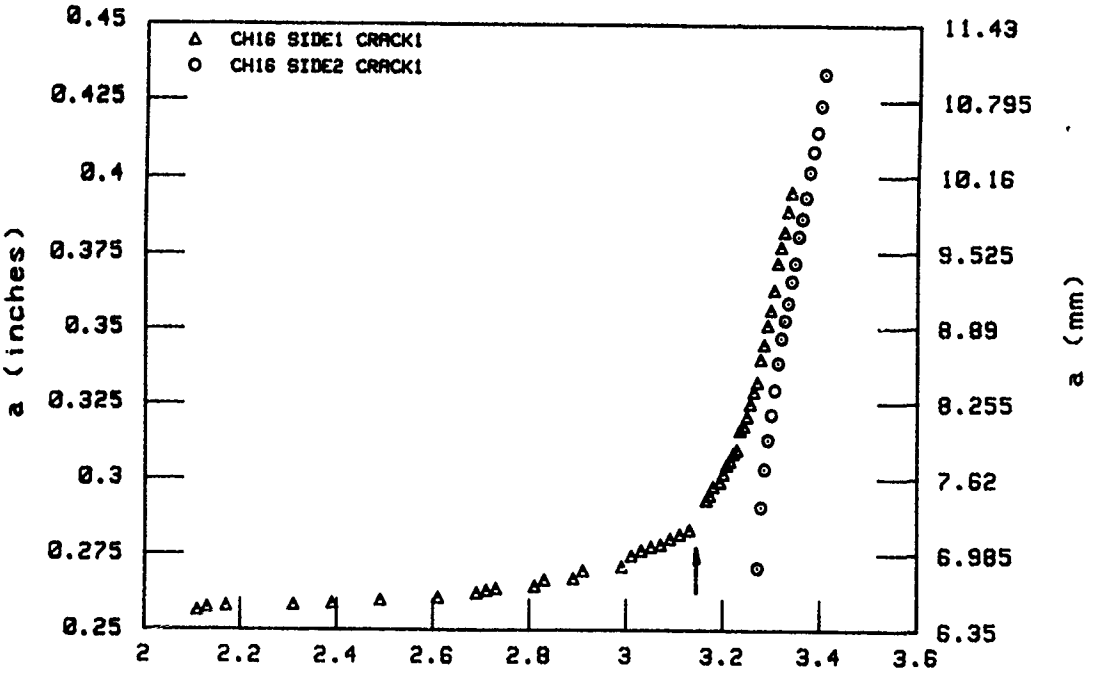

CH16/crack 1

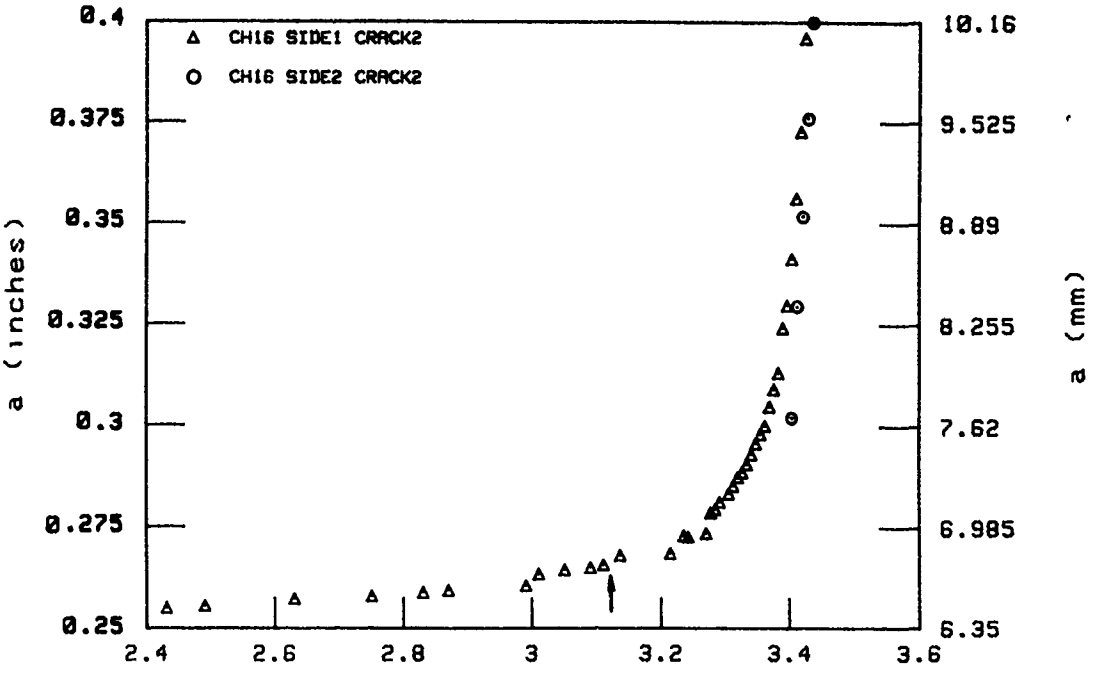

CH16/crack 2

a. (continued)

FIGURE 19. (Continued)

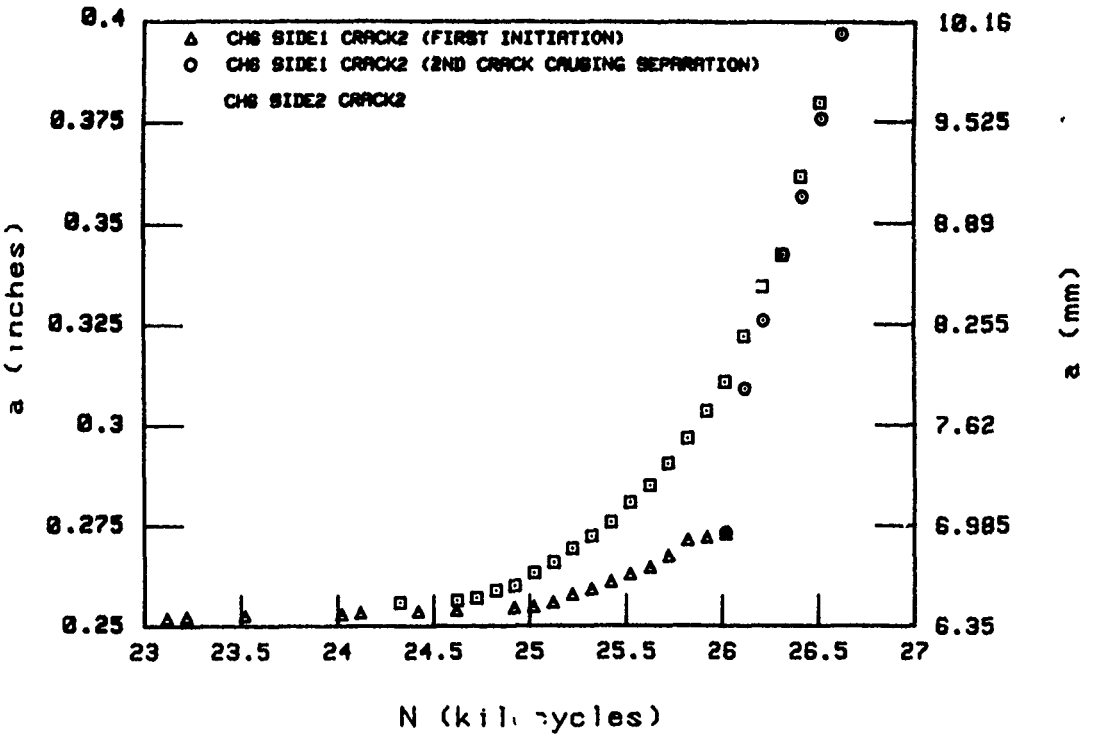

CH6/crack 2; corner vs plane preflawed, and inelastic versus elastic in Figure 19 because the preflaw was inadvertantly omitted at one notch root leading to major differences in initiation lives, and causing very asymmetric growth

a. (concluded)

FIGURE 19. (Continued)

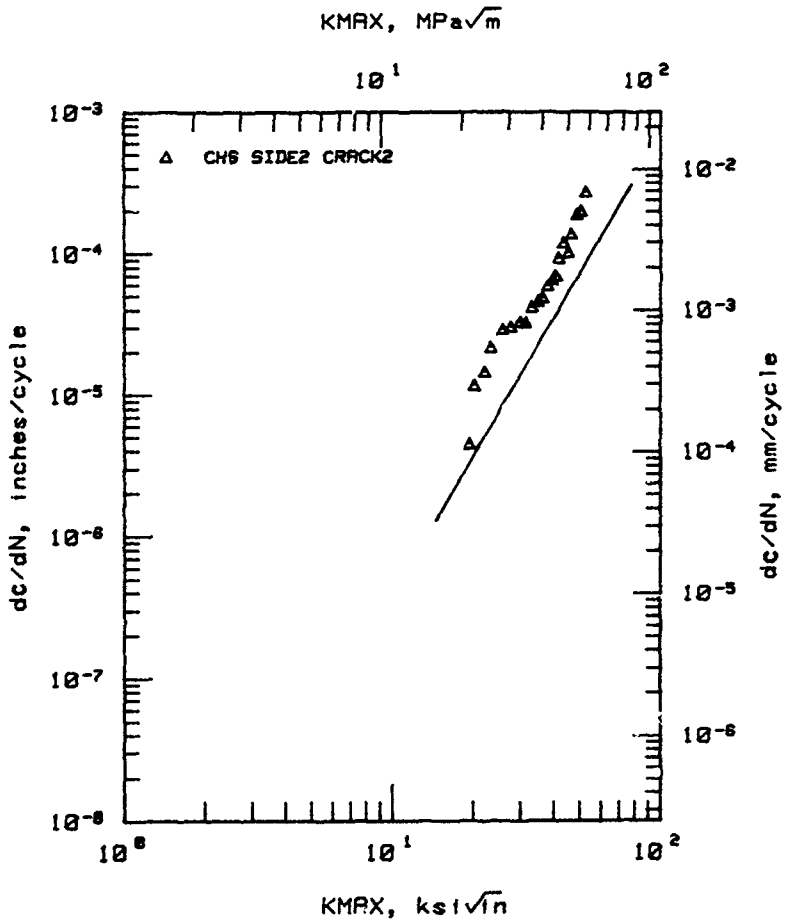

CH6/crack 2; analyzed as an axisymmetric through crack

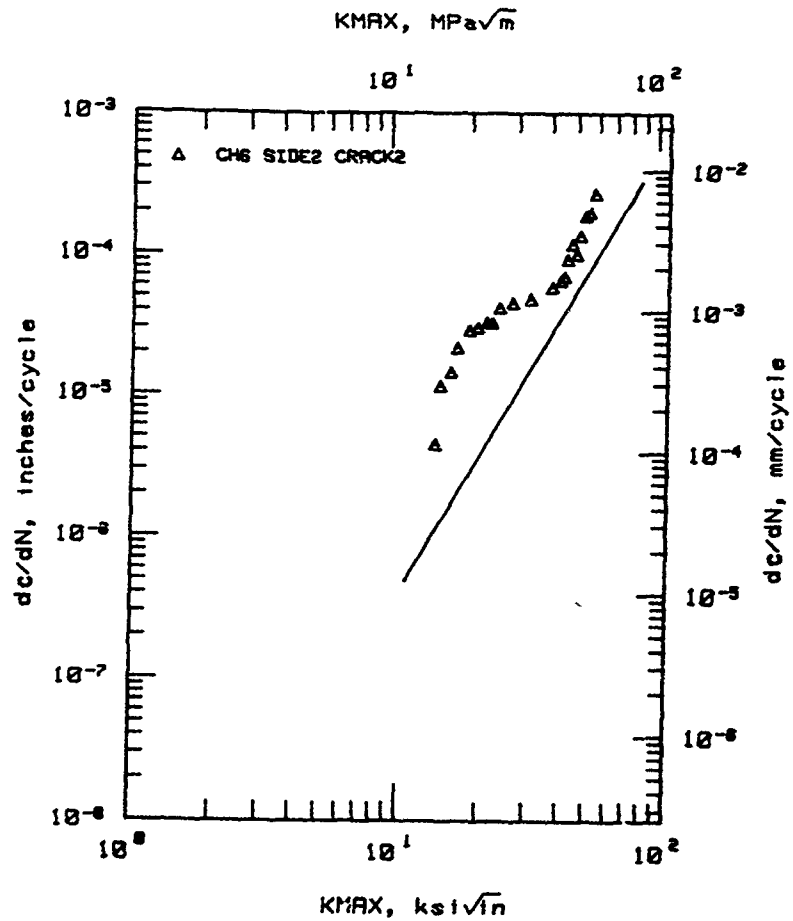

CH6/crack 2, analyzed as a corner crack in asymmetric cracked plate

b. crack growth rate versus K_{mx}

FIGURE 19. (Continued)

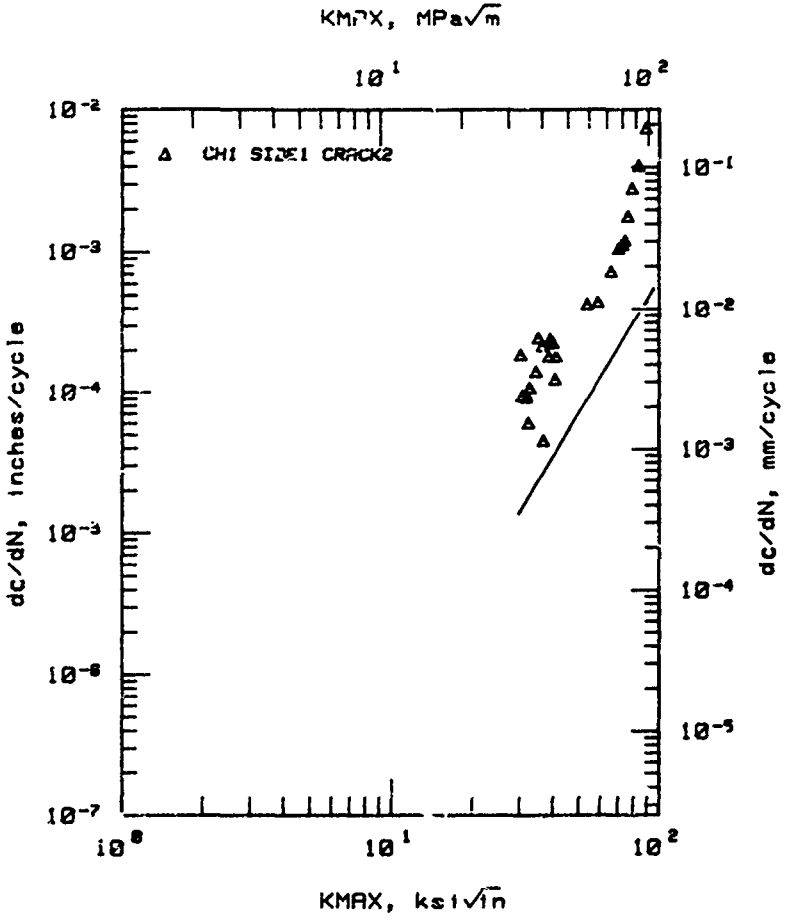

CH1/crack 1,2; analyzed as a through crack

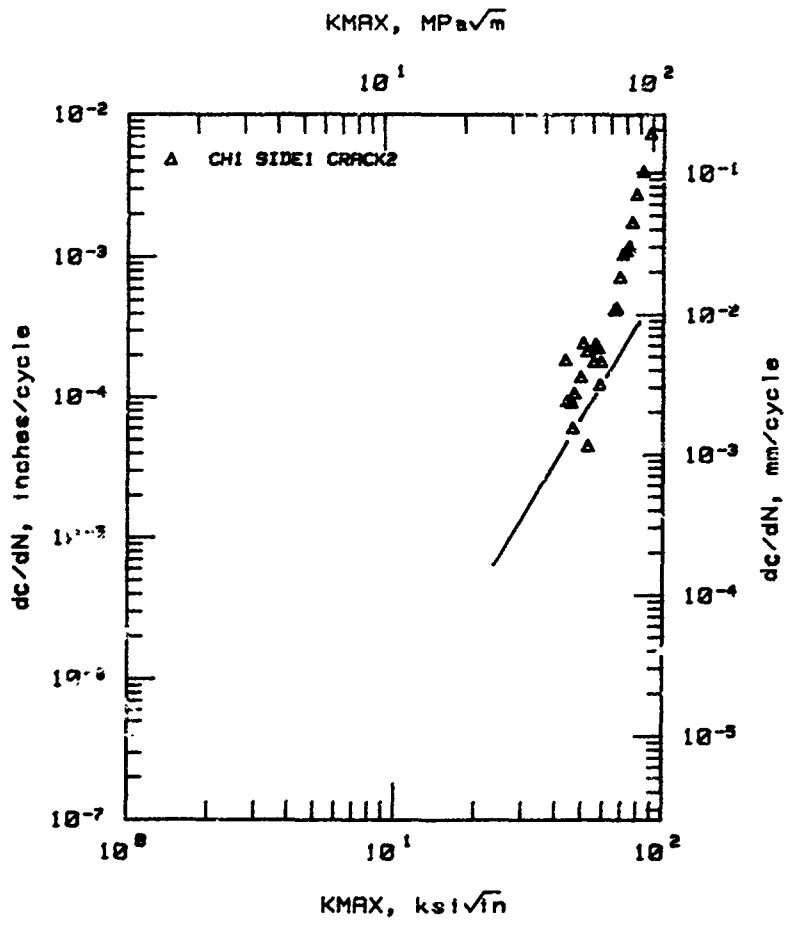

CH1/crack 1,2; analyzed as a corner crack

b. (continued)

FIGURE 19. (Continued)

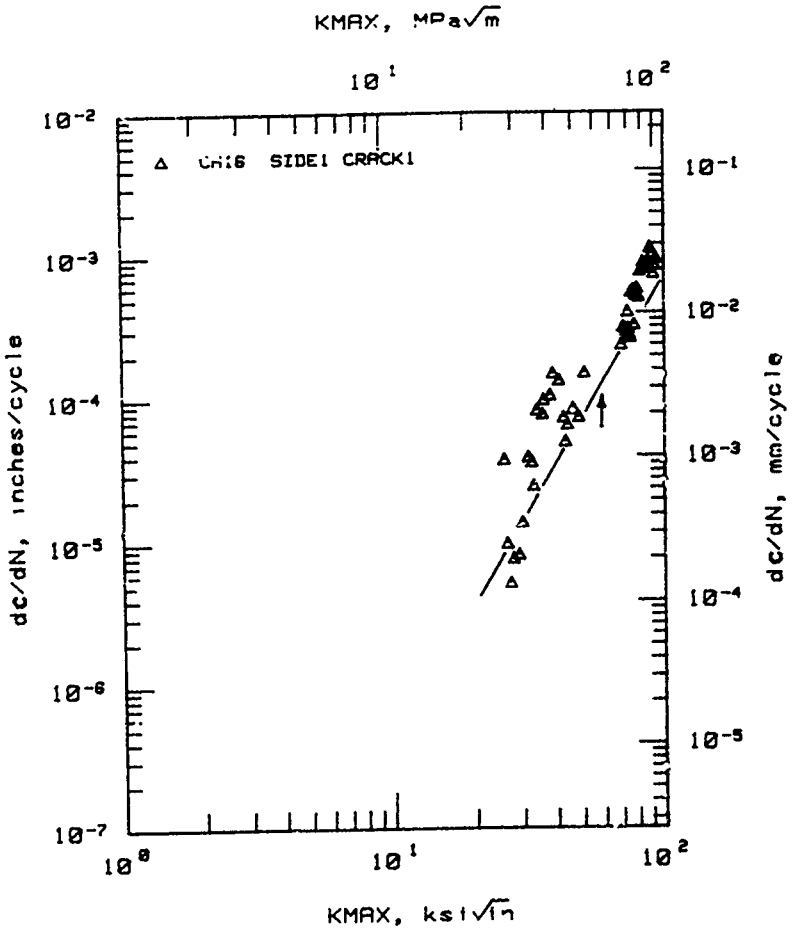

CH16/crack 1,1; analyzed as a through crack

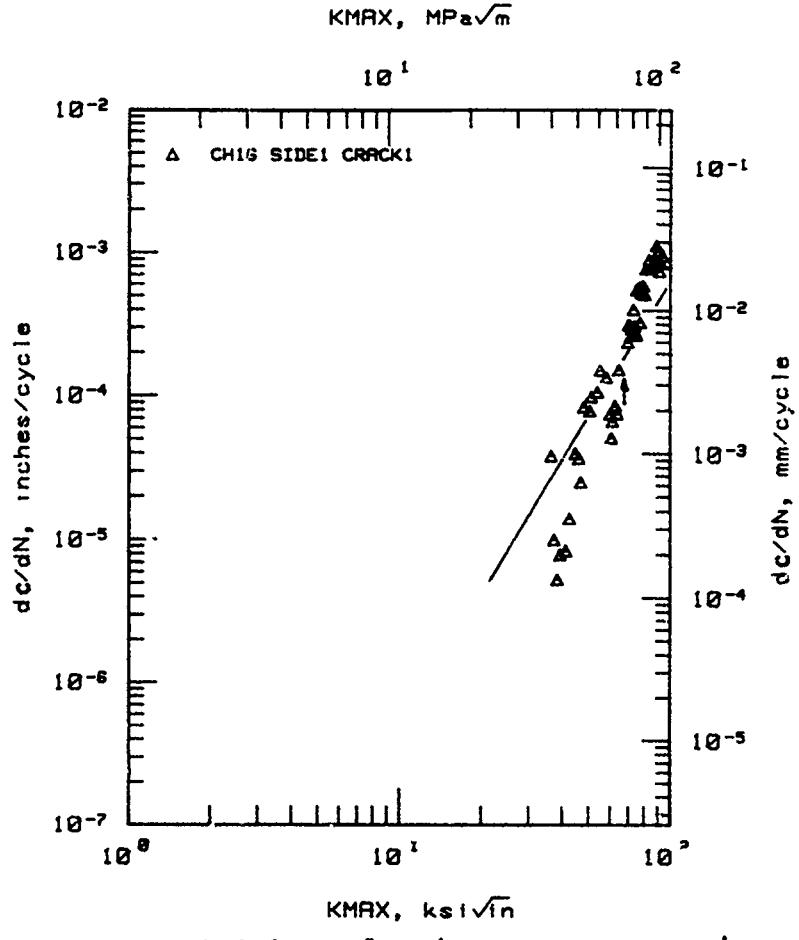

CH16/crack 1,1; analyzed as a corner crack

b. (concluded)

FIGURE 19. (Concluded)

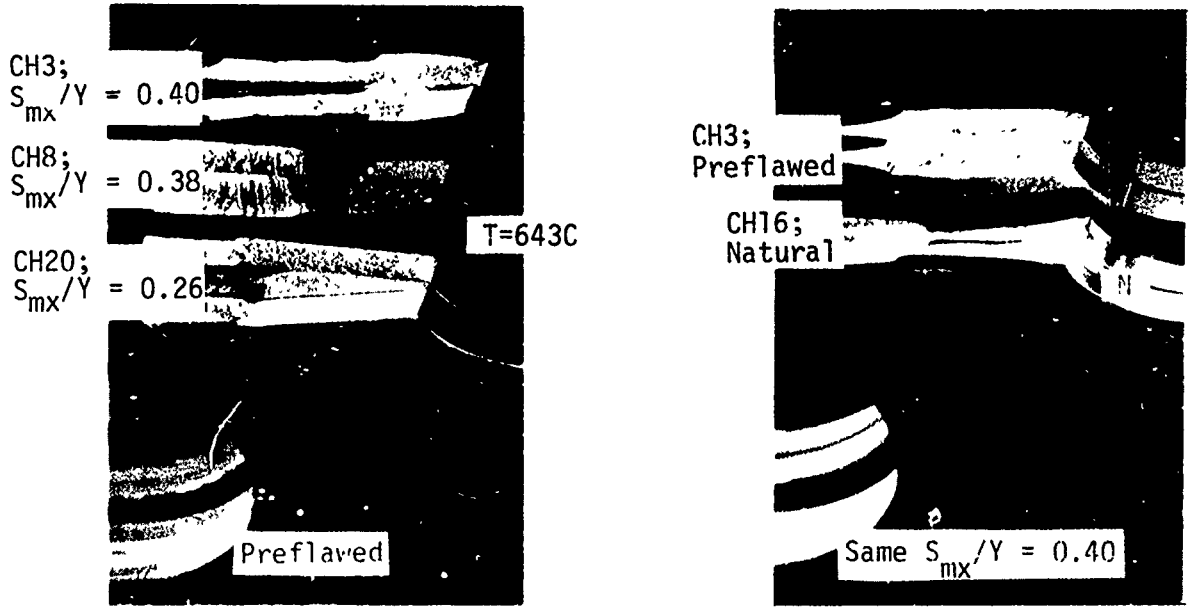

FIGURE 20. FRACTOGRAPHS OF ROOM AND ELEVATED TEMPERATURE FRACTURE SURFACES AT COMPARABLE ΔK

DISCUSSION OF THE RESULTS

This section presents a discussion of the experiments designed to explore the short-crack effect in Inconel 718. These experiments have been performed with a view toward developing a predictive model for RFC analyses valid at crack sizes below the current capabilities of LEFM*. Fractographic results are introduced as appropriate to aid in understanding the observed trends and their implications for Inconel 718 and other engine materials.

Center-Cracked Panel Specimens

The literature suggests that large values of r_p/a tend to be associated with a short-crack effect. The results for the CCP specimens share a number of common features related to the value of r_p/a.

Table 1 listed normalized values of crack tip plasticity--r_p/a--based on plane stress LEFM calculations. Note that two tests had r_p/a ratios between 0.1 and 0.2, while two other specimens represented the interval 0.2 to 0.3. The remainder had values of r_p/a between 0.3 and 0.32. The values of r_p/a considered represent the practical limit of what can be achieved subject to two constraints: (1) the fracture toughness, and (2) the desire to examine somewhat realistic stress levels and stress intensities. The fracture toughness constraint is set by the stress level that can be applied before pre-existing microstructural or microgeometric defects extend unstabily on the rising portion of a fatigue cycle. This bound leads to data generated for Inconel 718 at lower peak stresses (normalized to yield or flow stress) and much lower values of r_p/a as compared to the data generated for the lower strength materials which dominate the literature.

A value of $r_p/a = 0.1$ generally is considered as an upper bound limit for valid applications of LEFM. The values of r_p/a from 0.1 to 0.32 addressed in this study do not satisfy this confined flow requirement. But,

---

*It is to be emphasized that the short-crack effect is material-and application-specific (e.g., for discussion see [41]). Any analysis developed and demonstrated valid to a lower limit crack size for one material and application (load, geometry, etc.) is not general, and should not be applied indiscriminately.

neither are they indicative of large-scale plasticity relative to the crack length. (Values of r_p/a on the order of 100 have been found for short cracks in the absence of notch field effects [4].)

Because the conditions addressed by the CCP data at r_p/a near 0.1 meet or just exceed a usually accepted limit for confined flow, an LEFM characterization of the crack driving force is valid within usually accepted standards. For the remainder of the tests, values of K may be somewhat in error. But, as compared to cases in the literature where a short-crack effect is observed at very large values of r_p/a for finite growth-rate conditions, all cases considered represent very confined flow.

By most standards, this study deals with small r_p/a, whereas the literature tends to focus on large r_p/a. Therefore, analysis found appropriate for small r_p/a in this study are not sufficiently general to deal with large r_p/a. Likewise, because of the radical differences between brittle and ductile initiation, factors identified as being significant for large r_p/a in Reference 4 may not be keys to the behavior of data reported hereafter.

Relative differences in r_p/a may have led different authors to postulate very different models for the short-crack effect. Results where r_p/a is large all tend to be associated with plasticity, examples of which include ΔJ and ℓ_o (e.g., [42]), and the effects of closure and notches (e.g., [10,43,44]). On the other hand, many argue that LEFM is valid for very small cracks where r_p/a is small (e.g., [45-47]). An obvious question arises in this context: can r_p/a be used as a criterion to assess whether or not to expect a short crack effect in engine RFC analysis? Certainly some data indicate the answer is yes. But an answer based on this study must await the following discussion of the experimental results generated.

Influence of Stress Level. The influence of absolute stress level on the growth of short cracks is presented for R = 0.01 and room temperature in Figure 13. Included are results for four stress levels (for comparable crack lengths) that represent values of r_p/a^* equal to 0.31, 0.26, 0.22, and

---

* For all CCP specimens (CC prefixes), r_p/a is taken with respect to the crack length at wake removal, as listed in Table 1.

0.16, for CC13, CC11, CC9, and CC14, respectively. These develop at values of maximum stress divided by the flow stress* denoted as $\bar{S} = S_{mx}/Y$, that range from 0.67 down to 0.48. Note that these values of $\bar{S}$ are relatively large, but the corresponding values of r_p/a are rather small. As is evident from the figure, the crack growth patterns are similar for all four specimens. There are indications of initially higher growth rates over the first two to four data points.

Regarding the influence of closure as assessed by wake removal, this should be evident as a shift in growth rate following wake removal as shown schematically in Figure 1. On part (a) of Figure 13, this would appear as a change in slope in results just beyond the arrow** which denotes the cycle at which removal occurred. Although they are not well defined, trends in the growth rate before removal and that for the first few points after removal tend to show an abrupt increase in rate for CC13, CC11, and CC14. Wake removal† to reduce closure causes an increase in ΔK_{eff} for a given ΔK. Thus an increase in growth rate is expected. But, the increase observed is at most only a factor of three for these data which cover values of r_p/a approaching the practical limit for this material.

---

* Flow stress is a term relevant to analyses based on strip yield models and is usually defined as Y = (yield stress + ultimate stress)/2. For the present material, Y is larger than the 0.2 percent offset yield stress by a factor of 1.167.

** An arrow is used to denote the cycle number for wake removal whenever the technique is employed. Likewise, on da/dN versus K_{mx} plots, the arrow denotes the level of K (or crack length at wake removal). These symbols are used throughout the remainder of this report. The short line on the abscissa denotes the initial crack size on this and all subsequent a-N plots.

† Wake removal is by low power, EDM wire cutting using 50 μm diameter wire. The system is numerically controlled to a reference position set when the starter flaws are cut. Results indicate that such wire cutting alters the microstructure to a depth less than 10 μm. Once the crack reinitiates and grows through this < 10 μm layer, the results generated represent the base material and heat treatment. The editing procedure coupled with the growth rate calculation procedure automatically skips this region, so that it is not a factor in data interpretation.

The modest increase in growth rate due to wake removal is much less than the factors of 10 to 100 associated with the short-crack effects reported in the literature. But the values of r_p/a developed for this material are also orders of magnitude less than values typical for the ductile initiation materials that dominate the literature. The present data, therefore, are not incompatible with the literature; indeed, limited plasticity would be expected to generate limited closure. In the limit, as $r_p/a \rightarrow 0$, inelastic action becomes so confined that the closure load approaches the lower load in the applied cycle. Under this condition, $\Delta K_{eff} = \Delta K$ and wake removal can have no influence whatsoever.

For the highest value of r_p/a (CC13), only 40 μm remained after wake removal. Evidently, even when wake is removed to within the limits of current wire EDM capabilities, closure does not appreciably alter crack-growth rates at the practical upper limit of r_p/a for this material. It may well be that this same trend would be observed for other materials at comparable levels of r_p/a.

Based on the available data in the literature and the results in Figure 13, the value of r_p/a may be a major factor controlling the incidence of a short-crack effect. For the Air Force, the implication is that microcrack growth via a reversed plasticity mechanism in high-strength, fine-grained engine materials may not be strongly dependent on closure.

Results for CC11/crack 2 presented in Figure 13(a) are replotted on coordinates of da/dN and K_{mx} in Figure 13(b) to illustrate the trends in part (a) as compared to so-called long-crack data. As expected in view of the a-N data, this plot shows that the growth rate for the first two points lies above the trend for the ensuing crack growth. Correspondence of the data for this specimen with those of the long-crack reference curve is good in that, except for the first two "short-crack" results, these data fall along the R = 0.01 trend line of Figure 12(b). While a few data points for the early growth of this crack do lie above the long-crack trend, the difference in rates is small in comparison to data for which r_p/a is large.

In summary, the results covering normalized stress levels from 0.48 to 0.67 and initial stress intensities as low as 15 MPa $\sqrt{m}$ do not indicate

significant differences in the a-N trends observed. When plotted on da/dN-K_{mx} coordinates, the results for all samples also show similar trends. Thus, it is concluded for this fine-grained, high-strength material that changes in absolute stress do not cause changes in microcrack-growth behavior correlated in terms of K_{mx}, over the range of stress and finite growth rates considered. This conclusion could be false at much lower stresses.

Wake Removal. Some insight as to the significance of closure can also be gained by exploring different amounts of net wake under otherwise identical conditions. To emphasize the effect, different wakes have been considered at the largest value of r_p/a found practical in this material ($r_p/a = 0.31$) at the shortest crack length possible using available EDM facilities.

Comparison results have been developed in CC10 and CC12, with average net wakes at 40 μm and 115 μm. The data plotted in Figures 14(a) and 14(b) show little difference between the respective trends. For CC10, the results show high growth rates* when the cracks are small, after which the trends are similar to the data developed for CC12 as well as that generated using conventional long crack samples. With reference to Figure 14(a), an influence of wake removal cannot be seen for either specimen. This is contrary to the observations in Figure 13 for sample CC13, conditions for which are identical to CC12 (cf Table 1). As is evident in Figure 14(b), results for short crack growth in CC10 lie above the long-crack trend.

In summary, these results do not indicate that closure depends on the net wake as would be expected if extensive closure occurred. Since, with a few exceptions, applications of wake removal fall within the range of net wake considered in Figure 14, and since these represent the practical limit of r_p/a for this material, the results of Figure 14 imply that net wake is not a factor in this study. But, this does not mean that (in this study or in general) crack-growth rate and closure do not depend on the net wake.

---

* The fact that symmetric crack growth does not occur may in part be responsible for this observation, particularly for the second crack.

First, for the present experiments, the largest value of r_p/a that can be achieved is relatively small. And, the extent to which closure develops depends on the extent of inelastic action local to the crack tip. Small levels of r_p/a (as in the present $r_p/a \leq 0.32$), therefore, are expected to develop limited closure as compared to cases where $r_p/a \sim 10$ to 100 in the literature. For this reason, the absence of an influence of net wake may simply mean that plasticity-induced closure is not a controlling factor in this material. A second consideration relates to the fact that the effect of closure may be confined to a region very near the crack tip. This does not appear to be the case for the present study since evidence of increased growth rates after wake removal has already been discussed, and more will be introduced.†

Another approach for examining the influence of closure on the microcrack-growth process is to remove wake over a range of R. Varying R is useful because more negative values of R cause more compression yielding at the crack tip. In turn, this leaves the crack tip further open as compared to cases with more positive values of R, and thereby enhances the effect of closure on growth rate*. To emphasize closure, tests have been conducted at the largest value of r_p/a coupled with the most negative value of R possible. This has been achieved subject to the limitations of system stability using buckling restraints for samples CC12, CC19, CC15, and CC18. Results for these specimens, which represent values of R equal to 0.01, -0.6, -1, and -1, respectively, are plotted in Figure 15. Examination of the a-N data (Figure 15(a)) indicates their behavior is comparable to that already discussed. In some cases, the growth rate for the physically smaller cracks

---

† If closure had been confined to within 40 μm of the crack tip in this study, the a-N data would fail to show a change in growth rate as a result of wake removal in all cases. The 40 μm limitation is not inherent in the wake removal concept. Rather it is a constraint, imposed by the practical implementation of numerically controlled EDM using 50 μm diameter wire, to avoid cutting away the crack tip along with the wake. Application of the wake-removal concept, therefore, cannot be used to study closure effects if they are indeed confined this close to the tip.

* If, as just discussed, closure is not a major factor controlling microcrack growth at low values of r_p/a, more negative values of R are expected to cause only modest changes in growth rate.

is greater than for subsequent growth. And, for CC15/crack 1, there is an abrupt increase in growth rate following wake removal. But, as with the other specimens, there is no marked pattern in these trends, either in the behavior for physically small cracks or after wake removal. As evident in Figure 15(b), growth rates for small cracks and after wake removal lie above the long-crack trend [Figure 12(b)].

In summary, the results presented failed to show a marked dependence of growth rate on R, for small cracks and after wake removal. This result is consistent with the previously discussed data.

Summary for CCP Specimens at 20 C. Overall, the data for the CCP specimens indicate small cracks may grow at rates slightly in excess of the long crack trend. But, the difference in rates was small and always less than a factor of 4. Wake removal was observed to cause an abrupt increase in growth rate about as frequently as physically small cracks were observed to grow at higher rates as compared to the long crack trend. When wake removal was observed to have an effect, the ensuing trend showed rates increased (coincidentally) by a factor less than 4. This suggests that the limited value of r_p/a possible in the high-strength, fine-grained material limits plasticity-induced closure and does not exceed the confined flow limitation of LEFM (in a practical sense). Its influence, if any, on growth from preflaws leads to increased crack-growth rates by a factor less than 4 for physically small cracks over the range of conditions examined. As indicated throughout, the absence of a short-crack effect causing increased growth rates for small r_p/a is consistent with the literature where significant short-crack effects tend to be associated with r_p/a on the order of 10 to 100.

The Effect of Cycling at 643 C on a CCP Specimen. Specimen CC3 has been used as a preliminary check of whether results developed for small cracks at 20 C carry over to temperatures more representative of service. Comparison data for otherwise matched mechanical conditions therefore have been developed

at 20 and 643 C. Specifically, the crack geometry, R, and frequency* match as closely as possible the conditions for CC12. The maximum stress also has been chosen to match CC12, with provision made to simulate r_p/a accounting for temperature-reduced flow resistance based on handbook properties.

As is evident in Figure 16(a), the crack growth versus cycles response looks similar to that developed at 20 C. Both cracks show that an initially higher rate develops for the first two points, but neither (data missed for one crack) show any evidence of a closure effect upon wake removal. As evident in Figure 16(b), the data for CC3 lie above the 148 C trend line, which is taken to approximately a 20 C long crack trend for the GE data. Also, they show a similar shift from 148 C to 643 C--including the ΔK dependence--as do the long surface crack GE results shown in Figure 12(f). In this respect, whatever the source of the ΔK dependence of growth rate shift with temperature, it seems to develop the same extent for small through cracks and long surface cracks.

The limited data developed at 643 C for the fine-grained Inconel 718 used in this investigation show trends similar to that generated at 20 C. The only major difference is that the fracture surface for the 643 C data shows Mode I cracking occurs to longer crack lengths, as compared to its 20 C counterpart, for results developed in this study. This difference in fractography can be seen in Figure 20. Also, the fracture surfaces developed at 643 C are smooth as compared to their long crack 20 C counterparts. The fractographic evidence thus shows a decreasing propensity for surface roughness (and therefore roughness-induced closure) as temperature goes from 20 C to 643 C. It follows that, as compared to 20 C data, the same imposed ΔK and R may develop a larger effective stress intensity factor range at 643 C.

---

* Lower frequencies probably would develop trends different than that observed in this preliminary study.

Center-Notched Panel Specimens

Results developed using CNP specimens, designated by the prefix CH, share the same material-related constraints discussed in regard to the CCP samples. One constraint is the limited peak stress imposed by the fracture brittle nature of the material studied. Accordingly, the normalized nominal stresses ranged from 0.40 to 0.20. These are lower than the 0.67 to 0.43 investigated for the CCP samples since the notch field serves to locally elevate the stress. Because the notch field is local, this geometry permits testing at higher local levels of the ratio at plastic zone size, r_p, to surface crack length from the notch root, c. Values of this second constraint, r_p/c, are tied to values of peak stress and to the depth of the notch plastic field along the transverse net section, denoted as x_p. At low levels of S_{mx}, because the notch field is elastic, the crack's plastic zone is the dominant (only) plastic zone. When this is the case (i.e., $x_p = 0$), values of r_p/c of 0.21, 0.35, and 0.31 have been developed in samples CH6, crack 1; CH20; and CH2; respectively. These values of r_p/c are similar to values of r_p/a developed in the CCP samples. In all other cases, the crack grows (at least over part of its length) through an inelastic notch field. One depth of notch field has been successfully explored--460 μm. The value of r_p/c developed in this case is 0.85. This value of r_p/c is much larger than the 0.1 generally associated with valid applications of LEFM, but are very small in comparison to values often associated with short crack effects* as discussed for the CCP samples. Likewise, the depths of the notch plastic fields possible in this high-strength, fracture-brittle† material are small

---

* Recall that the present interpretation of this "short crack effect" terminology in an LEFM/RFC sense is a behavior that leads to nonconservative predictions--that is, a crack growth rate in excess of the LEFM long crack trend.

† The term fracture brittle herein denotes a material which exhibits limited plastic flow with cracking. Fatigue crack nucleation occurs with very localized and very little flow meaning only a limited wake of plasticity and very little propensity for closure. Crack growth occurs at relatively small values of r_p/a, even for rather large nominal stresses. This term does not imply a low fracture toughness.

compared to those found associated with short crack effects in the literature. As with the CCP specimens, tests on CNP samples have been used to explore whether or not the initial growth of short cracks occurs at rates in excess of LEFM predictions. Also, as with the CCP samples, CNP specimens have been used to assess the role of closure via the wake removal concept. Reference to Table 3 indicates that the CNP samples also have been used to study the influence of natural initiation and 3D effects (Figures 17 and 19), absolute stress level (Figure 18), and notch stress field (also Figure 18). An attempt had also been made to examine the influence of temperature. (While fractography is possible for the test at 643 C, all growth rate data have been lost due to a film processing problem--see Table 1.) Results for through cracks in preflawed CNP samples are presented first. Then Figures 17 and 19, which involve natural initiation and corner cracks, are considered. Note that cracks in preflawed samples can be (and have been) considered as plane fronted while those for corner cracks have aspect ratios a/c, of about 1 for a/t up to 0.25 and between 1 and 3 at breakthrough. After breakthrough, the transition to a plane-fronted crack with nearly equal surface lengths occurs very quickly.

Influence of Stress Level and Notch Fields. Results for samples CH3, CH4, CH20, and CH6 crack 1 can be used to examine the influence of absolute stress level on crack-growth rate behavior. But since the size of the notch plastic field and the value of r_p/c increase with increases in stress, both the stress level and the depth of the plastic field must be considered together.

Results for the CCP samples indicated that, by itself, r_p/a (note the nomenclature r_p/a for CCP means the same as r_p/c for CNP specimens) does not lead to differences in growth behavior over the range of values investigated. The extent to which this carries over to notches can be examined in the absence of notch plasticity effects using the results for CH6 crack 1 and

CH20. These data, plotted in Figure 18a on c-N† coordinates are similar to results for CC14, CC9, CC11, and CC12.

The only difference evident in comparing CNP and CCP results on c-N coordinates is the absence of an initially higher growth rate in the CNP samples, such as that observed in many of the CCP specimens. But this difference is not surprising since, for the CCP case, K increases only with $\sqrt{a}$ whereas the strain gradient due to the notch field in the CNP case causes K to increase very rapidly*. Thus, the factor of less than 4 increase in da/dN observed in the CCP results occurs in a situation where subsequent growth is not overshadowed by the influence of the notch field. Trends for inelastic action at the notch, developed in CH3 and CH4, are similar to that just discussed for elastic behavior in regard to CH6 crack 1 and CH20. This is evident in comparing the results for these specimens, as shown in Figure 18. The only exception occurs for CH3, crack 1, which shows growth rates over the first few points slightly above those for the ensuing cycles.

The c-N data for the CNP samples do not indicate trends that could point to even a modest short crack effect, as did the data for CCP specimens. But because the influence of the notch field masks the trend evident when only $\sqrt{a}$ drives K, the data must be examined on coordinates of dc/dN and K_{mx} before conclusions can be drawn. Data showing growth rate as a function of K_{mx} in the absence of inelastic notch action are plotted in Figure 18(b) for CH6 crack 1 and CH20. In comparison to the long crack trend, the results for CH6, crack 1,1 (the only results captured for small cracks) show growth rates for small cracks in excess of the long crack trend by more than an order of magnitude! Similar although less dramatic and somewhat scattered results develop for CH20 at crack 1,1, crack 1,2, and crack 2,2. This trend is not shown for crack 2,1 because data are not available for it at small crack sizes.

---

† The system of arrows to denote wake removal and a line to denote the initial crack length used for a-N plots is retained for c-N and dc/dN-K_{mx} plots.

* This can be seen by comparing values of d(K/S)/dc per Appendix F, Eq. F.3 for small cracks with F(ℓ)--the CNP case--and without F(ℓ)--the CCP case--in the definition of K, Eq. A7.1.

The increased values of dc/dN just examined for growth through elastic fields becomes more complex for growth through an inelastic field, as evident in Figure 18(b) for CH3 and CH4. As with cracks in the elastic notch field, a decrease in growth rate with increasing crack length is evident particularly for CH3 crack 1,1 and CH4 crack 2,1. However, in contrast with the results for the elastic field, this decrease ceases at a trend which lies a factor of 5 to 10 above the long crack trend [Figure 12(b)]. The data for an elastic notch field quickly approaches the long crack trend; however, following initially high growth rates in CH3 and CH4, growth rates 5 to 10 times that of the long crack trend are evident so long as the cracks grow in the inelastic field. As apparent, at least for CH3 crack 2,1 and CH4 crack 1,2 and crack 2,2, growth continues at rates 5 to 10 times greater than the long crack trend at crack lengths greater than 575 μm and less than 1 mm. Beyond this, there is a decrease in growth rate evident toward the long crack trend. But, only for CH4, crack 1,2, is this decrease steep enough to indicate that the growth rate would actually meet the long crack results.* This decrease in growth rate as the crack tip passes into the elastic field in CH3 and CH4 has also been observed in more ductile materials. References 18 and 43 present such trends for steels, whereas References 43 and 44 show such results for 2024 Aluminum. Plausible explanations for such behavior are considered in References 43 and 44.

For the situation just considered, approximate lower bound calculations indicate that x_p = 460 μm (Table 1). Given the accuracy of this approximation, it is reasonable to conclude that errors in the LEFM calculation of crack driving force due to local inelastic action are responsible for the 5 to 10 times increase in growth rates. Analysis for cases where cracks grow in an inelastic notch field have been presented in the literature. Several authors have discussed the use of detailed inelastic analysis for this problem (e.g., [48]). In the absence of such detailed solutions, engineering

---

* Given the critical crack size operative at the stress level causing inelastic action, stable tearing is expected to intervene long before growth rates approaching the long crack trend could develop. Further testing beyond this exploratory study are necessary to confirm the apparent very significant short crack effect due to inelastic notch action.

methods based on the influence of local yielding on the crack driving force have proven useful [18,43], and may be appropriate for engine RFC analysis.

Influence of Natural Initiation (Free Surface/Initiation Transients) and 3D Crack Geometry. Consider now the results for CH2 presented in Figure 17. This test involves natural initiation under conditions bounded below and above by test conditions for preflawed samples CH6 and CH20, respectively (Figure 18). Observe from Figure 17(a) that two cracks developed on side 1 whereas only one crack was observed on side 2. Crack 1,1 was first to initiate followed by crack 1,2. Both initiated and grew as circular corner cracks based on stereo macrofractography (35X) until $a/t \doteq 0.25$. At this point, a/c began to increase from a value of 1 to about 3 at breakthrough. Growth of crack 1 to beyond the camera field occurred before 2,2 appeared. Growth of crack 1 outpaced that of crack 2 leading to separation well before crack 2 grew appreciably. Several points concerning the behavior evident in Figure 17(a) are noteworthy as follows.

First, there is an interplay between cracks on adjacent faces of the plate at the same notch root. Crack 1,1 initiated first and grew quickly as a corner crack. Then, because the driving force for c is decreasing as $F'(c/W)$ takes the crack out of the dominance of the notch field (e.g., see Appendices B and F), growth across the transverse net section slows radically. Growth across the thickness is still in the dominance of the notch field so that, even though surface growth has slowed, the crack continues to propagate through thickness. As noted in Appendix B and discussed earlier in regard to Figure 9(c), continued growth in the thickness direction is toward increasing stress intensity factor (as $\sqrt{a}$ increases) so that the through-thickness growth process accelerates as a increases. As $a \rightarrow t$, breakthrough occurs and the shorter "just initiated" crack, being tied to its longer counterpart on the other face, propagates rapidly. The now almost-plane-fronted through crack continues to grow as any other long crack.

In view of the above, the rapid change in growth rate of crack 1,1 is due to the fact that crack initiation generates crack configurations that are not stable as the crack grows longer. Had the value of t/2r been larger,

the results of work cited in Reference 7 and noted in References discussed in Appendix A indicate corner crack initiation could occur along with multiple through thickness initiation. The nearly-plane-fronted through-thickness crack initiated would not exhibit the initial high growth rate and the ensuing transient evident for crack 1,1.

Another facet of the corner cracking process is that corner crack morphologies tend to involve extensive crystallographic cracking. While initially this leads to high rates (perhaps due to the absence of closure), the transition from a mixed Mode I/Mode II to Mode I cracking and the associated increased closure could lead to a continued reduction in rates with continued growth toward a stable crack geometry. In these respects, the result for crack 1,1 is interpreted as an initiation transient due to free surface effects admitted by natural initiation. It is due, for the most part, to the mechanics controlling crack initiation in gradients at a doubly free surface. For the case in point, this initiation transient influenced the first 800 μm of surface crack growth. However, the crack length over which this effect can occur is a function of the gradient, the peak stress, the notch geometry, the plate thickness, and other factors.

Another interesting feature evident in the data of Figure 17(a) is the stepped nature of the crack growth rate, even for longer cracks. Such steps are commonly observed in the growth of cracks during the transition from corner to plane-fronted cracks. To some extent, this can be ascribed to the interaction of separate cracks. But it is more likely attributed to the fact that c is growing in field where d(K/S)/dc is decreasing, whereas a is growing in a field where d(K/S)/da is increasing. This results in an unsteady balance wherein the growth along the crack front has to satisfy counteracting driving forces at the extreme tips of the crack front.

Whether or not the largely mechanics-controlled initiation transient is responsible for a significant portion of the short crack effects is not clear in the literature. But, it is certain that the shape of an initiated crack often differs from that associated with its steady-state "long crack" geometry. Some data in the literature for another engine material [49], IN 100, attest to this fact. In that case, on coordinates of da/dN and ΔK,

the results indicated that the growth rate first decreased and then increased becoming nearly coincident with the long crack trend as crack length increased. This is exactly the tendency for crack 1,1--as shown in Figure 17(b). As evident in the figure, the first crack to initiate also shows initial growth rates in excess of the long crack trend based on LEFM analyses. Note that the effect is enhanced by the use of a corner crack versus (an inappropriate) through crack K solution. In summary, the results for this test show two features often observed in what are called short crack effects. These are initially higher growth rate and a decreasing, then increasing, growth rate.

Comparison of the results in Figure 17 with the corresponding c-N data in Figure 18 shows trends for natural initiation similar to those observed for preflawed specimens. However, there are several differences. First, the trend for natural initiation involves several data points over which the growth rate is very much higher than for subsequent growth while the trend for preflawed geometries (through cracks) does not. As just discussed, this behavior is rationalized in terms of the double free surface which leads to initially high rates of cracking under locally large r_p/c. Decreases in growth rate to the long crack trend follow as a result of the 3D nature of the crack and the associated transient shapes leading to a stable value of a/c.

Another major difference is that natural cracks show significant scatter in initiation and consequent asymmetric crack growth, particularly at low stress levels. In some cases, multiple cracks initiate at the same notch root. Again this tendency is often accentuated at high stresses, as evident in the literature (e.g., [18]). Multiple cracking is evident in the results of CH6, crack 2. While planned for elastic local stress behavior, crack 1 initiated well before crack 2 in this specimen. Crack 1 therefore had grown well across the plate before crack 2 initiated. The asymmetric cracking and the related loss of section caused yield at the notch where crack 2 initiated. For this reason, this multiple initiation developed in an inelastic field. Yet another feature unique to corner cracks is the periods of dormancy, such as evident here in CH1, crack 1,1. Both multiple initiation and dormancy are

evident in Figure 19. Also, corner cracks develop from corner to through-thickness cracks. For this reason, data for small cracks following breakthrough is strongly influenced by the plastic instability process in the ligament prior to breakthrough.

The final feature unique to natural initiation is the development of Mode II cracks, along with the Mode I cracks observed with preflaws. With reference to Figure 20, note that the fracture surface near the initiation site for the natural initiation, denoted N, is very stepped and coarse compared to its preflawed counterparts. Related roughness-induced closure is expected for natural initiation as compared to preflawed cracks, and may cause a significant reduction in growth rate for cracks grown beyond the effect of the doubly free surface (Appendix A). In contrast, the locally enhanced plasticity associated with the doubly-free surface and the presence of Mode II cracks for the natural initiation may lead to decreased closure, particularly for negative values of R. Natural initiation thus may represent a fine balance between competing mechanisms.

Results for CH2, crack 1,1, have already been discussed in terms of a 3D solution applied until near a = 0.5t, after which K has been evaluated as a through crack. Changes in aspect ratio have been accounted for in analysis according to Figure 9(c). Note that the essential difference between these data and the through-crack results that bound it (CH1 and CH6, crack 1) is the occurrence of much larger growth rates for the natural initiation case. Obviously then if the desire is to study the growth of small cracks or to screen for short crack effects, the natural initiation process is significant in the presence of a free surface. When double free surfaces occur, natural initiation transients may be even more important. Another major difference is the driving force for an initiated crack to find the equilibrium crack shape under mechanics conditions which differ as it grows away from the notch. As this process depends on component geometry, it is difficult to predict when it will be most significant. But, earlier discussion of results for CH2 suggest that changes in crack shape can have a major influence on the growth rate of a part-through crack.

The significance of initiation transients and 3D crack geometry effects on the behavior of small cracks growing in an inelastic notch field can be extracted by study of data for CH1, crack 1,2, CH6, crack 2, and CH16, crack 1,1. These three sets of data are representative of 3D crack effects and initiation transients; only these results are discussed. In contrast to the c-N data for corner crack growth in an elastic notch field, the data for samples CH1 and CH16 shown in Figure 19(a) do not show the initially high growth rate to the extent found for CH2.

Analysis of these corner crack data is presented in Figure 19(b) on dc/dN-K_{mx} coordinates. This analysis has been done in two ways. First, the cracks have been considered as through cracks with length equal to that measured on the surface. In the second analysis they have been treated as corner cracks. For this second analysis, the aspect ratio has been changed as a function of surface crack length based on fractographic results and surface crack length data. Values of corner crack K determined in this manner show that, for a given surface crack length, K is less than that for the through crack case up to about $a/t = 0.5$ (see Appendix B). That is, for the same surface crack length, the value of K is reduced for corner cracks as compared to through cracks (Appendix B). Since $a/t \leq 0.5$ lies in the small crack domain these results suggest that an inappropriate through crack K underestimates the short crack effect that would be evident were a more appropriate corner crack K solution used for data analysis. Analyzed as corner cracks, the results are similar to the trend for CH2.

As has been noted for preflawed CNP data, the inelastic notch field operative in CH2 also is associated with growth rate trends in excess of the long crack data for growth through the notch field. Also, as was noted for preflawed data, the inelastic action of the notch seems to "wash out" the initially higher growth rates associated with small cracks in the CCP samples. Therefore, one could speculate that inelastic notch effects swamp the initiation transients and 3D effects observed to dominate the behavior for locally elastic conditions. In this respect, when local inelastic action occurs the value of r_p/a would appear to be the key driver for the short crack effect.

Summary of Results for CNP Samples. Data developed for preflawed CNP samples showed only a limited short-crack effect, consistent with the results for the CCP samples. Notch inelastic action was observed to significantly elevate the crack-growth rate as compared to that expected based on LEFM analysis. Natural initiation was associated with initially high growth rates attributed to the doubly free surface at corner-crack initiation sites. Fracture surfaces developed in these corner initiations showed mixed growth modes, and were very stepped and coarse. Closure and the development of constraint were asserted as the cause for reductions in growth rate as the corner crack grew. Three-dimensional crack configuration was also noted to be a factor when the configuration at initiation changed with crack advance to some other steady-state configuration.

Summary of Experimental Results for CCP and CNP Samples

The results developed for the precracked samples are not inconsistent with the use of r_p/a as a criterion to assess the possible extent of a short-crack effect. But results developed at nominally low values of r_p/a for both CCP and CNP geometries indicate the significance of free surfaces--a micromechanics contribution to r_p/a (or r_p/c). The CNP samples also showed transients in crack geometry from initiation through the development of a stable configuration are important. Likewise the CNP samples showed inelastic action at a notch field may by itself be responsible for a short-crack effect.

COMMENTARY: IMPLICATIONS FOR ENGINE MATERIALS AND RFC ANALYSIS

One disturbing facet of LEFM (and fracture mechanics in general) as applied herein is the difference in the value of stress intensity factor* that is encountered in the literature for, say, part-through cracks, for nearly the same geometry, cracking mode, etc. (See Appendix B for example.) Another disturbing facet of LEFM analysis (and fracture mechanics in general) is the need for geometry-specific analysis including the effect of boundaries on both peak stress and stress gradient. This tends to limit the utility of tabulated K solutions, at least in applications to cracks whose size is small compared to the dimensions of a component--e.g., a notch radius. To date, these aspects have not presented a problem in airframe Aircraft Structural Integrity Programs (ASIP) since LEFM based damage tolerant design and RFC analysis assume initial flaw sizes large in comparison to the crack sizes that exhibit a short-crack effect. But, even if initial flaw sizes are not assumed to be large, the shear loaded fastened joints popular in airframe construction tend not to exhibit short-crack effects, at least at finite growth rates [50,51]. The absence of a short-crack effect is apparently traceable to typically small values of r_p/c and the "propping" effect† that serves to reduce ΔK_{eff} but increases R [41]. Under these conditions, plasticity induced closure is virtually nonexistant, as is the inelastic action developed in open holes under otherwise identical conditions.

---

* While this statement is made and supported only for LEFM, it is also valid for some nonlinear fracture mechanics methods in that K forms a part of the parameter evaluation.

† Fasteners in shear loaded joints, such as interference-fit-fasteners, by virtue of their design create a tensile hoop prestress. As the joint is stressed in tension, the behavior at the high stress site at the fastener hole is controlled by radial unloading of the fastener. As load on the joint is removed, the fastener reloads. For this reason the cyclic loading seen by a material element at the high stress site in the hole is reduced, while the stress ratio (R) is increased - an effect known as "propping". Because of the high value of R, crack closure is less likely as compared to the open hole case.

For RFC analysis of engines must break virgin ground. And they must do this in fracture brittle materials, some of which have very small critical flaw sizes under service stress conditions. It follows then that microcrack growth in engine applications requires extensive phenomenological study, well beyond this preliminary effort. Once the phenomenology is in hand, models capable of characterizing key factors unique to microcracks can be formulated and tested.

This study has focused on identifying and characterizing factors that cause small cracks to grow differently than long cracks. Specifically, it was directed at cracks less than 1 mm long, and the objective was to develop and apply a framework valid for crack lengths less than 1 mm. Thereafter, the utility of this analysis was to be assessed, and consideration given to its use in engine RFC analysis. Based on the literature review [4], the key parameter controlling microcrack growth leading to nonconservative LEFM predictions was plasticity. Associated with plasticity were a host of related factors including inelastic notch fields, microfree surface effects, initiation transients and crack shape transients, and plasticity induced closure. Other factors were also noted such as the existance of a dominant singularity and microstructural features such as grain size, grain boundaries, etc.

The approach adopted to examine small crack growth in regard to engine RFC analysis recognized that deterministic applications of continuum fracture mechanics form the basis for most RFC analyses, as for example airframe ASIP [52]. Since deterministic fracture mechanics cannot deal with the variable crystallographic orientations at critical areas (at least polycrystalline materials), the study addresses cracking processes in an aggregate of material. Continuum mechanics likewise deals with an aggregate of material. The minimum volume of material to develop grain-to-grain compatibility is one criterion to judge the number of grains needed to develop the "bulk" response of an aggregate. Therefore, grain-to-grain compatibility can be used to set a lower bound to the crack sizes that can be dealt with if isotropic deterministic continuum mechanics descriptions of cracks are to be used. Discussions of single crystal, bicrystal, and surrounded bicrystal and

polycrystal deformation behavior (e.g., [53]) shed some light on this lower limit. Based on these results, the smallest crack addressed within such an analysis framework is one from 3- to 10-grain diameters along its least dimension. For the Inconel 718 studied, this lower limit crack dimension ranges from 30 to 100 μm. But for other materials used in engine applications, this dimension may be quite large. This lower limit associated with the use of continuum fracture mechanics restricts the scope of this study to rather fine-grained materials since the desired upper bound on crack size was 1000 μm. The lower limit crack dimension of 30 to 100 μm also restricts applicability of the results and continuum fracture mechanics† analysis to certain directionally solidified (DS) materials. Likewise, it essentially precludes consideration of single crystal (SC) materials using deterministic fracture mechanics--unless directional properties are expressly factored into the analysis.

Results presented in the literature show a short crack effect tends to be associated with large values of r_p/a* [4]. However, the material investigated admits only small values of r_p/a before brittle fracture intervenes, for both 20 C and temperatures typical of service. (This is attested to in the termination of CC17 at only $r_p/a = 0.23$ because of stable tearing tending to unstable growth, for a test at 643 C.) Given that large values of r_p/a tend to be associated with short crack effects in the literature, the small values admitted by the material studied suggest LEFM analyses might correlate most of the data generated. Indeed, in the absence of free surface effects or a notch which lead to locally large values of r_p/a at globally low levels, the results fail to indicate a short crack effect. Also, at small values of r_p/a (confined plasticity), plasticity induced crack closure is not expected to be a major factor. This is supported in a preliminary sense by

---

† Continuum fracture mechanics in this context is taken as an isotropic solution for crack driving force, which assumes the existance of a dominant singularity.

* The nomenclature relates specifically to CCP samples--but the discussion is general and r_p/a could be replaced by r_p/c used for CNP samples throughout this section.

the wake removal studies designed to isolate closure effects which showed only a limited effect of closure.

The peak value of r_p/a considered represents a value approaching the practical limit possible in the material studied. It is reasonable to expect that fine-grained high strength materials will also lead to similarly limited values of r_p/a, unless time-dependent flow or some other mechanism is involved. Thus, the results presented here may be indicative of the behavior of a broad class of engine materials. This assertion is supported to a limited extent by the literature for Rene 95 [45,54]. In that the largest practical values of r_p/a in these materials indicate flow is still confined, LEFM should be valid down to crack sizes associated with free surface effects (valid continuum fracture mechanics). This assertion is also supported in the literature, at least for Rene 95 [54]. That is, LEFM may provide a viable basis for RFC analysis for crack lengths (depths) down to about 100 μm in these materials, provided creep and oxidation (and oxidation-induced roughness) are kept in check through appropriate alloy selection.

For coarser-grained engine materials, larger values of r_p/a are possible. Also, microstructure may control growth to much larger crack lengths, since the lower bound crack length for the valid application of continuum fracture mechanics increases with grain size. These assertions are indirectly supported in the literature which shows that LEFM analysis does not achieve correlation in steels and aluminum alloys with coarser grain sizes, and noteably in a coarse-grained variant of a titanium alloy used in engines [55]. Adopting the titanium alloy as a vehicle for further discussion, results developed for that material show short crack effects at cracks a few mm long. Significantly, the short-crack effect can in that study [55] be ascribed to crack growth controlled by microstructure. But, it is also significant that this study involves conditions which violate the minimum crack length for valid application of deterministic continuum mechanics as noted earlier. The lesson to be learned is that continuum fracture mechanics must be applied with caution in dealing with coarse-grained high-strength materials. That is, r_p/a, based on bulk (continuum) calculations, is only valid if the crack is large compared to the microstructure. Therefore, care

must be taken in adopting a macroscopic value of r_p/a as an indicator of possible short crack effects, particularly in regard to DS and SC engine materials.

A general RFC analysis capability must address the limited viability of LEFM as r_p/a grows beyond values on the order of 0.1. ΔCTOD has been advanced in References 9 and 19 as a basis to extend the applicability of LEFM type analysis to higher values of r_p/a. ΔCTOD has the advantage of being related to physical parameters, but it may be difficult to calculate. Alternatively, analysis on ΔJ [56] based on adaptation of the J integral [57] to fatigue applications could be used. An important advantage of a J-based framework is its convenient calculation using J estimation procedures. Unfortunately, in the presence of a notch stress field and the notch's related influence on closure, determination of ΔJ requires detailed numerical evaluation just as would ΔCTOD.

Given that detailed analyses are required, the more general parameters such as ΔCTOD and ΔT [58] seem to offer the most promise. But it is desirable to use modifications of available LEFM analysis whenever possible in view of the complexity and cost associated with the evaluation of these parameters. As noted in Appendix C, ΔCTOD can be evaluated in terms of a pseudo plastic strip yield formulation based on LEFM technology (e.g., [59,60]. Since such models can be adapted to account for closure (e.g., [61,62]), this class of models may provide an economical alternative to detailed inelastic analysis without great loss in accuracy.

Regarding the influence of notch plasticity, analyses in the literature [18,43] indicate that for confined notch plasticity, LEFM analysis can be adapted to this situation. The key in this adaptation is modification of the far field stress to reflect stress-strain conditions that operate in the inelastic notch field. Once the inelastic field is fully traversed by the crack, LEFM can be used. Obviously, the situation of cracking in notch fields is complicated by the influence of local biaxiality (t/2r) near the site of crack initiation and the initial crack shape [7,63]. Since crack geometries at initiation are not necessarily the equilibrium "long crack" geometry, 3D K solutions for finite width may be required. And K so developed must reflect

both the peak stress and the stress gradient [26]. Also, the apparent dependence of crack-growth rate on far field stress state and normalized stress level (Appendix A) must be accounted for once applied gross section stress becomes an appreciable fraction of yield.

In summary, much work remains to be done before RFC analysis comes of age in applications where concern is directed at physically small cracks. Throughout, differences in micro-free surface effects on r_p/a between fine-and coarse-grained materials must be remembered. Lower bound limits on crack size for the applicability of LEFM must be set not only in terms of violating the confined flow restriction (r_p/a less than about 0.1) but also the continuum restriction (crack length or depth greater than about 10 times the grain size). Experiments should focus on natural initiation in test geometries that reflect key geometric parameters over the range of service conditions expected. Situations examined should reflect potential service conditions to develop creep and oxidation to the extent they occur in service.

Finally some cautions regarding developing and interpreting screening tests to see if a "material shows a small crack effect" are appropriate. In such studies, it should be remembered that for "continuum valid" applications of fracture mechanics, mechanics parameters seem to control whether or not a short-crack effect develops. This is not to say that materials considerations such as grain size are not important. Rather the situation is that changes in microstructure affect mechanical properties, which in turn affect mechanics parameters. As an example, grain size influences flow response which in turn figures into r_p/a. Grain size also figures into the lower bound crack size for deterministic continuum mechanics analysis.

Unfortunately it is difficult to study a material to screen crack growth behavior for a short-crack effect without the use of some test specimen. As has been emphasized by the results developed herein, certain test geometries enhance or play down the role of specific mechanics parameters noted in this study as drivers of the short-crack effect. It follows then that screening materials for "short-crack effects" using a given geometry tends to emphasize particular mechanics or materials parameters and factors known to control the microcrack growth rate. Therefore, the extent to which

any material exhibits a short-crack effect depends on the geometry used. For this reason, the question of whether or not a "material shows a short-crack effect" is not of consequence--unless it is asked in regard to a specific 3D geometry and loading that reflect some eventual service application.

CONCLUSIONS

The major conclusions of the experimental phase of this study are summarized below.

- In the absence of the elevated temperature, corner cracking, and inelastic notch fields, LEFM analysis is appropriate for small cracks in fine-grained Inconel 718 under engine conditions. Tests meant to simulate the mechanical service conditions showed an elevation of crack growth rate less than five times for short cracks. This increase operated over a very small crack growth increment.

- Inability to measure and/or analyze corner-initiating cracks can cause LEFM to become practically invalid for short cracks of that type. Consolidation of crack growth data by LEFM requires the accurate calculation of the stress intensity factor (SIF). The discussion of K solutions in this report establishes the widely varying solutions which are available in the literature. If the appropriate SIF cannot be determined or if the measurements needed to use the appropriate SIF cannot be made, then there is little hope that LEFM can consistently consolidate corner-initiating short cracks. Corner initiation can lead to elevated growth behavior caused by stress-state and transient-crack geometry effects.

- Notch root plasticity can elevate crack growth rates above the those predicted by LEFM. Growth rates 5 to 10 times the rates expected from LEFM analysis have been observed in tests.

REFERENCES

[1] Frost, N. E., Pook, L. P., and Denton, K., "A Fracture Mechanics Analysis of Fatigue Crack Growth Data for Various Materials", Engineering Fracture Mechanics, Vol. 3, pp 109-126, 1971.

[2] Ohuchida, H., Nishioka, A., and Usami, S., "Elastic-Plastic Approach to Fatigue Crack Propagation and Fatigue Limit of Materials with Crack", Vol. V, ICF3, Munich, 1973; see also "Fatigue Limit of Steel with Cracks", Bulletin of the JSME, Vol. 18, No. 125, November, 1975.

[3] Kitagawa, H., and Takahashi, S., "Applicability of Fracture Mechanics to Very Small Cracks or the Cracks in the Early Stages", Proc. Second International Conference on Mechanical Behavior of Materials, Boston, pp 627-631, 1976.

[4] Leis, B. N., Kanninen, M. F., Hopper, A. T., Ahmad, J., and Broek, D., "A Critical Review of the Short Crack Problem in Fatigue", AFWAL-TR-83-4019, January, 1983.

[5] Suresh, S., "Crack Deflection: Implications for the Growth of Long and Short Fatigue Cracks", Metallurgical Transactions A, Vol. 14A, November, 1983, pp 2375-2385.

[6] Schijve, J., "The Effect of an Irregular Crack Front on Fatigue Crack Growth", Engineering Fracture Mechanics, Vol. 14, pp 467-475, 1981.

[7] Leis, B. N., and Topper, T. H., "Long-Life Notch Strength Reduction in the Presence of Local Biaxial Stress", Journal of Engineering Materials and Technology, Trans. ASME, Vol. 99, No. 3, July, 1977, pp 215-221.

[8] Proceedings, International Conference on Multiaxial Fatigue, December, 1982, ASTM STP 853, edited by K. J. Miller and M. Brown, 1985.

[9] Kanninen, M. F., Ahmad, J., and Leis, B. N., "A CTOD-Based Fracture Mechanics Approach to the Short-Crack Problem in Fatigue", Mechanics of Fatigue, ASME AMD, Vol. 47, pp 81-90, 1981.

[10] Newman, J. C., Jr., "A Nonlinear Fracture Mechanics Approach to the Growth of Short Cracks", AGARD Specialists Meeting on Behavior of Short Cracks, Toronto, Canada, September 20-21, 1982.

[11] Suresh, S., Zamiski, G. F., and Ritchie, R. O., "Oxide-Induced Crack Closure: An Explanation for Near-Threshold Corrosion Fatigue Crack Growth Behavior", Met. Trans. A, Vol. 12A, 1981, pp 1435-1443.

[12] Ritchie, R. O., and Suresh, S., "Mechanics and Physics of the Growth of Small Cracks", in Behavior of Short Cracks in Airframe Components, AGARD CP 328, 1983, paper 1.

[13] Staehle, R. W., "A Point of View Concerning Mechanisms of Environment-Sensitive Cracking of Engineering Materials", In: Mechanisms of Environment Sensitive Cracking of Materials, Proceedings of an international conference organized by the Metals Society and held at the University of Surrey, Guildford, April, 1977.

[14] Smith, R. A., "On the Short Crack Limitations of Fracture Mechanics", Int. Journal of Fracture, 1977.

[15] Broek, D. and Schijve, J., "Fatigue Crack Growth; Effect of Sheet Thickness", Aircraft Engineering, 38, 11, (1966), pp 31-33.

[16] Schijve, J., Analysis of the Fatigue Phenomenon in Aluminium Alloys, Ph.D. Thesis, Technical University of Delft, Nat. Aerospace Inst., Amsterdam, TR-M-2122 (1964).

[17] Broek, D. and Schijve, J., The Influence of the Mean Stress on the Propagation of Fatigue Cracks in Aluminium Alloy Sheets, Nat. Aerospace Inst., Amsterdam, TR-M-2111 (1963).

[18] Leis, B. N., "Microcrack Initiation and Growth in a Pearlitic Steel", 15th National Fracture Symposium, June, 1982, ASTM STP 833, 1984, pp 449-474.

[19] Ahmad, J., Hopper, A. T., Kanninen, M. F., Leis, B. N., and Papaspyropoulos, V., "A Nonlinear Fracture Mechanics Predictive Procedure for the Short Crack Effect in Fatigue", in Proceedings of the Army Symposium on Solid Mechanics, 1982 - Critical Mechanics Problems in Systems Design, AMMRC MS 82-4, September, 1982.

[20] Atkinson, C., and Kanninen, M. F., "A Simple Representation of Crack-Tip Plasticity: The Inclined Strip-Yield Superdislocation Model", Int. J. Fracture, Vol. 13, 1977, p 151.

[21] Yagawa, G., and Nishioka, T., "Three-Dimensional Finite Element Analysis for Through-Wall Crack in Thick Plate", International Journal for Numerical Methods in Engineering, Vol. 12, pp 1295-1310, 1978.

[22] Smith, S. H., Unpublished stress intensity factor solution for finite width plate with hole, K_t = 2.5; used and reported in Reference 44.

[23] Shah, R. C., "Stress Intensity Factors for Through and Part-Through Cracks Originating at Fastener Holes", Mechanics of Crack Growth, ASTM STP 590, 1976, pp 429-459.

[24] Newman, J. C., Jr., "An Improved Method of Collocation for the Stress Analysis of Cracked Plates With Various Shaped Boundaries", NASA TN D-6376, 1971.

[25] Tada, H., Paris, P. C., and Irwin, G. R., The Stress Analysis of Cracks Handbook, Del Research Corp., Revised, 1977.

[26] Schijve, J., "Stress Intensity Factor of Small Cracks at Notches", Technical University of Delft, Report LR-330, July, 1981: see same title, Fatigue of Engineering Materials and Structures, Vol. 5, No. 1, 1982, pp 77-90.

[27] Novak, S. R., and Barsom, J. M., "Brittle Fracture (K_{IC}) Behavior of Cracks Emanating from Notches", ASTM STP 601, pp 409-447, 1976.

[28] Smith, R. A., and Miller, K. J., "Fatigue Cracks at Notches", International Journal of Mechanical Science, 19, pp 11-22, 1977.

[29] Broek, D., "The Propagation of Fatigue Cracks Emanating from Holes", Report No. TR 72134 C, National Aerospace Laboratory, 1972.

[30] Karlsson, A., and Backlund, J., "Summary of SIF Design Graphs for Cracks Emanating from Circular Holes", International Journal of Fracture, Vol. 14, No. 6, December 1978, pp 585-596.

[31] Newman, J. C., Jr., and Raju, I. S., "Stress-Intensity Factor Equations for Cracks in Three-Dimensional Finite Bodies", NASA TM 83200, August 1981.

[32] "Part-Through Crack Fatigue Life Prediction", ASTM STP 687, J. B. Chang, editor, 1979.

[33] Newman, J. C., Jr., "A Review of Stress-Intensity Factors for the Surface Crack", in Part-Through Crack Fatigue Life Prediction, ASTM STP 687, 1979.

[34] "The Surface Crack: Physical Problems and Computational Solutions", The American Society of Mechanical Engineers, J. L. Swedlow, editor, 1972.

[35] Broek, D., Elementary Engineering Fracture Mechanics, Noordhoff, 1974.

[36] Sova, J. A., Crews, J. H., Jr., and Exton, R. J., "Fatigue Crack Initiation and Growth in Notched 2024-T3 Specimens Monitored by a Video Tape System", NASA Technical Note No. D-8224, August, 1976.

[37] Newman, J. C., Jr., "Predicting Failure of Specimens with Either Surface Cracks or Corner Cracks at Holes", NASA TN D-8244, 1976.

[38] Bowie, O. L., "Analysis of an Infinite Plate Containing Radial Cracks Originating at the Boundary of an Internal Circular Hole", J. Math. and Physic., 25 (1956), pp 60-71.

[39] Tweed, J., and Rooke, D. P., "The Distribution of Stress Near the Tip of a Radial Crack at the Edge of a Circular Hole", Int. J. Engng Sci., Vol. 11, pp 1185-1195.

[40] Sternberg, E., and Sadowsky, M. A., "Three-Dimensional Solution for Stress Concentration Around a Circular Hole in a Plate of Arbitrary Thickness", J. App. Mech., Trans. ASME, March, 1949, pp 27-38.

[41] Leis, B. N., "Discussion of the Short Crack Effect in Airframe Materials and Components", in Behaviour of Short Cracks in Airframe Components, Agard Conference Proceedings No. 328, 1983, Section 16.

[42] El Haddad, M. H., Dowling, N. E., Topper, T. H., and Smith, K. N., "J Integral Applications for Short Fatigue Cracks at Notches", International Journal of Fracture, Vol. 16, No. 1, February, 1980.

[43] Leis, B. N., "Fatigue Crack Propagation Through Inelastic Gradient Fields", Int. J. Pres. Ves. & Piping, 10, pp 141-158, 1982; see also "Displacement Controlled Fatigue Crack Growth in Elastic-Plastic Notch Fields and the Short Crack Effect", Engineering Fracture Mechanics, to appear.

[44] Leis, B. N., and Galliher, R. D., "Growth of Physically Short Center Cracks at Circular Notches", Low Cycle Fatigue and Life Prediction, ASTM STP 770, pp 399-421, 1982.

[45] Gangloff, R. P., Res. Mechanics Letters, Vol. 1, pp 299-306, 1981; see also Gangloff, R. P., "Electric Potential Monitoring of Fatigue Crack Formation and Growth from Small Defects", ASTM Symposium on Fatigue Crack Growth Rate Testing and Data Analysis, (to be published), October, 1979.

[46] Friedl, K. H., Scarlin, R. B., and Zelizko, V., "The Propagation of Short Fatigue Cracks in 12% Chromium Steels", Advances in Fracture Research, Vol. 2, 1981.

[47] Lankford, J., "Initiation and Early Growth of Fatigue Cracks in High Strength Steel", Engineering Fracture Mechanics, 1977, Vol. 9, pp 617-624.

[48] Hammouda, M. M., and Miller, K. J., "Elastic-Plastic Fracture Mechanics Analyses of Notches", ASTM STP 668, pp 703-719, 1979.

[49] Lankford, J., Cook, T. S., and Sheldon, G. P., "Fatigue Microcrack Growth in a Nickel-Base Superalloy", Int. J. of Fracture, in press.

[50] Wang, D. Y., "A Study of Small Crack Growth Under Transport Spectrum Loading", in Behaviour of Short Cracks in Airframe Components, Agard Conference Proceedings No. 328, 1983, Paper 14.

[51] Potter, J. M., and Yee, B.G.W., "Use of Small Crack Data to Bring About and Quantify Improvements to Aircraft Structural Integrity", in Behaviour of Short Cracks in Airframe Components, Agard Conference Proceedings No. 328, 1983, Paper 4.

[52] Wood, H. A., and Engle, R. M., Jr., "USAF Damage Tolerant Design Handbook: Guidelines for the Analysis and Design of Damage Tolerant Aircraft", Technical Report AFFDL-TR-79-3021, Interim Report for Period January 1977 to November 1978.

[53] McGregor-Tegart, W. J., Elements of Mechanical Metallurgy, McMillan, 1966.

[54] McCarver, J. F., and Ritchie, R. O., "Fatigue Crack Propagation Thresholds for Long and Short Cracks in Rene 95 Nickel-base Superalloy", Materials Science and Engineering, Vol. 55, No. 1, August, 1982, pp 63-67.

[55] Brown, C. W., and Hicks, M. A., "A Study of Short Fatigue Crack Growth Behavior in titanium Alloy IMI 685", Fatigue of Engineering Materials and Structures, Vol. 6, No. 1, 1983.

[56] Dowling, N. E., and Begley, J. A., "Fatigue Crack Growth During Gross Plasticity and the J Integral", Mechanics of Crack Growth, ASTM STP 590, pp 82-103, 1976.

[57] Rice, J. R., "A Path Independent Integral and the Approximate Analysis of Strain Concentrations by Notches and Cracks", J. Appl. Mech., pp 379-386, 1968; see also Brown University Report E39, May 1967.

[58] Atluri, S. N., Nishioka, T., and Nakagaki, M., "Incremental Path Independent Integrals in Inelastic and Dynamic Fracture Mechanics", Engineering Fracture Mechanics, Engineering Fracture Mechanics, Vol. 20, No. 2, pp 209-244, 1984.

[59] Seeger, T., Ein Bertrag nur Berechnung von statisch und myblisch belasteten Rebocheichen noth dem Dugdale-Barenblat Modell, (A Contribution to the Calculation of Statically and Cyclically Loaded Cracks With the Dugdale-Barenblat Model), Institut fur Statick und Stahtban, Darmstadt (1973).

[60] Kanninen, M. F., Atkinson, C., and Feddersen, C. E., "A Fatigue Crack-Growth Analysis Method Based on a Simple Representation of Crack-Tip Plasticity", Cyclic Stress-Strain and Plastic Deformation Aspects of Fatigue Crack Growth, ASTM-STP 637, 1977, p 122.

[61] Fuhring, H., Berechnung von elastisch-plastischen Beanspruchungsablaufen in Dugdale-Rißscheiben mit Rißuferkontakt auf der Grundlage nichtlinearer Schwingbruchmechanick, Institut fur Statick und Stahlban, Darmstadt (1977), (Calculation of Elastic-Plastic Loading in Dugdale Cracks with Crack Closure on the Basis of Non-linear Fatigue Fracture Mechanics).

[62] Newman, J. C., Jr., "Prediction of Fatigue-Crack Growth Under Variable-Amplitude and Spectrum Loading Using a Closure Model", NASA Technical Memorandum 81942, January, 1981.

[63] Leis, B. N., Kanninen, M. F., and Ahmad, J., "Effect of Local Stress State on the Growth of Short Cracks", Multiaxial Fatigue, ASTM STP 853, 1985, (To Appear).

[64] Paris, P. C., and Sih, G. C., "Stress Analysis of Cracks", ASTM STP 381, (1965), pp 30-83.

[65] Broek, D., and Schijve, J., The Influence of the Mean Stress on the Propagation of Fatigue Cracks in Aluminum Alloy Sheets, Nat. Aerospace Inst., Amsterdam, TR-M-2111, (1963).

NOMENCLATURE

RFC	-	Retirement for cause
DTD	-	Damage tolerant design
LEFM	-	Linear-elastic fracture mechanics
ΔCTOD	-	Crack-tip-opening displacement range
μ	-	Biaxial stress ratio
S_{mx}	-	Maximum stress
S	-	Far-field stress
Y	-	Flow stress
t	-	Thickness
W	-	Width
r	-	Radius of hole
R	-	Stress ratio
K	-	Stress intensity factor
ΔK_{eff}	-	Effective stress intensity factor range
K_{mx}	-	Maximum stress intensity factor
CCP	-	Center crack panel
CNP	-	Center hole notched
c, a	-	Surface crack length in CNP and CCP specimens, respectively
N	-	Number of cycles
da/dN, dc/dN	-	Crack growth rate
K_t	-	Net-section stress accentuation factor
a/c	-	Crack aspect ratio
r_p	-	Plastic zone size
SC	-	Single crystal
DS	-	Directionally solidified
x_p	-	Notch plastic field, measured along transverse net section

APPENDICES

This section contains six appendices which report work done in support of this study, the results of which are used/referenced in summary or parametric form in main body of the report. Included are:

A Influence of Stress Biaxiality on Fatigue Crack Propagation Rate, Including Free Surface Effects

B Survey of Results of Stress Intensity Factor Solutions for Plates with Holes, Including Crack Configuration

C Analytical Consideration of Crack Tip Plasticity--Pseudoplastic Extension of LEFM to Small Cracks

D Accuracy and Precision in Crack Length Measurement

E Data Tables

F Considerations in the Choice of Stress Intensity Factor Solution for Finite Width CNP Specimens.

Each appendix is introduced with the background that identified the need for the effort reported, and is self standing. Where references are used, they are listed in the List of References.

Appendix A. Influence of Stress Biaxiality on Fatigue Crack Propagation Rate

Thickness to diameter ratio in CNP specimens is known to control the biaxial stress field at the notch root [40]. In a mechanics sense, this biaxiality is embedded in the stress intensity factor--which represents Mode I cracking (not loading). But it is known that crack-growth rate depends on stress biaxiality, μ. Note that the dependence of dc/dN on μ is not accounted for in (Mode I) K. Note too that short-crack data for growth in biaxial fields are compared to uniaxial long-crack data. Therefore, it is necessary to account for the presence of stress biaxiality to complete consideration of 3D effects in the CNP specimen. Also, because the extent of the local plasticity varies, this dependence of dc/dN on μ should be expressed as a function of normalized stress level.

Even after accounting for the macroscopic free surface effect in a mechanics sense [64] (via 1.122 applied to K for cracks at surfaces), and accounting for stress biaxiality as outlined in the following, there remains an unaccounted factor associated with surface cracks. As one passes from the surface to the interior of a body, there is an increase in the grain to grain compatibility. This develops since as compared to fully surrounded interior grains, those on the surface deform in the presence of fewer neighbours that limit flow in other directions. Furthermore this flow may occur on slip systems with an exterior normal component--which incurs no constraint at all at the free surface. The more slip systems, the more likely it is that slip systems are favorably oriented, therefore the greater the flow involved.

Without micromechanics analysis it is difficult to calculate the significance of this effect and the depth to which it may be a factor. However it can be inferred from consideration of differences in stress-strain (flow) behavior. Such data, presented as a function of the number and orientations of grains studied and the number of slip systems available (active) for various pure materials* suggest this microscopic free surface

---

* For a discussion of this subject, see for example [53].

effect is operative in a surface layer as few as 3, but up to 10 grains deep. For the present material, this means easier flow and therefore higher growth rates can be expected due to this microfree surface effect for cracks from 30 μm to 100 μm long.

It should be noted that the effect of free surface can create surface cracks that are "open" compared to their longer counterparts [63]. Moreover, its influence would be greatest when the crack is small, and would decrease with crack growth. In this sense, crack closure serves as a macroscopic vehicle to rationalize a process driven by a micromechanics phenomenon. Bulk flow properties, therefore, should not be used to develop closure models for short cracks. Finally, the length over which the effect is observed is indirectly tied to the material via grain size. For this reason, any associated short crack effect due to the micromechanics of free surface flow may be erroneously concluded to be "material" dependent. A more complete discussion of free surface effects and biaxiality is contained in Reference 63.

The issue of free surface aside, the dependence of dc/dN on μ was formulated in terms of a colinear strip yield model following the lead in earlier analysis tasks (compare Appendix C). This effort was funded in part by the analysis appropriation and by Battelle. Results of this formulation are presented in J. Ahmad, B. N. Leis, and M. F. Kanninen, "Analysis of Fatigue Crack Propagation Under Biaxial Loading Using an Inclined Strip Yield Zone Representation of Crack Tip Plasticity", accepted for publication in Fatigue of Engineering Materials and Structures. Figure 11 presents a summary of the findings of this study. The related text discusses some of the implications.

Appendix B. Survey of Results of Solutions for Plates with Holes, Including Crack Configuration

Results of the review indicated the 3D crack configuration may be a factor in explaining the nonunique correlation of dc/dN on ΔK or K_{mx}. Given that the first test performed using both the aluminum and the Inconel 718 indicated corner cracking developed for natural initiation, a survey of through thickness and part through thickness stress intensity factor solutions was initiated. The survey had a limited scope given that much of the experimental work utilized preflawed CCP or CNP samples anticipated to produce through cracks. The survey, performed and reported by Mr. T. P. Forte, was funded in part by Battelle and this contract out of the reporting appropriation and represented a small but significant fraction of that effort. A summary of the results of the survey follows.

Numerous stress intensity factor (SIF) solutions are available in the literature for cracks eminating from holes in plates. Unfortunately, however, there are significant differences between the results for the various solutions. Table B-1 contains a partial list of the references containing alternative SIF solutions for single and double through-thickness cracks as well as single and double corner cracks emanating from holes. This survey has been undertaken to compare some of the more popular stress intensity factors for the case of (1) symmetric through cracks, and (2) single corner cracks. (Double corner cracks and single through cracks are not prevelant in this study and as such have not been considered.) The study was further limited to the case of uniaxial, uniform, remote stress loading, perpendicular to the crack plane; in finite width plates; at crack sizes small compared to the hole diameter. Lastly, only those SIF solutions that were readily programmable were considered.

The ultimate goal of the survey of SIF solutions was to select the solution most appropriate for the analysis of the short crack, crack growth rate data developed in the current study. For this reason, the focus was on solutions applicable to short cracks (less than one-tenth the hole diameter in length). Of the many solutions available, those geometrically similar to the CNP test specimen (Figure 5b) developed using finite element analysis

techniques were of interest. (Recall that the test specimen nominal dimensions were: width = 2.25 inches, hole diameter = 0.5 inch, and thickness = 0.09 inch.) In addition, solutions incorporating finite width corrections were desired. Note that the finite width corrections were sought not only to compensate for the increase in the SIF as a growing crack consumes the width of the plate, but more importantly to compensate for the differences in the near-hole stress fields between infinite and finite width plates. These differences are reflected by differences in stress concentrations and in the shape of the stress gradient.

TABLE B-1. SOURCES OF SIF SOLUTIONS FOR CRACKS EMANATING FROM CIRCULAR HOLES

THROUGH-THICKNESS CRACKS

One Crack

1. Tweed, J. and Rooke, D. P., Int. J. Engr. Sci., V11, 1973 pp 1185-1193
2. Bowie, O.L., J. Math. Phys., V35, 1956, pp 60-71
3. Shah, R. C., ASTM-STP-590, Mechanics of Crack Growth, 1976, pp 429-459
4. Oladimeji, M. K., Engr. Fract. Mech., V15, No. 3-4, 1981, pp 391-405
5. Broek, D., Elementary Engineering Fracture Mechanics, Noordhoff International Publishing, Leyden, 1974.

Two Cracks

6. Bowie, O. L., (same as 2 above).
7. Shah, R. C., (same as 3 above).
8. Oladimeji, M. K., (same as 4 above).

TABLE B-1. (Continued)

9. Broek, D., (same as 5 above).

10. Karlsson, A. and Backlund, J., Int. J. Fract. Mech. V14, No. 6, 1978, pp 585-596.

11. Newman, J. C., NASA TN D-6376, 1971.

CORNER CRACKS

One Crack

12. Shah, R. C., (same as 3 above).

13. Broek, D., (same as 5 above).

14. Newman, J. C., NASA TN D-8244, 1976.

15. Newman, J. C. and Raju, I. S., ASTM-STP-791, Fracture Mechanics, 14th Symposium, Volume 1, Theory and Analysis, 1983, pp I 238-I 265.

16. Hall, L. R. and Finger, R. W., AFFDL TR 70-144, Edited by Wood, H. A., Et al, 1970, pp 235-262.

17. Liu, A. F., Engr. Fract. Mech. V4, 1972, pp 175-179.

18. Smith, S. H., WPAFB, ASD TR-18, 1974.

Two Cracks

18. Newman, J. C., NASA TN D-8244, 1976.

19. Newman, J. C. and Raju, I. S., (same as 15 above).

20. Shah, R. C., (same as 3 above).

21. Broek, D., (same as 5 above).

Comparison of SIF Solutions

The comparison of the various SIF solutions has been made graphically using computer generated plots. The normalized coordinates used for the abscissa and ordinate were the SIF divided by the applied remote stress, K/S, and the crack length (measured from the edge of the hole to the crack tip, in the width direction) divided by the hole diameter, c/D.

Symmetric Through Cracks

SIF solutions from References 7, 8, 16, and 17 were plotted on a single plot so that differences could be observed. As expected, each solution showed an increasing SIF with increasing crack length, but the large difference in the SIF for the solutions was somewhat unexpected. At a crack length to diameter ratio of 0.02 the values of K/S ranged from 0.38 to 0.62 with the lowest value being associated with Reference 6 and the largest with Reference 11*. For the 0.5 inch diameter hole the ratio of c/D of 0.02 corresponds to a 0.010-inch crack. At a c/D ratio of 0.10, a 0.050-inch length crack, the value of K/S ranged from 0.73 to 1.11, again the lowest value was associated with Reference 7 and the largest with Reference 17.

In each of the above two examples, for different c/D values the spread in K/S was largely due to the low values of K/S from Reference 7. Most likely this was because the solution from Reference 7 did not include a finite width correction. Comparing the other solutions, the variation in K/S at c/D = 0.02 was reduced to a range of 0.45 to 0.62 and at c/D = 0.10 to a range of 0.96 to 1.11. This result to some extent exhibits the influence of the finite width correction.

---

* This SIF solution was developed for a diameter to plate width ratio of 0.25. The corresponding ratio for the test specimen was 0.222. To offset this difference two sets of calculations were made, one with a hole size of 0.5 inch and a width of 2.0 inches, and a second with a width of 2.25 inches and a 0.5625 inch diameter hole. These provided closely spaced bounds for the test specimen geometry.

The SIF solution selected for the analysis of the short crack growth rate data was taken from Reference 17. The choice was made because this solution was derived from a finite element analysis of a model most nearly matching the test specimen geometry, c/D = 0.25 for the model and 0.222 for the specimen. As noted in the report, this solution most closely matched the limiting value of $K = 1.122\ K_t\ S\ \sqrt{\pi c}$ over the crack interval from 25 μm to 490 μm.

Single Corner Cracks

SIF solutions from References 5, 6, 11-13, and 18 were plotted on a series of three plots, one for each of the following ratios: a/c = 1, 2, and 3. As with the through-thickness cracks, c was the length of the crack measured from the hole's edge in the width direction; a, on the other hand, was the length of the crack in the depth (through thickness) direction. The variation in K/S as a function of c/D was similar to that of the through thickness SIF solutions. The variation tended to increase with increasing a/c. The closest agreement among the various solutions was for the case of a/c of 1 and c/D less than 0.04. In this regime the applicable SIF solutions (from References 5, 13, 14, and 18) exhibited only minor differences. For example, at c/D of 0.04, K/S ranged between 0.45 and 0.54.

An important criteria in the selection of a corner crack SIF solution for the analysis of the test data was that the corner crack solution reduce to a through-thickness crack as a/c approached infinity. This was taken as the upper limiting bound for candidate corner crack solutions. In the lower limit, i.e., for small quarter-circular with c/D less than 0.04, it was felt that the corner crack solution should be similar to the solutions given by References 5, 13, 14, and 18 since they were in such close agreement. Each of these conditions was satisfied through the use of the correction factor given in Figure 11 of Reference 13. This factor reflected the

relationship between the SIF for a corner crack and that of a through-thickness crack, each having the same value of normalized crack length c/D.* A plot of the SIF solution adopted for the analysis of the test data is shown in Figure B-1. Note that part of the figure shows an expanded plot of c/D less than 0.10.

In adopting the SIF solution shown in Figure B-1 it was necessary to prescribe the relationship between a and c, for a corner crack that begins as a quarter-circular crack and gradually transitions into a through-thickness crack as c increases. Such a relationship was established from consideration of the observed crack growth behavior. In general, the crack started as quarter-circular and grew as quarter-circular until c/D = 0.05, at which length they began to transition into through-thickness cracks. At c/D = 0.07, the cracks were approximately 2/3 through the thickness and at c/D = 0.075, the cracks were all but completely plane fronted through-thickness cracks. Using this information, and the correction factor given in Figure 11 of Reference 13, it was possible to define a smooth, continuous relationship between c/D and K/S for cracks that begin as corner cracks, transition to through-thickness cracks, and grow to failure as through-thickness cracks. The correction for corner cracks shown in Figure B-1 was used in analysis throughout the text discussing figures designated as "analyzed as a corner crack".

---

* Combining a SIF solution for a single corner crack and a double through-thickness crack was considered reasonable for two reasons. First, because of the close agreement between the single corner crack solution and the double through-thickness crack solution, as modified using the data in Figure 11 of Reference 13, for short cracks, and because the difference in SIF solutions betweeen single and double corner cracks, for the crack sizes of interest, was less than 3 percent.

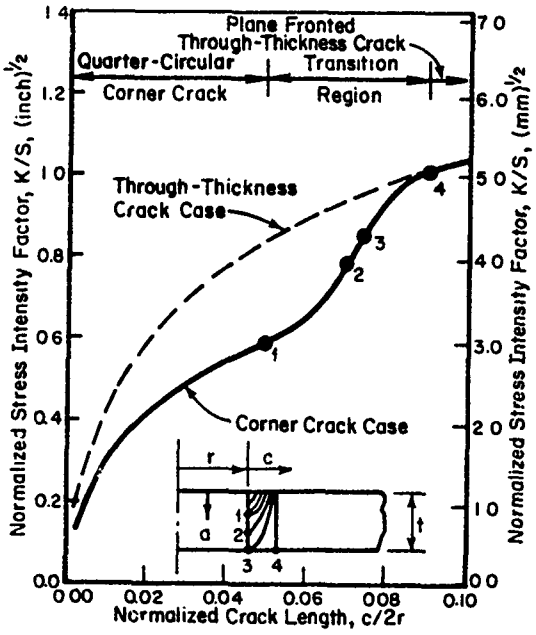

a. corner-crack domain - expanded scale

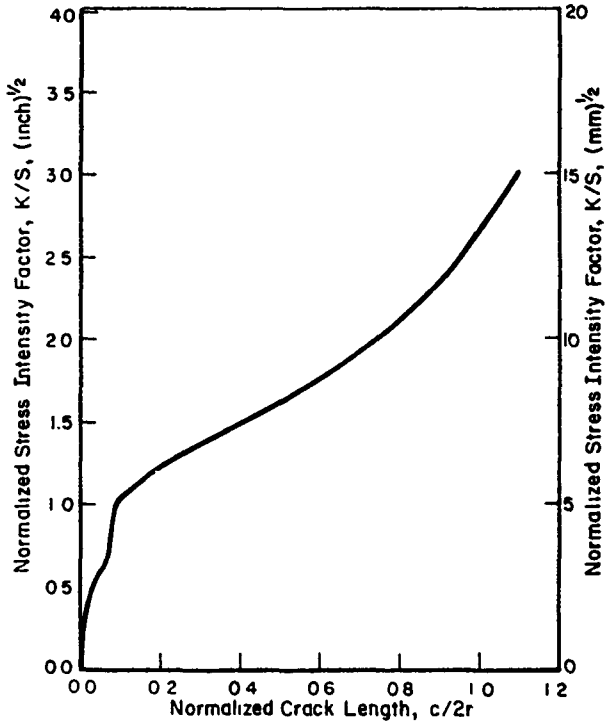

b. full range of normalized crack length

FIGURE B-1. NORMALIZED STRESS INTENSITY FACTOR VERSUS NORMALIZED CRACK LENGTH FOR CRACKS EMINATING FROM CIRCULAR HOLES, CENTRALLY LOCATED IN FINITE WIDTH PLATES

Appendix C. Analytical Consideration of Crack Tip Plasticity-- Pseudoplastic Extension of LEFM to Small Cracks

This appendix reports on a task whose purpose was to analytically examine the influence of crack tip plasticity as a function of crack length. The desire was to find a simple and inexpensive method to extend the applicability of LEFM to smaller crack sizes with significant crack tip plasticity.

The effort pressed forward in four subtasks and is so reported. These subtasks were: (1) review the relevant literature, (2) develop a simple analysis framework to account for crack tip plasticity, (3) evaluate an economical procedure to generate solutions for a variety of geometries within the analysis framework of Subtask 2 and (4) develop a means to account for microcrack closure. Commitments to these efforts involved an almost equal split of about 80% of the analysis appropriation, a portion of the appropriation for the literature review, and a small but significant portion of the experimental appropriation for model verification for Subtask 2. Results of these subtasks follow.

Literature Review

Results of this effort are presented in our earlier report [4].

Analysis Framework for Crack Tip Plasticity-- Pseudoplastic Model and Application/Evaluation

Results of this effort are reported in two papers [9,19] that present and summarize the framework and outline its application and verification in terms of results for the aluminum CNP sample noted in Table 1.

Exploratory Evaluation of an Economical Solution Generation Procedure

As detailed in References 9 and 19, our analysis framework makes use of a pseudoplastic characterization of crack driving force. It uses the usual LEFM K solution in conjunction with a singularity canceling relationship that also follows from LEFM considerations. The boundary point least squares (BPLS) solution procedure offers a very economical means to develop this information. For this reason a study of the utility and accuracy of BPLS was undertaken for an edge cracked panel and a symmetrically cracked CNP. Unfortunately, problems with the solution procedure developed as the crack length decreased. After a persistant attempt by Dr. L. E. Hulbert in cooperation with Ms. V. Papaspyropoulus, the BPLS effort was abandoned leaving only the finite element approach detailed in Reference 19 as the basis to make the required LEFM analysis.

Crack Closure

This is the last of the analytical tasks initiated in regard to crack tip plasticity. Need for this task was identified as a result of the literature review which showed closure to be a key factor in some explanations of short-crack effects. The effort focused on an extension of earlier work by Kanninen et al [20] based on an inclined strip yield formulation, following the lead of others [59], who had applied strip yield models to this type of analyses. The advantages of such a framework were (1) it is a direct extension of the colinear strip formulation already in use, (2) it has the potential to be implemented in the absence of detailed inelastic analysis and (3) the concept already had been used in Europe and later the U.S. to account for closure for long cracks [59,61,62]. The work was terminated in view of funding limitations, awaiting definitive results showing a significant closure effect for Inconel 718. Subsequent to our critical review and concurrent to our feasibility study, Newman [10] independently demonstrated with appropriate calibration of his model that closure could simulate short crack trends observed in the literature.

Appendix D. Accuracy and Precision in Crack Length Measurement

Measurement of physically small cracks involves problems and techniques not always encountered with physically long cracks. Accuracy and precision are important considerations in choosing editing and analysis procedures and in data interpretation for short cracks. For this reason details concerning accuracy and precision, and also the threshold for detection, have been summarized under funding from the reporting appropriation. This summary is presented in this appendix.

Accuracy of a measurement technique is a measure of the agreement between the absolute measurements obtained using the technique with those obtained using some other technique which serves as a standard. The photographic method used in this study does not allow simultaneous measurement of the crack length by another suitable measurement technique. Therefore, in the strictest sense one cannot establish the accuracy of the present method; however, information is available to give a rough estimate of expected accuracy. Specimens which were to undergo wake removal were removed from the load frame after initiating and growing the crack to some specified length. The cracks were then measured using a monocular microscope equipped with a micrometer-driven X-Y table. The micrometer accuracy was $\pm$ 0.00025 inch*. These measurements were used to guide the machinist carrying out wake removal. Comparison between these lengths and those obtained using the photographic method gives a one point check of accuracy (see Table D-1).

Two things should be noted. First, the number of load cycles experienced by the specimen at the time of measurement is reported in Table D-1. Often the last picture prior to wake removal was taken a number of cycles before load cycling was stopped. Thus, a small increment of crack growth could occur before microscopic measurement. Second, this one point check of agreement is not a true measure of accuracy. A proper determination

---

* As inch units form the basis for this study, the results are reported in that units system. Summary results and conclusions are presented with SI equivalents.

TABLE D-1a. COMPARISON OF CRACK LENGTHS AT WAKE REMOVAL MEASURED BY MICROSCOPE AND THE PHOTOGRAPHIC METHOD*

Specimen	Microscope			Photographic Method				Error			
	Side 1 Length	Side 2 Length	Cycle	Side 1 Length	Side 1 Cycle	Side 2 Length	Side 2 Cycle	Relative (%) Side 1	Relative (%) Side 2	Absolute (inches) Side 1	Absolute (inches) Side 2
CC-9	.0171	.0183	8500	.0171	8480	.0185	8430	0.0	10.9	0.0	.0002
CC-10	.0150	.0143	3750	.0277	3720	.0241	3720	84.7	68.5	.0127	.0102
CC-11	.0153	.0206	8430	.0169	9270	.0226	8490	10.3	9.6	.0016	.0020
CC-12	.0164	.0153	4350	.0165	4350	.0155	4350	.5	1.6	.0001	.0002
CC-13	.0178	.0188	4510	.0190	4490	.0147	4490	6.5	-22.0	.0012	-.0041
CC-14	.0162	.0148	13400	.0154	13300	.0139	13300	-4.8	-6.4	-.0008	-.0009
CC-15	.0228	.0223	7500	.0229	7400	.0232	7400	.5	4.0	.0001	.0009
CC-3	.0298	.0287	2590	.0299	2580	.0278	2580	.3	-3.1	.0001	-.0009
CC-18	.0180	.0188	7600	.0188	7500	.0183	7500	4.3	-2.4	.0008	-.0005
CC-19	.0353	.0224	1980	.0357	1980	.0230	1980	1.2	2.8	.0004	.0006

* All lengths are in inches, which formed the basis for measurement (.03937 inches = 1 mm). All microscopic measurements are ±.00025 inches.

TABLE D-1b. COMPARISON OF CRACK LENGTHS AT WAKE REMOVAL MEASURED BY MICROSCOPE AND THE PHOTOGRAPHIC METHOD (CONT'D)*

Specimen	Side 1 Crack 1 M'scope Cycle	Side 1 Crack 1 Photo. Cycle	Side 1 Crack 1 Error % Absolute	Side 1 Crack 2 M'scope Cycle	Side 1 Crack 2 Photo. Cycle	Side 1 Crack 2 Error % Absolute	Side 2 Crack 1 M'scope Cycle	Side 2 Crack 1 Photo. Cycle	Side 2 Crack 1 Error % Absolute	Side 2 Crack 2 M'scope Cycle	Side 2 Crack 2 Photo. Cycle	Side 2 Crack 2 Error % Absolute
CH-1	.0409	.0302	-26.2	0	0	--	.0776	.0707	-8.9	0	0	--
	3082	3074	-.0107	3082	3082	--	3082	3074	-.0069	3082	3082	--
CH-3	.0147	.0146	-.7	.0041	.0057	39.0	.0154	.0149	-3.2	.0029	.0016	-44.8
	211	205	-.0001	211	211	.0016	211	205	-.0005	211	246	-.0013
CH-4	.0063	.0071	12.7	.0343	.0300	-12.5	.0091	.0054	-40.7	.0461	.0429	-6.9
	370	367	.0007	370	367	-.0043	370	367	-.0037	370	367	-.0032
CH-16	.0316	.0332	5.0	.0162	.0140	-13.5	0	0	--	0	0	--
	3131	3131	.0016	3131	3131	-.0022	3131	3131	--	3131	3131	--

* All lengths are in inches, which formed the basis for measurement (.03937 inches = 1 mm). All microscopic measurements are $\pm$.00025 inches.

of accuracy would involve a number of comparisons of mean values obtained by making repeat measurements of crack length at various stages in its growth.

For the 32 sets of data listed in Table D-1, the mean absolute error is - 0.00002 inch (.5 μm) and the standard deviation on the mean is 0.0041 inch (104 μm). These numbers suggest a high variability in the accuracy of the method, but a very good agreement in the mean. Note that error bands for K derived from applying $\pm$ 0.004 inch to crack length would be on the order of the width of the symbols used in the da/dN -K_{max} plots in this report. It can be expected that some of the variability observed arises from the procedure being used to estimate accuracy. Estimates of relative error are also reported. For cracks 0.014-0.017 inches in length, the average relative error is 13.7%, with values ranging from -0.7% to 84.7%.

Precision indicates the inherent variability of the measurement technique. In this study measurement precision is defined as the standard deviation on the mean value of crack length determined for a set of replicate measurements. Because of variations in film quality from roll to roll, the precision was determined for each roll by averaging the standard deviations found for 3 sets of 15 replicate readings made on 3 film images chosen at random. These average values are reported in Table D-2. For the 45 values shown, the mean value is 0.0002 inch (5 μm) with a standard deviation of 0.0002 inch (5μm). Error bands for this precision would be smaller than the height of the symbols used on the plots in this report.

Editing of the crack length record was done by requiring a $2\bar{\sigma}$ increase in successive readings, applying the appropriate standard deviation determined for each roll of film to the raw data for that roll. Determination of precision was not made for specimens CC-10, 11, 12, and 13. They were edited with an assumed value of σ equal to 0.0002 inch. The resulting data sets were satisfactory.

The threshold for crack detection is significant because it limits the amount of information obtainable in the range of crack lengths over which anomolous growth behavior is expected. Table D-3 summarizes the smallest crack lengths detected for each test. Initial EDM flaw length, natural crack length, and total crack length are included. The three factors most affecting

TABLE D-2 SUMMARY OF MEASUREMENT PRECISIONS*

Specimen	Side	Roll	σ_{avg}	Specimen	Side	Roll	σ_{avg}
CC-9	1	1	.000100	CH-1	1	1	.000204
		2	.000138			2	.000164
	2	1	.000155		2	1	.000271
		2	.000365			2	.000335
		3	.000067				
				CH-3	1	1	.000344
CC-15	1	1	.000146			2	.000344
		2	.000189		2	1	.000529
	2	1	.000243			2	.000481
		2	.000126				
				CH-4	1	1	.000224
CC-3	1	1	.000173			2	.000806
		2	.000509		2	1	.000211
	2	1	.000107			2	.000510
CC-18	1	1	.000131	CH-16	1	1	.000240
		2	.000389			2	.000221
	2	1	.000072		2	1	.000256
		2	.000079				
				CH-20	1	1	.000154
CC-19	1	1	.000106		2	1	.000172
		2	.000092				
	2	1	.000097	CH-6	1	1	.000122
		2	.000133			2	.000144
					2	1	.000658
CC-14	1	1	.000099			2	.000221
	2	1	.000164				
		2	.000062				
		3	.000081				

* All σ are expressed in inches, which formed the basis for measurement (.03937 in = 1 mm).

TABLE D-3a. THRESHOLD FOR CRACK DETECTION*

Specimen	Side	Initial EDM Half Flaw Length	Average Half Crack Length Measured from Initial EDM Flaw	Total Half Crack Length, a
		Cracks Starting from Small EDM Flaws		
CC-9	1	.0105	.0028	.0133
	2	.0092	.0009	.0101
CC-10	1	.0106	.0091	.0197
	2	.0083	.0084	.0167
CC-11	1	.0153	.0016	.0169
	2	.0097	.0049	.0146
CC-12	1	.0096	.0019	.0115
	2	.0087	.0023	.0110
CC-13	1	.0093	.0012	.0105
	2	.0138	.0009	.0147
CC-14	1	.0096	.0011	.0107
	2	.0094	.0023	.0117
CC-15	1	.0088	.0023	.0111
	2	.0090	.0011	.0101
CC-3	1	.0085	.0011	.0096
	2	.0073	.0024	.0097
CC-18	1	.0076	.0009	.0085
	2	.0087	.0022	.0109
CC-19	1	.0103	.0012	.0115
	2	.0110	.0020	.0130

* All lengths are in inches, which formed the basis for measurement.
(.03937 inches = 1 mm)
All measurements are $\pm$.00025 inches.

TABLE D-3b. THRESHOLD FOR CRACK DETECTION (CONT'D)

Cracks Starting from .5 inch Diameter Holes					
Specimen	Side	Crack	Depth of EDM Starter Notch	Crack Length Measured from EDM Starter Notch	Total Crack Length c
CH-1	1	1	0	.0080	.0080
		2	0	.0097	.0097
	2	1	0	.0197	.0197
CH-2	1	1	0	.0154	.0154
		2	0	.0027	.0027
	2	1	0	.0010	.0010
CH-3	1	1	.0028	.0009	.0037
		2	.0018	.0044	.0062
	2	1	.0029	.0035	.0064
		2	.0020	.0005	.0025
CH-4	1	1	.0014	.0032	.0046
		2	.0017	.0024	.0041
	2	1	.0014	.0044	.0058
		2	.0018	.0024	.0042
CH-16	1	1	0	.0064	.0064
		2	0	.0051	.0051
CH-20	1	1	.002		.0049
		2	.002		.0027
	2	1	.002		.0123
		2	.002		.0059
CH-6	1	1	.001		.0021
		2a	0		.0019
		2b	0		.0043
	2	1	.001		.0122
		2	0		.0064

the threshold for detection were film image quality, the presence of surface irregularities such as pits, and the tightness of the crack. Including the preflaws (about 0.01 inch), the mean crack length, a, for earliest detection is 0.0123 inches (312 μm) with a standard deviation of 0.0029 inches (74 μm) for the center cracked panels. For the plates with holes, the mean crack length, c, including the preflaws (about 0.001 inch), at earliest detection was 0.0063 inches (160 μm) with a standard deviation of 0.0045 inches (110 μm). Corresponding means and standard deviations of thresholds for detection in the absence of the preflaws were 0.0025 $\pm$ 0.0023 inch (63.3 $\pm$ 57.5 μm) in CCP samples and 0.0055 $\pm$ 0.0053 inch (137 $\pm$ 132 μm) in CNP samples.

In summary, the results reported here suggest that the photographic method used in this study is capable of highly accurate measurements but is also subject to variability in accuracy for crack lengths on the order of those of interest to this study. Further study of the system is required to make a categorical statement of its measurement accuracy. The precision of the digitizing method was found to be generally on the order of 0.0002 inches (5 μm). Therefore data trends for small increments of crack growth could be easily studied. The threshold for crack detection varied from specimen to specimen. Generally the threshold beyond the preflaw was on the order of 0.05 to 0.15 mm.

APPENDIX E. DATA TABLES

The following tables list the data generated in this study and presented in graphical form in this report. All data has been edited and labeled as detailed in the section on data reduction. Test conditions are given in Table 1, and the specimen geometries are shown in Figure 5.

CC9

Side 1

a	N
0.10858	15280.
0.10044	15160.
0.06233	14080.
0.05931	13960.
0.05689	13840.
0.05436	13720.
0.05223	13600.
0.05194	13480.
0.04833	13360.
0.04709	13240.
0.04572	13120.
0.04398	13000.
0.04319	12880.
0.04070	12760.
0.03968	12640.
0.03849	12520.
0.03704	12400.
0.03613	12280.
0.03528	12160.
0.03502	12040.
0.03340	11920.
0.03192	11800.
0.03112	11680.
0.03057	11560.
0.02999	11440.
0.02930	11320.
0.02856	11200.
0.02825	10900.
0.02760	10780.
0.02714	10660.
0.02594	10540.
0.02566	10420.
0.02483	10300.
0.02436	10180.
0.02152	9500.
0.02099	9340.
0.02069	9260.
0.02013	9180.
0.01944	9100.
0.01579	8780.
0.01845	8480.
0.01753	8280.
0.01712	8180.
0.01668	7980.
0.01607	7680.
0.01536	7480.
0.01486	6720.
0.01289	6400.
0.01154	5700.
0.01108	5300.
0.01009	5100.

Side 2

a	N
0.10034	15240.
0.09425	15120.
0.08722	14960.
0.08257	14840.
0.07765	14720.
0.07341	14600.
0.06965	14480.
0.06493	14320.
0.06170	14200.
0.05932	14080.
0.05661	13960.
0.05357	13840.
0.05108	13720.
0.04771	13520.
0.04530	13360.
0.04262	13120.
0.03997	13000.
0.03323	12280.
0.03166	12080.
0.03119	11960.
0.02901	11680.
0.02859	11560.
0.02708	11440.
0.02618	11320.
0.02564	10900.
0.02427	10620.
0.01688	8400.
0.01622	8200.
0.01601	8100.
0.01477	7800.
0.01454	7600.
0.01428	7500.
0.01391	7400.
0.01381	7200.
0.01331	7120.

Side 1

a	N
0.12413	7060.
0.1151	7010.
0.10858	6960.
0.09843	6860.
0.08815	6710.
0.08272	6660.
0.07492	6560.
0.06892	6410.
0.06335	6310.
0.05919	6210.
0.05498	6110.
0.05221	6010.
0.05022	5960.
0.04891	5910.
0.04757	5860.
0.04689	5810.
0.04074	5560.
0.03804	5460.
0.03755	5360.
0.03538	5310.
0.03485	5160.
0.03339	5060.
0.03231	5010.
0.03065	4910.
0.02953	4760.
0.02793	4260.
0.02560	4210.
0.02372	4060.
0.02334	4010.
0.02768	3720.
0.02623	3600.
0.02583	3470.
0.02516	3380.
0.02453	3320.
0.02381	3130.
0.02312	3040.
0.02199	2930.
0.02140	2900.
0.02089	2840.
0.01967	2810.

Side 2

a	N
0.16138	7310.
0.14703	7260.
0.13513	7210.
0.12756	7160.
0.11869	7110.
0.11092	7060.
0.10491	7010.
0.09808	6960.
0.09329	6910.
0.09032	6860.
0.08446	6810.
0.08067	6760.
0.07683	6710.
0.07408	6660.
0.07181	6610.
0.06837	6560.
0.06565	6510.
0.06345	6460.
0.06083	6410.
0.05968	6360.
0.05867	6310.
0.05606	6260.
0.05413	6210.
0.05148	6160.
0.04859	6110.
0.04800	6060.
0.04504	6010.
0.04348	5960.
0.04109	5910.
0.04084	5860.
0.03960	5760.
0.03974	5710.
0.03837	5660.
0.03749	5610.
0.03684	5560.
0.03568	5510.
0.03509	5460.
0.03443	5360.
0.03267	5260.
0.03160	5210.
0.03100	5110.
0.02928	5060.
0.02875	5010.
0.02824	4910.
0.02696	4810.
0.02646	4660.
0.02595	4610.
0.02546	4460.
0.02483	4410.
0.02409	3720.
0.02243	3630.
0.02170	3600.
0.02126	3450.
0.02041	3330.
0.01858	3300.
0.01674	3270.

CC11

Side 1

a	N
0.09944	12810.
0.09321	12750.
0.08920	12690.
0.08533	12630.
0.08146	12570.
0.08025	12510.
0.07555	12390.
0.07116	12330.
0.06859	12270.
0.06433	12210.
0.06176	12150.
0.05977	12090.
0.05700	12030.
0.05638	11970.
0.05369	11910.
0.05282	11850.
0.05039	11790.
0.04747	11730.
0.04705	11670.
0.04511	11550.
0.04463	11490.
0.04379	11430.
0.04091	11370.
0.03926	11310.
0.03758	11250.
0.03670	11190.
0.03534	11130.
0.03326	11010.
0.03258	10890.
0.03178	10770.
0.03034	10710.
0.02727	10530.
0.02637	10470.
0.02573	10410.
0.02496	10230.
0.02422	10170.
0.02375	10050.
0.02186	9990.
0.02084	9930.
0.01964	9810.
0.01912	9750.
0.01846	9390.
0.01688	9270.

Side 2

a	N
0.11619	12990.
0.11165	12930.
0.10622	12870.
0.10225	12810.
0.09768	12750.
0.09511	12690.
0.09132	12630.
0.08842	12570.
0.08430	12510.
0.08194	12450.
0.07945	12390.
0.07586	12330.
0.07417	12270.
0.07125	12210.
0.06927	12150.
0.06724	12090.
0.06612	12030.
0 06448	11970.
0.06192	11910.
0.06033	11850.
0.05929	11790.
0.05793	11730.
0.05639	11670.
0.05408	11550.
0.05178	11490.
0.05062	11430.
0.04802	11370.
0.04679	11250.
0.04580	11190.
0.04526	11130.
0.04403	11070.
0.04292	11010.
0.04204	10950.
0.04061	10830.
0.04012	10770.
0.03896	10710.
0.03787	10590.
0.03669	10530.
0.03594	10470.
0.03534	10410.
0.03464	10350.
0.03304	10170.
0.03219	9930.
0.03130	9810.
0.02951	9750.
0.02876	9630.
0.02819	9330.
0.02771	9270.
0.02504	9030.
0.02461	8790.
0.02419	8730.
0.02247	7400.
0.02154	6680.
0.02058	6560.
0.01634	6440.
0.01458	6290.

CC12

Side 1		Side 2	
a	N	a	N
0.09645	7590.	0.11347	7610.
0.08878	7530.	0.10359	7550.
0.08179	7470.	0.09497	7490.
0.07724	7410.	0.08927	7430.
0.07286	7350.	0.08159	7370.
0.06752	7290.	0.07614	7310.
0.06435	7230.	0.07095	7250.
0.06111	7170.	0.06690	7190.
0.05749	7110.	0.06349	7130.
0.05517	7050.	0.05918	7070.
0.05267	6990.	0.05557	7010.
0.04982	6930.	0.05396	6950.
0.04840	6870.	0.05075	6890.
0.04577	6810.	0.04836	6830.
0.04492	6750.	0.04598	6770.
0.04281	6690.	0.04446	6710.
0.04152	6570.	0.04299	6650.
0.03859	6510.	0.04088	6590.
0.03712	6450.	0.03983	6530.
0.03562	6390.	0.03771	6470.
0.03463	6330.	0.03691	6410.
0.03362	6270.	0.03533	6350.
0.03265	6210.	0.03368	6290.
0.03122	6150.	0.03262	6230.
0.03016	6090.	0.03177	6170.
0.02953	6030.	0.03090	6110.
0.02889	5970.	0.02991	6050.
0.02819	5910.	0.02903	5990.
0.02718	5850.	0.02819	5930.
0.02583	5670.	0.02728	5870.
0.02534	5550.	0.02618	5810.
0.02328	5430.	0.02561	5850.
0.02260	5370.	0.02493	5790.
0.02211	5310.	0.02441	5730.
0.02136	5190.	0.02363	5670.
0.02075	5070.	0.02279	5550.
0.01948	4950.	0.02222	5490.
0.01885	4890.	0.02159	5430.
0.01833	4770.	0.02082	5310.
0.01787	4710.	0.02001	5190.
0.01730	4590.	0.01918	5070.
0.01649	4350.	0.01837	4950.
0.01597	4230.	0.01787	4890.
0.01493	4170.	0.01726	4770.
0.01435	3750.	0.01656	4650.
0.01386	3570.	0.01610	4470.
0.01281	3450.	0.01554	4350.
0.01153	2730.	0.01491	4230.
		0.01404	3990.
		0.01291	3480.
		0.01103	2540.

CC13

Side 1

a	N
0.10786	7230.
0.09492	7170.
0.08644	7110.
0.08175	7050.
0.07726	6990.
0.06985	6930.
0.06757	6870.
0.06185	6810.
0.06044	6750.
0.05592	6690.
0.05422	6630.
0.05072	6570.
0.04845	6510.
0.04662	6450.
0.04553	6390.
0.04427	6330.
0.04040	6270.
0.03861	6050.
0.03786	5990.
0.03645	5930.
0.03342	5870.
0.03283	5810.
0.03241	5750.
0.03172	5690.
0.02967	5570.
0.02829	5510.
0.02776	5450.
0.02614	5330.
0.02499	5150.
0.02408	5090.
0.02334	4790.
0.02163	4730.
0.02080	4670.
0.01969	4550.
0.01895	4490.
0.01785	4430.
0.01694	4290.
0.01594	3990.
0.01502	3870.
0.01353	3510.
0.01380	3450.
0.01320	3330.
0.01250	3150.
0.01208	3090.
0.01162	2850.
0.01051	2790.

Side 2

a	N
0.11410	7310.
0.09976	7250.
0.09030	7190.
0.08162	7130.
0.07480	7070.
0.06875	7010.
0.06447	6950.
0.05946	6890.
0.05573	6830.
0.05269	6770.
0.04859	6710.
0.04573	6650.
0.04437	6590.
0.04089	6530.
0.03850	6470.
0.03739	6410.
0.03482	6350.
0.03241	6290.
0.03070	6230.
0.02892	6170.
0.02787	6110.
0.02712	6050.
0.02560	5990.
0.02452	5930.
0.02369	5870.
0.02279	5810.
0.02134	5690.
0.02069	5630.
0.01896	5570.
0.01805	5450.
0.01723	5210.
0.01647	5150.
0.01517	5030.
0.01467	4490.

CC14

Side 1

a	N
0.10403	26480.
0.10167	26360.
0.09848	26260.
0.09709	26160.
0.09569	26060.
0.09160	25960.
0.08871	25860.
0.08718	25760.
0.08588	25660.
0.08304	25560.
0.08184	25460.
0.08067	25360.
0.07968	25260.
0.07915	25160.
0.07345	25060.
0.07146	24960.
0.07016	24860.
0.06842	24760.
0.06795	24660.
0.06614	24560.
0.06489	24460.
0.06403	24360.
0.06253	24260.
0.06182	24160.
0.06011	23960.
0.05737	23860.
0.05602	23760.
0.05561	23660.
0.05366	23460.
0.05285	23360.
0.05123	23060.
0.04849	22860.
0.04688	22560.
0.04566	22360.
0.04365	22260.
0.04323	22160.
0.04240	22060.
0.04199	21960.
0.04091	21760.
0.04045	21660.
0.03940	21460.
0.03731	21260.
0.03677	21060.
0.03622	20960.
0.03548	20860.
0.03443	20460.
0.03309	20360.
0.03265	20160.
0.03171	19960.

Con't

a	N
0.03079	19760.
0.03034	19660.
0.02975	19560.
0.02887	19460.
0.02837	19060.
0.02780	18760.
0.02724	18660.
0.02638	18360.
0.02594	18260.
0.02527	18160.
0.02484	18060.
0.02411	17760.
0.02344	17330.
0.02274	16910.
0.02233	16730.
0.02166	16490.
0.02123	16430.
0.02080	16070.
0.02025	16010.
0.01984	15710.
0.01939	14990.
0.01867	14930.
0.01818	14870.
0.01746	14330.
0.01701	14270.
0.01659	13850.
0.01507	12760.
0.01454	11860.
0.01399	11220.
0.01348	10680.
0.01234	10380.
0.01183	10040.
0.01141	9160.
0.01072	9080.

Side 2

a	N
0.11675	27580.
0.10929	27380.
0.10310	27160.
0.09674	26960.
0.09212	26780.
0.08709	26560.
0.08271	26360.
0.07914	26160.
0.07567	25960.
0.07173	25760.
0.06859	25560.
0.06565	25360.
0.06407	25160.
0.06158	24960.
0.05969	24760.
0.05659	24560.
0.05477	24360.
0.05217	24160.
0.05007	23960.
0.04804	23760.
0.04597	23360.
0.04389	23160.
0.04162	22760.
0.03994	22560.
0.03868	22360.
0.03753	22160.
0.03628	21960.
0.03516	21760.
0.03423	21560.
0.03293	21360.
0.03214	21160.
0.03140	20960.
0.03088	20760.
0.02969	20560.
0.02800	20160.
0.02739	19860.
0.02675	19660.
0.02596	19460.
0.02545	19260.
0.02489	19160.
0.02449	18960.
0.02374	18660.
0.02318	18360.
0.02237	17960.
0.02193	17660.
0.02095	16840.
0.01619	14620.
0.01579	13900.
0.01507	13840.
0.01464	13540.
0.01350	12700.
0.01300	12100.
0.01260	11620.
0.01220	10900.
0.01167	10180.

CC15

Side 1

a	N
0.10326	13720.
0.09851	13620.
0.09390	13520.
0.08862	13420.
0.08751	13320.
0.08293	13220.
0.08129	13120.
0.07784	13020.
0.07557	12920.
0.07234	12820.
0.07149	12720.
0.06742	12620.
0.06665	12520.
0.06431	12420.
0.06223	12320.
0.06124	12220.
0.05843	12120.
0.05753	12020.
0.05562	11920.
0.05271	11720.
0.05219	11620.
0.05100	11520.
0.04906	11420.
0.04782	11320.
0.04664	11220.
0.04577	11120.
0.04460	11020.
0.04415	10820.
0.04270	10720.
0.04177	10620.
0.04051	10520.
0.03964	10220.
0.03813	10120.
0.03764	9720.
0.03438	9620.
0.03360	9520.
0.03303	9420.
0.03250	8920.
0.03147	8720.
0.02994	8620.
0.02894	8420.
0.02836	8000.
0.02688	7900.
0.02626	7800.
0.02543	7700.
0.02432	7600.
0.02284	7200.
0.02228	6900.
0.02171	6600.
0.02124	6400.
0.01940	6300.
0.01879	5800.
0.01836	5400.
0.01773	5200.
0.01686	5000.
0.01637	4800.
0.01470	4200.
0.01406	3700.
0.01385	3300.
0.01311	3100.
0.01204	2900.
0.01112	2800.

Side 2

a	N
0.11178	13920.
0.10735	13820.
0.10236	13720.
0.09839	13620.
0.09387	13520.
0.09128	13420.
0.08722	13320.
0.08444	13220.
0.08099	13120.
0.07812	13020.
0.07517	12920.
0.07306	12820.
0.07023	12720.
0.06705	12620.
0.06508	12520.
0.06348	12420.
0.06082	12320.
0.05911	12220.
0.05799	12120.
0.05535	12020.
0.05432	11920.
0.05299	11820.
0.05244	11720.
0.05131	11620.
0.04912	11520.
0.04877	11420.
0.04776	11320.
0.04371	11020.
0.04338	10920.
0.04248	10820.
0.04166	10720.
0.04118	10620.
0.03985	10520.
0.03898	10420.
0.03804	10320.
0.03608	10220.
0.03581	10120.
0.03536	9920.
0.03465	9720.
0.03348	9620.
0.03297	9520.
0.03268	9420.
0.03238	9320.
0.03199	9220.
0.03122	9120.
0.03082	9020.
0.02989	8820.
0.02957	8720.
0.02811	8520.
0.02753	8420.
0.02592	8100.
0.02515	8000.
0.02456	7800.
0.02414	7700.
0.02353	7600.
0.02144	6900.
0.02057	6700.
0.01997	6400.
0.01947	6300.
0.01855	5500.
0.01772	5400.
0.01663	4700.
0.01531	4400.
0.01440	3900.
0.01391	3700.
0.01331	3100.
0.01251	2500.
0.01203	2300.
0.01139	2000.
0.01063	1600.
0.01008	1200.

Side 1		Side 2	
a	N	a	N
0.10252	4450.	0.02784	2580.
0.09348	4390.	0.02571	2400.
0.08758	4330.	0.02450	2340.
0.08528	4270.	0.02384	2280.
0.07683	4090.	0.02239	2160.
0.07330	4030.	0.02217	1920.
0.06823	3970.	0.01816	1800.
0.06548	3910.	0.01757	1680.
0.06091	3850.	0.01674	1440.
0.05732	3730.	0.01557	1320.
0.05369	3670.	0.01402	1200.
0.05080	3610.	0.01387	1140.
0.04909	3550.	0.01167	840.
0.04782	3430.	0.01127	660.
0.04537	3370.	0.00970	600.
0.04279	3310.		
0.04033	3250.		
0.03848	3070.		
0.03683	3010.		
0.03574	2950.		
0.03351	2830.		
0.03228	2770.		
0.02957	2650.		
0.02989	2580.		
0.02875	2520.		
0.02736	2460.		
0.02671	2400.		
0.02597	2340.		
0.02495	2280.		
0.02447	2220.		
0.02333	2140.		
0.02223	2080.		
0.02184	2020.		
0.02080	1960.		
0.02008	1900.		
0.01929	1840.		
0.01844	1780.		
0.01804	1480.		
0.01690	1420.		
0.01634	1360.		
0.01557	1300.		
0.01437	1180.		
0.01383	1120.		
0.01317	1060.		
0.01258	940.		
0.01217	820.		
0.01173	760.		
0.00962	700.		

CC18

Side 1

a	N
0.03892	11700.
0.03648	11400.
0.03328	11200.
0.03188	10800.
0.03094	10600.
0.03012	10400.
0.02852	10000.
0.02742	9600.
0.02650	9300.
0.01803	6800.
0.01714	6400.
0.01679	6300.
0.01640	6000.
0.01593	5900.
0.01563	5400.
0.01508	5100.
0.01413	4800.
0.01333	4700.
0.01298	4600.
0.01262	4300.
0.01237	4100.
0.01173	3600.
0.01129	3100.
0.01087	2900.
0.01056	2700.
0.01017	2200.
0.00975	1900.
0.00948	1200.
0.00912	900.
0.00851	800.

Side 2

a	N
0.03460	11700.
0.03273	11600.
0.03145	11500.
0.03107	11400.
0.03026	11300.
0.02944	11200.
0.02894	11100.
0.02860	11000.
0.02817	10900.
0.02771	10800.
0.02737	10700.
0.02704	10600.
0.02655	10500.
0.02599	10200.
0.02559	10100.
0.02465	10000.
0.02422	9900.
0.02330	9700.
0.02275	9500.
0.02238	9400.
0.02016	9300.
0.02176	9100.
0.02120	9000.
0.02054	8800.
0.02004	8600.
0.01947	8500.
0.01924	8400.
0.01900	8300.
0.01859	8200.
0.01834	7500.
0.01816	7400.
0.01787	7200.
0.01762	7100.
0.01735	7000.
0.01569	6100.
0.01531	6000.
0.01505	5800.
0.01480	5600.
0.01441	5500.
0.01240	3700.
0.01209	3600.
0.01186	3400.
0.01146	3300.
0.01131	3000.
0.01110	2800.
0.01090	2600.

CC19

Side 1

a	N
0.10051	2700.
0.08440	2640.
0.07392	2580.
0.06489	2520.
0.06116	2460.
0.05797	2400.
0.05224	2340.
0.04719	2280.
0.04396	2220.
0.04172	2160.
0.03939	2100.
0.03735	2040.
0.03574	1980.
0.03439	1920.
0.03238	1860.
0.03122	1800.
0.03033	1740.
0.02997	1680.
0.02806	1620.
0.02645	1560.
0.02514	1500.
0.02441	1440.
0.02374	1380.
0.02209	1320.
0.02121	1260.
0.02051	1200.
0.01982	1140.
0.01882	1080.
0.01840	1020.
0.01764	960.
0.01682	900.
0.01643	840.
0.01596	780.
0.01516	720.
0.01493	660.
0.01406	600
0.01343	540
0.01289	480
0.01261	420
0.01177	360
0.01148	300.

Side 2

a	N
0.09585	2700.
0.07719	2640.
0.06437	2580.
0.05596	2520.
0.05182	2460.
0.04762	2400.
0.04214	2340.
0.03605	2280.
0.03242	2220.
0.02961	2160.
0.02602	2100.
0.02387	2040.
0.02303	1980.
0.02100	1920.
0.01939	1860.
0.01805	1800.
0.01714	1740.
0.01622	1680.
0.01495	1620.
0.01402	1560.
0.01299	1500.

Crack 1/Side 1

c	N
0.01537	29120.
0.01701	29130.
0.02029	29140.
0.02254	20150.
0.02357	29180.
0.025	29190.
0.02582	29220.
0.02684	29230.
0.02787	29300.
0.02910	29310.
0.02971	29330.
0.03094	29340.
0.03238	29360.
0.0332	29490.
0.03381	29520.
0.03463	29580.
0.03545	29630.
0.03668	29670.
0.03791	29690.
0.03955	31620.
0.04201	31640.
0.04303	31660.
0.04406	31750.
0.04467	31830.
0.04631	32080.
0.04754	32220.
0.04816	32230.
0.05	32630.
0.05594	32840.
0.06025	33140.
0.06557	33180.
0.07541	33280.
0.08074	33310.
0.08566	33390.
0.09221	33410.
0.09713	33450.
0.10041	33480.
0.10553	33510.
0.11004	33540.
0.11516	33580.
0.12090	33610.
0.12602	33650.
0.13033	33680.
0.13586	33720.
0.15061	33820.
0.15615	33860.

Crack 1/Side 2

c	N
0.0	33180.
0.00102	33190.
0.00963	33200.
0.01926	33210.
0.02623	33220.
0.03135	33230.
0.03832	33240.
0.03934	33250.
0.04795	33280.
0.05	33290.
0.05594	33320.
0.06639	33370.
0.07172	33400.
0.07623	33440.
0.08258	33470.
0.08627	33510.
0.09037	33540.
0.09529	33570.
0.10266	33610.
0.10553	33650.
0.11066	33680.
0.11537	33720.
0.125	33790.
0.13135	33830.
0.13525	33860.
0.14119	33910.
0.14508	33940.
0.15143	33980.
0.15594	34010.
0.16107	34940.
0.16557	34080.
0.17131	34120.
0.17480	34140.

CH1

Crack 1/Side 1

c	N
0.13840	3130.
0.13033	3125.
0.12300	3120.
0.03022	3074.
0.01500	3014.
0.01223	2994.
0.01150	2954.
0.01109	2934.
0.01036	2854.
0.00924	2794.
0.00886	2734.
0.00841	2714.
0.00797	2214.
0.00757	2014.
0.00711	1934.

Crack 1/Side 2

c	N
0.21499	3190.
0.20957	3185.
0.20480	3180.
0.19712	3175.
0.19027	3170.
0.18704	3165.
0.18127	3160.
0.17800	3155.
0.17008	3150.
0.16305	3145.
0.15529	3140.
0.14767	3135.
0.14175	3130.
0.13696	3125.
0.12769	3120.
0.07069	3074.
0.06258	3054
0.05313	3034.
0.04929	3014.
0.04249	2994.
0.04004	2974.
0.03447	2954.
0.03270	2934.
0.03204	2914.
0.02986	2894.
0.02776	2874.
0.02552	2854.
0.02029	2814.
0.01967	2774.

CH1
(Concluded)

Crack 2/Side 1

c	N
0.16519	3331.
0.11435	3326.
0.09086	3321.
0.07385	3316.
0.06297	3311.
0.05607	3306.
0.05094	3301.
0.04485	3296.
0.04038	3291.
0.03670	3283.
0.03454	3278.
0.02486	3255.
0.02431	3250.
0.02318	3240.
0.02176	3235.
0.02077	3230.
0.01826	3195.
0.01788	3185.
0.01635	3180.
0.01533	3165.
0.01343	3155.
0.01317	3145.
0.01278	3140.
0.01156	3130.
0.01115	3125.
0.00969	3120.

CH16

Crack 1/Side 1

c	N
0.14527	3341.
0.13890	3334.
0.13202	3327.
0.12705	3320.
0.12170	3313.
0.11270	3306.
0.10605	3299.
0.10103	3292.
0.09458	3285.
0.08972	3278.
0.08208	3271.
0.07892	3264.
0.07495	3257.
0.07075	3250.
0.06763	3243.
0.06621	3236.
0.05970	3229.
0.05854	3222.
0.05601	3215.
0.05467	3208.
0.05174	3201.
0.04906	3194.
0.04750	3180.
0.04465	3173.
0.04319	3166.
0.03317	3131.
0.03167	3111.
0.03019	3091.
0.02827	3071.
0.02755	3051.
0.02626	3031.
0.02458	3011.
0.02092	2991.
0.01959	2911.
0.01704	2891.
0.01650	2831.
0.01447	2811.
0.01363	2731.
0.01306	2711.
0.01217	2691.
0.01064	2611.
0.00987	2491.
0.00887	2391.
0.00837	2311.
0.00785	2171.
0.00738	2131.
0.00636	2111.

Crack 1/Side 2

c	N
0.18353	3405.
0.16466	3391.
0.15830	3384.
0.15158	3377.
0.14330	3370.
0.13633	3363.
0.13049	3356.
0.12161	3349.
0.11584	3342.
0.10844	3335.
0.10267	3328.
0.09671	3321.
0.08843	3314.
0.07942	3307.
0.07132	3300.
0.06298	3293.
0.05327	3286.
0.04075	3279.
0.02057	3272.

Crack 2/Side 1

c	N
0.14603	3425.
0.12282	3418.
0.10635	3411.
0.09136	3404.
0.07986	3397.
0.07424	3390.
0.06318	3383.
0.05914	3376.
0.05488	3369.
0.05019	3362.
0.04812	3355.
0.04585	3348.
0.04318	3341.
0.04073	3334.
0.03873	3327.
0.03753	3320.
0.03536	3313.
0.03341	3306.
0.03135	3292.
0.02950	3285.
0.02871	3278.
0.02360	3271.
0.02273	3243.
0.02304	3236.
0.01864	3215.
0.01809	3137.
0.01576	3111.
0.01512	3091.
0.01449	3051.
0.01343	3011.
0.01060	2991.
0.00943	2871.
0.00887	2831.
0.00803	2751.
0.00735	2631.
0.00580	2491.
0.00505	2431.

CH4

Crack 1/Side 1

c	N
0.15881	500.
0.14617	495.
0.13093	490.
0.11924	485.
0.10631	480.
0.09699	475.
0.08899	470.
0.07400	465.
0.06518	460.
0.05785	455.
0.04537	450.
0.03938	445.
0.03304	435.
0.02351	430.
0.02072	425.
0.01768	420.
0.01580	415.
0.01359	400.
0.00877	375.
0.00689	357.
0.00633	337.
0.00578	332.
0.00508	317.
0.00457	312.

Crack 1/Side 2

c	N
0.19253	515.
0.17490	510.
0.15791	505.
0.14380	500.
0.12909	495.
0.11773	490.
0.10548	485.
0.09609	480.
0.08252	475.
0.07260	470.
0.06747	465.
0.05755	460.
0.04932	455.
0.04184	450.
0.03839	445.
0.03097	440.
0.02689	435.
0.02506	430.
0.01977	420.
0.01828	415.
0.01632	405.
0.00576	362.
0.00144	357.

CH4
(Concluded)

Crack 2/Side 1		Crack 2/Side 2	
c	N	c	N
0.15403	450.	0.19473	470.
0.15226	445.	0.18753	465.
0.15033	435.	0.17767	460.
0.14474	430.	0.17042	455.
0.13895	425.	0.16331	450.
0.12795	420.	0.15585	445.
0.11707	415.	0.14685	440.
0.11144	410.	0.14001	435.
0.10176	405.	0.13119	430.
0.09503	400.	0.12494	425.
0.08418	395.	0.11761	420.
0.07225	390.	0.11030	415.
0.06242	385.	0.10037	410.
0.05440	380.	0.09216	405.
0.04075	375.	0.08480	400.
0.02998	367.	0.07664	395.
0.02468	362.	0.07015	390.
0.02054	357.	0.06457	385.
0.01632	352.	0.05758	380.
0.01558	347.	0.05181	375.
0.01251	342.	0.04286	367.
0.01166	337.	0.04019	362.
0.00860	327.	0.03625	357.
0.00748	317.	0.03237	352.
0.00640	287.	0.02985	347.
0.00507	277.	0.02747	342.
0.00405	257.	0.02523	337.
		0.02323	332.
		0.02050	327.
		0.01835	322.
		0.01717	317.
		0.01595	312.
		0.01424	302.
		0.01298	297.
		0.01141	292.
		0.01036	287.
		0.00981	282.
		0.00934	277.
		0.00870	272.
		0.00826	267.
		0.00728	250.
		0.00654	245.
		0.00609	235.
		0.00561	215.
		0.00486	200
		[illegible]	[illegible]

CH3

Crack 1/Side 1

c	N
0.14154	309.
0.13080	302.
0.12047	295.
0.10724	288.
0.09532	281.
0.08754	274.
0.07394	267.
0.06577	260.
0.05392	253.
0.04572	246.
0.03593	239.
0.02984	232.
0.02381	225.
0.01817	218.
0.01457	205.
0.01335	200.
0.01212	190.
0.01117	180.
0.00991	165.
0.00757	150.
0.00624	140.
0.00531	125.
0.00442	120.
0.00365	115.

Crack 1/Side 2

c	N
0.19808	344.
0.18869	337.
0.17888	330.
0.15883	323.
0.14799	316.
0.13426	309.
0.12154	302.
0.11064	295.
0.10010	288.
0.08816	281.
0.07700	274.
0.06557	267.
0.05530	260.
0.04741	253.
0.03792	246.
0.03088	239.
0.02396	232.
0.02001	225.
0.01724	210.
0.01491	205.
0.01368	200.
0.01257	185.
0.01031	165.
0.00910	150.
0.00746	130.
0.00636	110.

CH3
(Concluded)

Crack 2/Side 1		Crack 2/Side 2	
c	N	c	N
0.15018	385.	0.19828	372.
0.10881	358.	0.12060	365.
0.08309	351.	0.08516	358.
0.05407	344.	0.05925	351.
0.03920	337.	0.03752	344.
0.02739	330.	0.01993	337.
0.02344	323.	0.01231	330.
0.01927	316.	0.00748	323.
0.01618	309.	0.00774	316.
0.01332	302.	0.00490	302.
0.01009	281.	0.00368	287.
0.00891	274.	0.00252	253.
0.00811	253.	0.00155	246.
0.00622	205.		

CH20

Crack 1/Side 1

c	N
0.15868	4030.
0.14962	3970.
0.14721	3910.
0.14069	3850.
0.13845	3790.
0.13072	3730.
0.12740	3670.
0.12427	3610.
0.11947	3550.
0.11651	3490.
0.11118	3430.
0.10786	3370.
0.10450	3310.
0.10300	3250.
0.09716	3190.
0.09324	3130.
0.08962	3070.
0.08762	3010.
0.08544	2929.
0.08026	2869.
0.07752	2809.
0.07417	2749.
0.06995	2689.
0.06825	2629.
0.06556	2569.
0.06177	2509.
0.05998	2449.
0.05633	2389.
0.05380	2329.
0.04994	2285.
0.04778	2245.
0.04611	2205.
0.04458	2165.
0.04259	2125.
0.04042	2085.
0.03904	2045.
0.03731	2005.
0.03515	1965.
0.03375	1925.
0.03207	1885.
0.03076	1845.
0.02963	1805.
0.02807	1725.
0.02552	1645.
0.02258	1600.
0.02207	1580.
0.02158	1500.
0.01936	1480.
0.01886	1460.
0.01801	1440.
0.01667	1400.
0.01620	1320.
0.01505	1300.
0.01461	1280.
0.01416	1240.
0.01321	1040.
0.01171	1020.
0.01136	880.
0.01014	860.
0.00908	800.
0.00637	580.
0.00578	500.
0.00531	420.
0.00486	400.

Crack 1/Side 2

c	N
0.20237	4570.
0.19586	4510.
0.19141	4450.
0.18459	4390.
0.17977	4330.
0.17300	4270.
0.16763	4210.
0.16322	4150.
0.15784	4090.
0.15182	4030.
0.14775	3970.
0.14354	3910.
0.13785	3850.
0.13281	3790.
0.12800	3730.
0.12680	3670.
0.12133	3610.
0.11683	3550.
0.11320	3490.
0.10978	3430.
0.10371	3370.
0.10317	3310.
0.09606	3250.
0.09372	3190.
0.09120	3130.
0.08986	3070.
0.08663	3010.
0.08041	2950.
0.07552	2809.
0.07255	2749.
0.07012	2689.
0.06533	2629.
0.06488	2569.
0.06141	2509.
0.05872	2449.
0.05601	2329.
0.05030	2285.
0.04761	2245.
0.04571	2205.
0.04493	2165.
0.04237	2125.
0.04071	2085.
0.03897	2045.
0.03690	2005.
0.03436	1965.
0.03317	1925.
0.03109	1885.
0.03052	1845.
0.02929	1765.
0.02704	1685.
0.02654	1645.
0.02551	1605.
0.01321	1060.
0.01232	660.

CH20
(Concluded)

Crack 2/Side 1

c	N
0.14836	4570.
0.14080	4510.
0.13166	4450.
0.12331	4390.
0.11571	4330.
0.10876	4270.
0.10392	4210.
0.09690	4150.
0.08953	4090.
0.08530	4030.
0.07911	3970.
0.07218	3910.
0.06608	3850.
0.05764	3790.
0.05318	3730.
0.04835	3670.
0.04401	3610.
0.04046	3550.
0.03660	3490.
0.03197	3430.
0.02870	3370.
0.02647	3250.
0.02100	3190.
0.01989	3130.
0.01833	3070.
0.01630	3010.
0.01593	2950.
0.01466	2929.
0.01418	2869.
0.01350	2809.
0.01199	2749.
0.01058	2689.
0.01005	2449.
0.00813	2245.
0.00784	2205.
0.00713	2165.
0.00495	1805.
0.00439	1540.
0.00333	1520.
0.00304	1400.
0.00269	1120.

Crack 2/Side 2

c	N
0.14729	4570.
0.14002	4510.
0.13106	4450.
0.12405	4390.
0.11958	4330.
0.10873	4270.
0.10190	4210.
0.09723	4150.
0.09023	4090.
0.08623	4030.
0.07934	3970.
0.07323	3910.
0.06597	3850.
0.06256	3790.
0.05449	3730.
0.04967	3670.
0.04640	3610.
0.04148	3550.
0.03783	3490.
0.03429	3430.
0.02981	3370.
0.02940	3310.
0.02369	3250.
0.02237	3190.
0.02037	3130.
0.01910	3070.
0.01832	3010.
0.01691	2950.
0.01511	2809.
0.01389	2689.
0.01338	2569.
0.01255	2509.
0.01111	2389.
0.00958	2085.
0.00913	2005.
0.00769	1925.
0.00590	1605.

Crack 1/Side 1

c	N
0.14301	14840.
0.13917	14630.
0.13368	14420.
0.12871	14210.
0.12350	14000.
0.11859	13790.
0.11390	13580.
0.10899	13370.
0.10373	13160.
0.09858	12950.
0.09504	12740.
0.08927	12530.
0.08471	12320.
0.08058	12110.
0.07624	11900.
0.07217	11690.
0.06894	11480.
0.06433	11270.
0.06119	11060.
0.05677	10850.
0.05447	10640.
0.05166	10430.
0.04896	10220.
0.04656	10010.
0.04146	9800.
0.03800	9590.
0.03556	9380.
0.03245	9170.
0.03000	8960.
0.02661	8750.
0.02423	8540.
0.02189	8330.
0.02053	8120.
0.01901	7910.
0.01720	7700.
0.01553	7490.
0.01432	7280.
0.01378	7070.
0.01252	6860.
0.01147	6650.
0.01061	6440.
0.00981	6230.
0.00928	6020.
0.00825	5810.
0.00790	5600.
0.00699	5390.
0.00606	4970.
0.00567	4760.
0.00529	4550.
0.00499	4130.
0.00439	3920.
0.00385	3360.
0.00301	3080.
0.00268	3010.
0.00211	2940.

Crack 1/Side 2

c	N
0.20234	17360.
0.20168	17290.
0.20033	17220.
0.19876	17150.
0.19704	17080.
0.19482	17010.
0.19387	16940.
0.19387	16870.
0.19053	16800.
0.18927	16730.
0.18280	16520.
0.17614	16310.
0.17194	16100.
0.16802	15890.
0.16029	15680.
0.15601	15470.
0.15031	15260.
0.14563	15050.
0.13981	14840.
0.13631	14630.
0.12971	14420.
0.12514	14210.
0.12087	14000.
0.11493	13790.
0.11037	13580.
0.10516	13370.
0.10060	13160.
0.09734	12950.
0.09198	12740.
0.08691	12530.
0.08430	12320.
0.07864	12110.
0.07457	11900.
0.06934	11690.
0.05805	11060.
0.05605	10850.
0.05488	10640.
0.05003	10430.
0.04760	10220.
0.04444	10010.
0.04014	9800.
0.03623	9590.
0.03258	9380.
0.03009	9170.
0.02684	8960.
0.02572	8750.
0.02219	8540.
0.02056	8330.
0.01780	8120.
0.01577	7910.
0.01356	7490.
0.01219	7280.

CH6
(Concluded)

Crack 2/Side 1

c	N
first crack	
0.02312	26020.
0.02206	25920.
0.02142	25820.
0.01738	25720.
0.01459	25620.
0.01290	25520.
0.01098	25420.
0.00910	25320.
0.00785	25220.
0.00583	25120.
0.00476	25020.
0.00451	24920.
0.00397	24620.
0.00368	24420.
0.00331	24120.
0.00284	24020.
0.00256	23520.
0.00224	23220.
0.00192	23120.
crack causing failure	
0.14711	26620.
0.12576	26520.
0.10653	26420.
0.09223	26320.
0.07591	26220.
0.05901	26120.
0.02319	26020.
0.02226	25920.
0.02015	25820.
0.01750	25720.
0.01477	25620.
0.01244	25520.
0.01082	25420.
0.00908	25320.
0.00792	25220.
0.00560	25120.
0.00426	24920.

Crack 2/Side 2

c	N
0.18376	26720.
0.15122	26620.
0.12977	26520.
0.11149	26420.
0.09224	26320.
0.08443	26220.
0.07215	26120.
0.06082	26020.
0.05386	25920.
0.04697	25820.
0.04067	25720.
0.03524	25620.
0.03105	25520.
0.02611	25420.
0.02268	25320.
0.01962	25220.
0.01613	25120.
0.01358	25020.
0.01037	24920.
0.00924	24820.
0.00746	24720.
0.00692	24620.
0.00639	24320.

Appendix F. Considerations in the Choice of K Solution for Finite Width CNP Specimens

Because the focus of this study is on physically small cracks, it is important that the K solution used adequately characterize the crack driving force local to the notch root. This means that for finite width specimens, a finite width correction for the far boundary must be applied. But, more important for short cracks is the need to account for variations in the peak stress and the stress gradient as a function of width. To this end, this appendix considers the choice of the K solution such that the chosen solution matches the limit given by Equation 2a for small cracks. Specifically this appendix considers bounds on the validity of Equation 2a as a function of crack size so as not to erroneously bias the selection process. The bounds on crack length are chosen with respect to (1) the error in stress as a function of c introduced by setting stress equal to K_tS and (2) dominance of the crack's stress field and the notch stress field as a function of crack length.

The error made by fixing σ, the local stress in the material element at the crack tip, equal to K_tS can be estimated by comparison of K_tS with the value of K_tS reduced by the gradient. Backlund and Karlsson [30] discuss analysis convenient for this purpose, for small cracks. Their work notes that Equation 2a can be more accurately written as follows:

$$K/S = (1.22\ K_t + (0.683\ \partial\sigma_y/\partial x|_{x=r})c)\ \sqrt{\pi c}\ ; \qquad (F.1)$$

but, it should be emphasized that this form is also only valid for small cracks. In view of this result, Equation 2a can be used for crack lengths up to about 490 μm within a +5% error. Such an error is considered acceptable in a practical context in that typically load is only controlled to within ±1%. Therefore, an upper bound to the validity of Equation 2a is tentatively taken as 490 μm. In the limit, as $c \to 0$, Equation 2a approaches the exact result so that the corresponding lower bound to the validity of Equation 2a is zero crack length.

Consider now control of the crack driving force in terms of the coupled effects of the crack stress field and the notch stress field. The

purpose here is to calculate the range of crack lengths controlled by these fields. Because differences in accounting for the notch stress field is the essential difference between the various K solutions for a CNP, the desire is to limit the comparison of Equation 2a and the various K solutions to the range of crack lengths where K is controlled by terms involving $F(\ell)$. To simplify the analyses, an infinite plate solution with crack length expressed as a function of notch root radius is used as the basis for the study. Thereafter, the results are made specific to the present application by the introduction of the crack length and notch dimensions relevant to this study. In view of the above analysis the results are accurate in an absolute sense within +5%, for cracks less than 490 μm long.

The results of Newman as expressed by Tada [25] for the situation considered indicate K has the form

$$\frac{K}{S} = F(\ell)\ \sqrt{\pi c} \qquad (F.2)$$

where $\ell = c/(r+c)$, and r = the radius of the hole. Dominance of the stress field of the crack, embedded in terms involving $\sqrt{\pi c}$, and that of the notch, embedded in terms involving $F(\ell)$, can be established by examining the rate of change in K/S as a function of c. To this end:

$$\frac{d}{dc}(K/S) = \frac{\pi}{2}\ (\pi c)^{-\frac{1}{2}}\ F(\ell) + (\pi c)^{\frac{1}{2}}\ \frac{d}{dc}\ F(\ell) \qquad (F.3)$$

Since $\ell = c/(r+c)$, then

$$\frac{d}{dc}(F(\ell)) = \frac{d}{d\ell}\ F(\ell) \cdot \frac{d\ell}{dc}$$

$$= \frac{d}{d\ell}\ F(\ell)\ \left(\frac{1}{r+c} - \frac{c}{(r+c)^2}\right)$$

Here $F'(\ell)$ is the slope of the function $F(\ell)$ (denoted F(c/W) in regard to Equation 2) for the function catalogued by Tada et al [25].

Thus for the CNP of interest:

$$\frac{d}{dc}(K/S) = -(\pi c)^{-\frac{1}{2}} F(\ell) + (\pi c)^{\frac{1}{2}} F'(\ell) \frac{1}{(0.25+c)} - \frac{c}{(0.25+c)^2}$$

$c \to 0$:	$\to \infty$	finite
c = .001":	(1.57)(17.84)(3.36)	(0.056)(6.5)(3.96)
c = .01":	(1.57)(5.64)(3.1)	(0.18)(6.27)(3.69)
c = .1":	(1.57)(1.78)(1.8)	(0.56)(2.5)(1.93)
c = 1":	(1.57)(0.56)(1.12)	(1.77)(0.06)(0.14)

As noted earlier, for c > 490 μm, discrepancies in Equation 2a between $K_t S$ and the actual stress for that crack length are considered to be excessive. Another upper bound follows from Equation A6.2 which shows that at about 800 μm the $\sqrt{\pi c}$ term in Equation 2 begins to dominate K/S, whereas for smaller cracks the notch field F(ℓ) dominates. Obviously the smaller of these two upper limits controls, so that 490 μm is adopted as the upper bound on the validity of Equation 2a. As is evident from the behavior of d(K/S)/dc there is also a lower bound in c below which crack growth driving force is also controlled by the $\sqrt{\pi c}$ term. The above table shows the influence of the $\sqrt{\pi c}$ related terms in Equation 2a will be balanced by those related to F(ℓ) for $c \geq$ ~0.002" (50 μm) and $c \leq$ ~0.1" (25 mm). Since the upper bound here exceeds that noted above, the previously stated upper bound of 490 μm is retained. It will be used in conjunction with a lower bound on the validity of Equation 2a which, based on the tabulated results, should be less than the initial balance point between the $\sqrt{\pi c}$ term and those related to F(ℓ). Since this initial balance occurs at about 0.002 inch or 50 μm, a lower bound for present purposes is a crack size less than 0.002 inch. For the present, a length of 0.001 inch or 25 μm is arbitrarily selected. This avoids transients associated with small cracks related to the unbounded tendency of d(K/S)/dc as $c \to 0$.

Note that calculated values of d(K/S)/dc for various K solutions are significantly different for short cracks. However, once the crack is about

3.5 mm long the values of d(K/S)/dc are comparable. Note too that as $c \to 0$, d(K/S)/dc approaches infinity. That is, the crack driving force for small cracks at notches is changing very rapidly. It is doubtful that a "steady state" growth process can develop under such conditions in real materials. But it is also clear that as $c \to 0$ continuum mechanics becomes inappropriate for applications to real materials. In view of the above analysis, it is asserted that K does not adequately characterize the driving force for growth for values of c less than 25 μm. The use of K already has been so restricted in this study by the lower bound associated with the free surface effect.